A compact Ge-BGO Compton suppression spectrometer

Wintraecken, Y.J.E.

Award date:
1996

A compact Ge-BGO Compton suppression spectrometer

Y.J.E. Wintraecken

Collaboration: K.V.I., Groningen - Netherlands
Canberra Semiconductors N.V., Olen - Belgium
Quartz & Silice, de Meern - Netherlands

Eindhoven University of Technology
Department of Technical Physics
Nuclear Physics Techniques

Report on graduate study
1 February 1992 - 17 February 1993
Supervision: M.J.A. de Voigt
S.L. Micek

Graduate committee:

Prof. dr. M.J.A. de Voigt	- Eindhoven, University of Technology
dr. S.S. Klein	- Eindhoven, University of Technology
dr. F. de Waele	- Eindhoven, University of Technology
Prof. dr. S.L. Micek	- Jagellonian University, Cracow
dr. J.C. Bacelar	- K.V.I., Groningen
dr. P. Burger	- Canberra Semiconductors N.V, Olen
dr. P. Schotanus	- Quartz & Silice, de Meern

Abstract

A compact Ge-BGO Compton suppression spectrometer is being designed and built in the group Nuclear Physics Techniques at the Eindhoven University of Technology. The designed spectrometer is unique in the fact that the Ge detector and the BGO veto shield are within one cryostat, so attenuation of Compton scattered γ-rays in cryostat material is avoided.

In designing the spectrometer we first optimized the Peak to Total ratio of the spectrometer by means of Monte Carlo calculations for different crystal sizes and crystal shapes. The final Ge-BGO configuration shows the highest Peak to Total ratio (E_γ = 1.33 MeV; P/T = 0.77) acquired by simulation until now (1993).

Secondly, we simulated the light output of the BGO veto shield. We examined the influence of crystal shape and crystal size as well as the influence of different surface treatments of the crystal on the photon collection. This resulted in a veto shield which is conically shaped and consists of BGO with diffuse as well as specular surfaces. According to the simulations the minimum detectable energy deposition in the crystal amounts to 15 keV.

According to the calculations the equilibrium temperature of the spectrometer amounts to 100 kelvin when cooled, which is appropriate to operate the Ge. The cooling down time of the setup amounts to 2-3 days.

Contents

Introduction

This report describes the work done during a period of a year (February 1992 - February 1993) in the group Nuclear Physics Techniques at the Physics department of the Eindhoven University of Technology. During this period we developed and built a Ge-BGO Compton suppression spectrometer mostly on the basis of information acquired by Monte Carlo simulations.

In July 1990 the project started as a new FOM project to build a compact Compton suppression spectrometer at the institute. At present, the construction of the compact Compton suppression spectrometer reaches its final stage (February 1993). The spectrometer will be used as a single Compton suppression spectrometer. Another possible application is to serve as a segment of the 4π cluster detector of the Eurogam project, at the moment situated in Daresbury, U.K. The project can also contribute to the Euroball project.

Compton suppression spectrometers normally consist of a high resolution semi-conductor detector, which is cooled in a cryostat, surrounded by a scintillator crystal, which has an inferior energy resolution and is at room temperature.

The spectrometer built in Eindhoven deviates from the normally built spectrometers, because there is no material between the Ge semi-conductor detector and the BGO scintillator veto shield. Absorption of γ-rays by material between Ge and BGO is thereby avoided. Because the Ge needs to be operated at temperatures below 110 kelvin, the Ge detector as well as the scintillator are cooled.

In Chapter 1 the setup of the Compton suppression spectrometer is discussed. Because an anti-Compton spectrometer consists of a semi-conductor detector surrounded by a scintillator, properties of both detection materials are discussed in this chapter.

Chapter 2 discusses γ-ray interactions with matter. The Geant software package is used for simulation of the γ-ray and secondary interactions. By Monte Carlo calculations the geometry of the spectrometer is optimized, keeping in mind the physical and mechanical restrictions.

The light output of the BGO veto shield is discussed in chapter 3. The light yield can be calculated using another Monte Carlo simulation program, named LGUIDE [Mic92a]. To test the program measurements and calculations are compared for a long rectangular BGO crystal. In order to optimize the light collection of the veto shield the influence of different surface treatments is studied using the program.

Ge detectors must be operated at temperatures below 110 kelvin. Consequently, the spectrometer must be cooled. In chapter 4 the equilibrium temperature of the spectrometer is calculated. We also predict a cooling down time for the new setup, using cooling down time of an existing setup.

Finally, in Chapter 5 design considerations as well as mechanical and electrical restrictions of the spectrometer are discussed.

The report ends with a discussion and recommendations for future development of the Ge-BGO Compton suppression spectrometer at the Eindhoven University of Technology.

Chapter 1

Compton suppression spectrometers, semi-conductor detectors and scintillation crystals; summary of literature

§ 1.1 Compton suppression spectrometers

To detect γ-rays mostly scintillation crystals or semi-conductor detectors are used. At present only Si and Ge semi-conductors are commercially available. For γ-ray detection Ge is superior to Si because of its much higher attenuation (§ 1.2). The number of scintillation materials is much larger. Properties of several inorganic scintillators and semiconductors materials are compared in table 1.1.1. [Der81,Eij92,Kno79].

Table 1.1.1. *Properties of NaI(Tl), BGO, BaF_2, Si and Ge.*

Material	Scintillator material			Semiconductor	
	NaI(Tl)	BGO	BaF_2	Ge	Si
Density (g/cm^3)	3.67	7.13	4.88	5.38	2.34
Index of refraction	1.85	2.15	1.50	-	-
Radiation length (cm) [a]	2.6	1.1	2.0	1.5	4.2
Hygroscopic ?	Yes	No	No	No	No
Scintillation decay time (ns)	230	300	600 0.8	-	-
Yield [b]	40	9	10 1.4	675	530
Emission of maximum wavelength (nm)	410	480	310 220	-	-

[a] Radiation length for 511 keV γ-rays.
[b] Scintillation photons or electron-hole pairs per keV energy loss.

NOTE: BaF_2 HAS A FAST AND A SLOW COMPONENT. IN THE ABOVE TABLE THE UPPER VALUES REPRESENT THE SLOW COMPONENT.

Ge detectors have a far better energy resolution than scintillators. However, Ge detectors suffer from a major limitation. A major fraction of the γ-rays which interact with the germanium deposits only a part of their energy in the crystal, resulting in a spectrum that consists of a sharp (photo)peak (complete energy deposition of the γ-rays) and a continuum at lower energies (partial energy deposition of the γ-rays). The process responsible for this continuum is known as Compton scattering (See Chapter 2). This is partly remedied by using larger Ge crystals. However, the maximum volume of a Ge crystal amounts to 500 cm^3. Moreover, Ge crystals are very expensive and paid per unit volume (cm^3).

In order to reduce this continuum several suppression methods can be used. Three different Compton suppression methods are given in [Kno79]: (1) Compton rejection by anti-coincidence; (2) sum coincidence; (3) pair spectrometry. The only continuum reduction method for the 0.1 MeV $\leq E_\gamma \leq$ 12 MeV region is the application of an anti-Compton shield (method 1), which surrounds the Ge-crystal. When γ-rays do not deposit their full energy in the Ge-crystal and Compton scatter out of the germanium, the scattered photon can be detected by the veto shield. If energy is deposited in the Ge as well as the veto shield the event is rejected by an anti-coincidence circuit. The ratio of the number of γ-rays which deposit their complete energy in the Ge detector to the total number of γ-rays which had an interaction in the detector is called the Peak to Total ratio and will be used to optimize the shape of the veto shield (Chapter 2). The shield is mostly made of a scintillation crystal, because it can have a great variety in size and shape. The lower energy resolution is of minor importance, because only a veto signal is needed.

In order to develop a compact anti-Compton spectrometer both the semi-conductor detector and the scintillation crystal should have a high density and high average atomic number (high attenuation of the γ-rays). For our purpose bismuth germanate (§ 1.3) is most suitable (see table 1.1.1). But the low light output and slow scintillation decay time of BGO make timing accuracy very dependent upon crystal geometry and optical coupling between BGO and photomultiplier (See Chapter 3). On the other hand, BGO is easy to handle (non-hygroscopic) and facilitates the use of a wide variety of crystal shapes, surfaces (polished, rough) and external reflectors (MgO, teflon, Al, etc).

Present anti-Compton spectrometers have separate cryostats for the Ge detector and the scintillator shield. Cryostats are made of metal, which can cause absorption of γ-rays. The γ-rays absorbed in the metal can not be detected by the scintillation crystal, and consequently the veto signal will not be given.

The purpose of our work is to build a compact Ge-BGO Compton suppression spectrometer consisting of a HPRE (high purity reverse electrode) Ge detector (§ 1.2) surrounded by a BGO veto shield in one cryostat, so that Ge as well as BGO will be cooled. A schematic drawing of the spectrometer can be seen in figure 1.1.1. The major advantages of one cryostat for both crystals are: (1) a more compact Compton spectrometer; (2) no material between Ge and BGO which can absorb scattered photons. Major disadvantage is the complicated geometry of the cryostat in order to keep the system vacuum tight.

Previous research done at the Eindhoven University of Technology [Pey90,Ver91] concerned the read-out of BGO by photodiodes. Advantages of photodiodes with respect to photomultiplier tubes are: (1) photodiodes are small compared to photomultiplier tubes, which is convenient to build a compact spectrometer; (2) photodiodes have a higher quantum efficiency compared to PMTs; (3) the low power demand of photodiodes compared to PMTs. On the other hand, the advantages of photomultipliers with respect to photodiodes are: (1) the complete coverage of the read-out surface (in our setup a 5" PMT completely covers the BGO read-out surface: diameter = 106 mm$\varnothing$), while the largest diameter of a photodiode assembly amounts to: diameter = 90 mm$\varnothing$ [Bur92]; (2) the amplification of photo-multipliers is large (10^6-10^7) and has of a high signal to noise ratio, while photodiodes have no amplification; (3) The cost of photomultipliers is rather low compared to the cost of photodiodes. Calculations on spectrometers read out by photodiodes and photomultipliers are compared. The simulated photon collection of the

BGO-PMT detection device is better than the light yield acquired using a BGO-photodiode assembly [Mic92a,Mic92d], so our veto shield will be read out by a PMT.

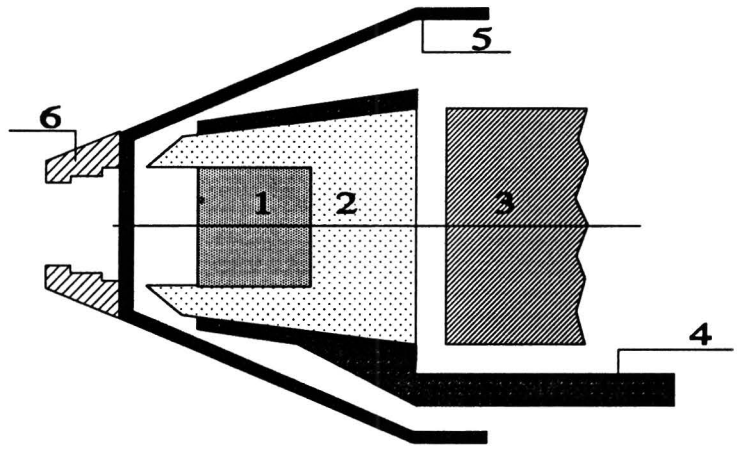

Figure 1.1.1. *Schematic setup of the built Compton suppression spectrometer.*

(1)	GE	: SEMI-CONDUCTOR DETECTOR	(4)	CU	: COPPER COOLING ROD
(2)	BGO	: SCINTILLATION CRYSTAL	(5)	AL	: ALUMINIUM CRYOSTAT
(3)	PMT	: PHOTOMULTIPLIER TUBE	(6)	PB	: LEAD COLLIMATOR

§ 1.2 Semi-conductor detectors

Semi-conductor detectors are based on crystalline semi-conductor materials, i.e. silicon or germanium. The advantage of semi-conductor detectors is their energy resolution which is far better than that of scintillators. The energy resolution of detectors is largely determined by the number of information carriers (n). Its variance is $\sqrt{n}$, and the resolution is a fraction $1/\sqrt{n}$ of the signal.

The use of semi-conductor detectors as radiation detectors can result in a much larger number of information carriers for a given radiation event than is possible with any other detector type. The basic information carriers are electron-hole pairs created along the path of the charged particle through the detector.

For γ-ray detection Ge is preferred over Si because of its higher atomic number and higher density (table 1.2.1 [Kno79]), which results in a much stronger attenuation for γ-rays. Disadvantage of germanium is that it must be cooled when operated, because of its smaller bandgap compared to silicon (explanation of the term bandgap is given in § 1.3). Normally, liquid nitrogen (LN_2) is used to cool the germanium (the liquid nitrogen temperature is 77 kelvin).

Commonly, Ge detectors are semiconductors with a p-i-n structure (See figure 1.2.1 [Kno79]) in which the intrinsic region (i) is sensitive for ionizing radiation, e.g. γ-rays.
A germanium detector converts γ-ray energy into electron-hole pairs. Due to an applied electric field over the p and n electrodes the electrons or holes are collected. The amount of collected charge carriers (electrons/holes) gives information about the incident energy.

Table 1.2.1. *Properties of intrinsic silicon and germanium.*

Material	Si	Ge
Atomic number	14	32
Atomic weight {g.mol^{-1}}	28.09	72.60
Density (300 K) {g cm^{-3}}	2.33	5.33
Forbidden energy gap (300 K) {eV}	1.115	0.665
Forbidden energy gap (0 K) {eV}	1.165	0.746
Energy per electron-hole pair (300 K) {eV}	3.62	-
Energy per electron-hole pair (77 K) {eV}	3.76	2.96

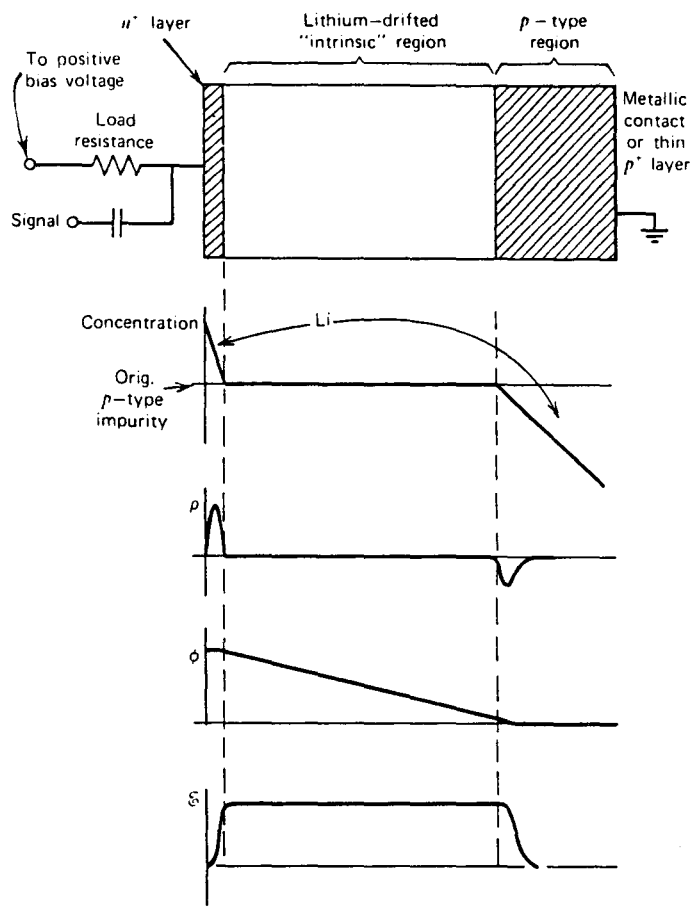

Figure 1.2.1. *Semi-conductor (Ge(Li)) detector consisting of a p-i-n structure. Also shown are the corresponding profiles for impurity concentration, charge density* ρ, *electric field potential* ϕ *and electric field* ε.

The first semi-conductor useful for γ-ray detection were made from lithium (Li) compensated germanium, also known as Ge(Li) detectors. Because of the high mobility of the lithium ions in germanium at room temperature Ge(Li) detectors must be operated and stored at liquid nitrogen temperature at all times. The minimum detectable energy of Ge(Li) detectors is limited by the thickness of the dead layer formed on the crystal by lithium drifting. Attenuation of γ-rays can occur in the dead layer. For low energy γ-rays the attenuation in the dead layer is relevant.

In more recent years intrinsic germanium detectors, also known as HP Ge detectors (high purity germanium detectors) have been constructed. These detectors are operated in the same way as Ge(Li) detectors, but have the advantage that they do not need to be stored at liquid nitrogen temperature. Cooling is only necessary if a high voltage is applied, normally done when the detector will be used for measurements.

Another advantage of intrinsic detectors is the possibility of using n-type semi-conductors rather than the p-type Ge necessary for the lithium drifting process. These are the HP RE Ge detectors (high purity reverse electrode germanium detectors). The schematic setups of HP Ge and HP RE Ge detectors are shown in figure 1.2.2.

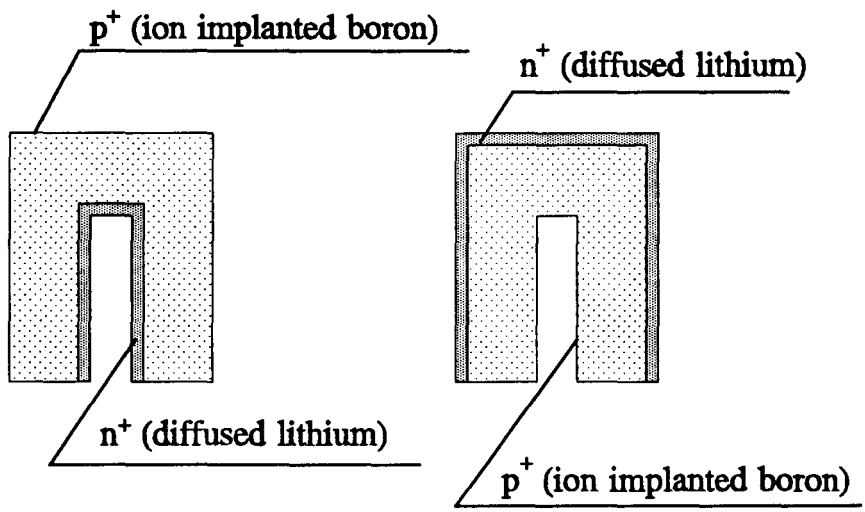

Figure 1.2.2. *Coaxial detector cross sections, left: reverse electrode high purity Ge detector; right: conventional high purity Ge detector.*

The reverse electrode high purity detectors are somewhat less sensitive to radiation damage. To improve the minimum detectable energy of the RE HP Ge detector a very thin dead layer at the detector entrance window can be formed by ion-implantation, which results in a lower detection threshold (below 10 keV [Leo87]).

§ 1.3 Scintillation crystals

Scintillation crystals are the most widely used γ-ray detectors in nuclear and particle physics today. The scintillation mechanism in inorganic materials depends on the energy

states determined by the crystal lattice of the material. The electrons have only discrete bands of energy available as seen in figure 1.3.1.

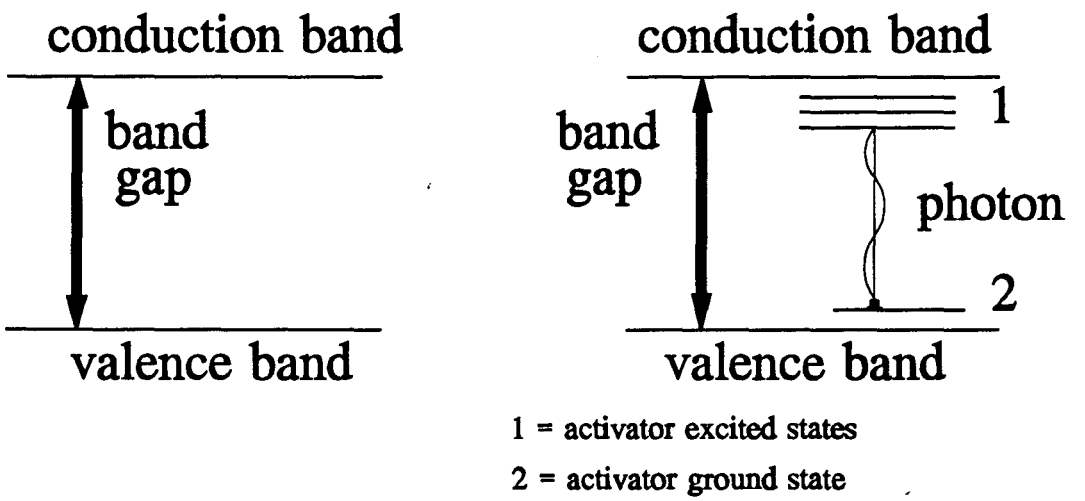

Figure 1.3.1. *Energy band structure of crystalline (inorganic) scintillators, left: intrinsic scintillator; right: doped scintillator.*

The lower band, known as valence band, contains those electrons, which are essentially bound at lattice sites, whereas the conduction band represents those electrons which contain sufficient energy to be free to migrate throughout the crystal. In between there is a forbidden band or bandgap. This forbidden region gives rise to an energy gap E_g between the conduction and valence band.

In pure crystals the electrons can not have an energy within the bandgap. Depending on the material, photons can be induced, which will have an energy larger or equal to the bandgap energy. These photons will again be absorbed in the crystal and are not detectable.

However, if impurities are present, energy levels (donor and acceptor states) within the forbidden region can exist. As a result of the energy states in the forbidden region, an electron can de-excite to the valence band from an activator excited state, thereby emitting a (scintillation) photon. The energy of this photon is less than the bandgap E_g. Absorption of the photon can thus only occur at activator states. Since the concentration of activator states is small, the chance on absorption inside the crystal is rather low. Consequently, the photons can traverse some distance through the crystal. Detection is therefore possible.

When a γ-ray interacts with the scintillator material, it induces a high energetic electron, which induces a large number of electrons to be elevated from the valence band to the conduction band. These electrons will migrate freely throughout the crystal, until they encounter an activator state. The electron will have a high probability to occupy the activator state, losing energy by phonon emission, forming a self trapped exciton. This exciton can recombine by photon emission or quenching. The de-excitation process will occur very quickly. Typical half lives for excited states are on the order of 10^{-7} s.

As already discussed in § 1.1 we chose to use BGO as a scintillator, because of its high attenuation for γ-rays. Since we want to build a Compton suppression spectrometer in one

cryostat the properties of BGO should be examined at liquid nitrogen temperatures (77 K).

In BGO the activator is the Bi atom. Trivalent bismuth has a mercury like $6s^2$ electronic configuration. The first excited configuration is the 6s6p state. The lowest excited state of Bi^{3+} is the $^3P_0$ state. However, a $^3P_0 \rightarrow {}^1S_0$ emission is forbidden using the selection rules [Eng72,Kra88,Eij92].

1: $\Delta J = 0, \pm 1$; no $J = 0 \rightarrow J = 0$
2: $\Delta S = 0$

The observed fluorescence of Bi^{3+} originates from the thermal population of the $^3P_1$ state and of the transition $^3P_1 \rightarrow {}^1S_0$. First thermal excitation from the $^3P_0 \rightarrow {}^3P_1$ will occur. After this transition, emission of the scintillation photon can occur. So, the lifetime will decrease for increasing temperature. Non radiative decay can occur via exciton migration or direct energy transfer to quenching centres, e.g. impurities, defects. Multiple phonon emission can also contribute to non radiative decay. The scintillation intensity of the BGO is dependent on radiative and non radiative decay. Since for increasing temperature the non radiative decay increases, the fluorescence yield (intensity of radiative decay) will decrease. In figure 1.3.2. [Web73] the lifetime and the relative fluorescence yield is plotted against the temperature.

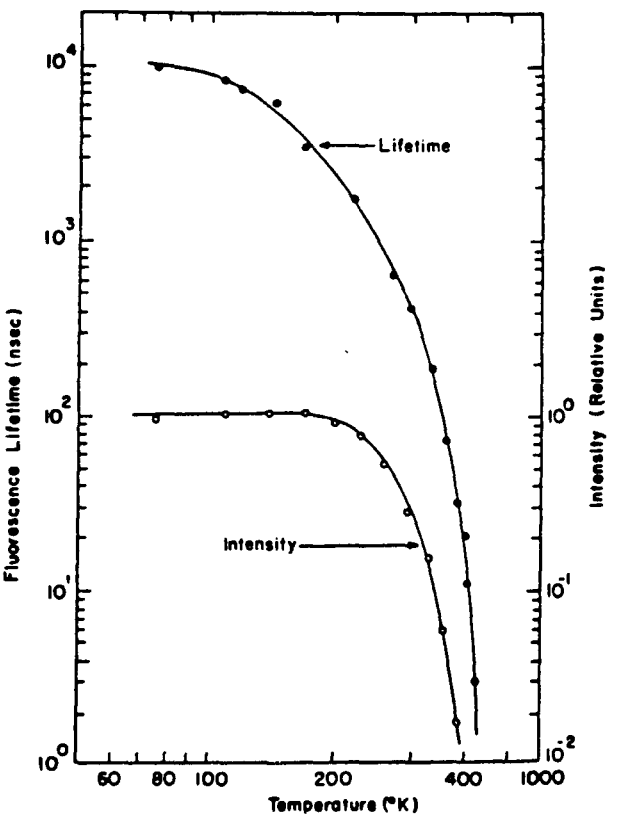

Figure 1.3.2. *Temperature dependence of the fluorescence lifetime and intensity for* $Bi_4Ge_3O_{12}$.

[Pil79] showed that the emission wavelength will increase for decreasing temperature. The quantum efficiency of the photomultiplier can be taken constant, because of the small wavelength-shift of the scintillation photons (See figure 1.3.3).

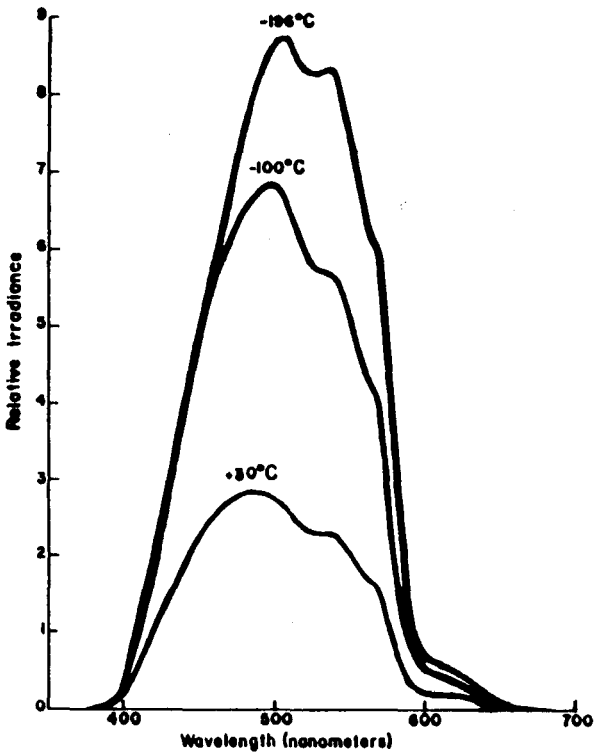

Figure 1.3.3. *Emission spectrum of BGO as function of temperature.*

Chapter 2

Optimizing the Peak to Total ratio using Monte Carlo simulations

§ 2.1 Monte Carlo calculations

For more than 25 years people have built Compton suppression spectrometers [Mic67, Mic86,Byr85,Eji89]. During this period, several Monte Carlo calculations have been carried out to predict the suppression and/or Peak to Total ratio. The first calculations did not consider secondary particles or multiple scattering. Nowadays, several software packages [For85,Bru87,Los87] are available which can simulate all possible interactions and can handle rather complicated geometries. Results obtained using such computer calculations are reported frequently in literature [Tab87,Nol85,Lie84,Bea92,Eks92,Kut92, Bax92] and are compared with experimental results. They show that Monte Carlo calculations are a powerful tool in predicting the Peak to Total ratio and Compton suppression.

In the next section (§ 2.2) the Geant software package is described. In § 2.3 all physical interactions of importance are discussed. The results of optimizing the Peak to Total ratio obtained using Geant for several Ge BGO-anti-Compton shield geometries are discussed in § 2.4. Finally in § 2.5, some additional remarks are made.

§ 2.2 The Geant computer code

The Geant software package is developed at the CERN institute in Geneva. Although Geant is developed specially for high energy physics, all physical processes of importance above 10 keV can be taken into account. The 10 keV-limit gives no problems, because the region of interest will be $0.1 \text{ MeV} \leq E \leq 12 \text{ MeV}$.

We chose to use Geant (version 3.17) in favour of other software packages, although in our laboratory some people worked with EGS [Ver91,Man92a]. This choice was made because geometrical problems are much easier to handle with Geant.

To use the Geant library, one has to write a Fortran [Nyh85] program. Through common blocks the program communicates with Geant. The main program contains statements about the matter with which the particles should interact, the geometry of the material, the physical processes Geant should take into account and the parameters of the event file created by running the program.

Matter is defined by its chemical composition, e.g. BGO is defined by $Bi_4Ge_3O_{12}$ (see table 2.2.1). To define an object only its shape and dimensions, e.g. tube (inner radius, outer radius, length) and the material it is composed of, e.g. BGO or Ge, are needed. The physical processes which should be simulated are simply called by common-blocks. After running Geant for one particle, all physical interactions which occurred and their positions are available. Storing all this information takes too much memory, but we want to have as much information as possible. Therefore we have to compromise. First, we divide the BGO-crystal into three pieces. This has two major advantages: (1) we can simulate a

Table 2.2.1. *Defining matter.*

	Bi	Ge	O	Ge
A (atomic weight)	208.92	72.59	15.99	72.59
Z (atomic number)	83	32	8	32
W (molecular constitution)	4	3	12	1

rather complicated structure of the BGO-crystal; (2) we can easily estimate the influence of one of the BGO-pieces by just leaving it out. Then we choose to store 8 parameters for each incident particle which had a first interaction with the spectrometer (particles which had no first interaction with the spectrometer can only contribute to the Compton continuum by scattering from the surrounding material (e.g. copper, lead collimator) to the Ge detector. The effect of this approximation is discussed in § 2.5). These 8 parameters are: energy deposited in Ge-crystal (1), energy deposited in the main BGO (2), the back BGO (3) and the nose BGO (4), the radius and depth of the first interaction in Ge-crystal (5-6) and the radius and depth of the first interaction in BGO-crystal (7-8). For additional information of the program, see Appendix B and [Bru87].

§ 2.3 Physical interactions taken into account

When particles hit matter a lot of interactions can take place. In Geant almost all interactions can be included. But we are only interested in the interaction of electromagnetic radiation (photons) with matter, and of course the induced secondary particles. For the energy region of interest (0.1 MeV $\leq$ E $\leq$ 12 MeV) only five physical processes should be taken into account: photoelectric effect, Compton scattering, pair production, annihilation and bremsstrahlung.

In the photoelectric effect, a photon is absorbed by an atom and one of the atomic electrons is released. The energy of the (photo)electron is given by equation 2.3.1.

$$T_e = h\nu - E_b \qquad (2.3.1)$$

with: T_e = kinetic energy of the (photo)-electron.
$h\nu$ = energy of the incident photon.
E_b = binding energy of the electron.

In the energy-region we are interested the binding energy of the electron is negligible compared to the incident photon energy, so $T_e \approx h\nu$. This electron is emitted under an angle ϕ (See figure 2.3.1) with an angular distribution which depends on the energy of the incident photon [Eva67,Hei57]. The range varies from 27 μm for 0.1 MeV (photo)-electrons to 1.1 cm for 12 MeV [Eva67] (photo)electrons in Ge, so it is likely that in the photoelectric process the complete energy of the incident photon is absorbed inside the material in which the photoelectric effect took place.

Compton scattering is the process by which a photon scatters from a nearly free atomic

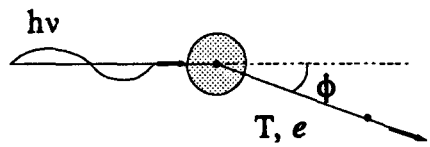

Figure 2.3.1. *Photo-electrical effect.*

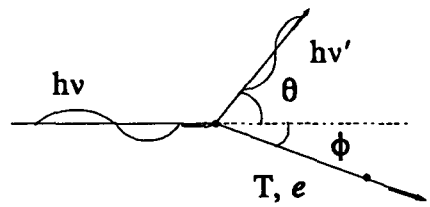

Figure 2.3.2. *Compton scattering.*

electron, resulting in a less energetic photon in a new direction and a scattered electron (see figure 2.3.2). Neglecting the binding energy of the electron, conservation of linear momentum and energy yields (formula 2.3.2):

$$h\nu' = \frac{h\nu}{1 + \alpha(1 - \cos\theta)} \qquad (2.3.2)$$

with: $h\nu$ = incident photon energy.
$h\nu'$ = energy of the scattered photon.
α = $h\nu/m_0c^2$; (m_0c^2 = electron rest mass ≈ 511 keV).
θ = angle under which the photon is scattered.

The probability for Compton scattering at an angle θ can be determined by the Klein-Nishina formula for the differential Compton cross section (equation 2.3.3)[Eva67]:

$$\frac{d\sigma}{d\Omega} = r_0^2 \left[\frac{1}{1 + \alpha\,(1 - \cos\theta)}\right]^3 \left[\frac{1 + \cos^2\theta}{2}\right] \cdot \qquad (2.3.3)$$

$$\left[1 + \left(\frac{\alpha^2(1 - \cos\theta)}{(1 + \cos^2\theta)\,(1 + \alpha(1 - \cos\theta))}\right)\right]$$

with: r_0 = the classical electron radius {m}.
Ω = solid angle {sr}.

The polar plot of the Klein-Nishina differential Compton cross section is shown in figure

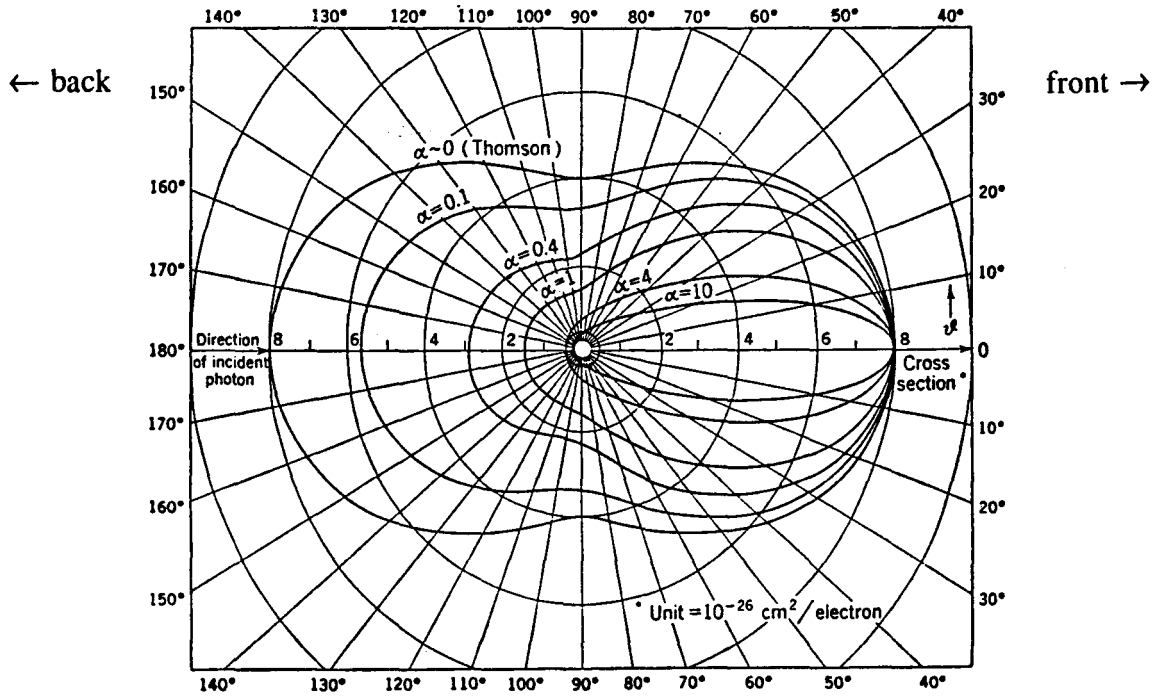

Figure 2.3.3. *The number of photons scattered into unit solid angle ($d\sigma/d\Omega$), at a mean scattering angle θ.*

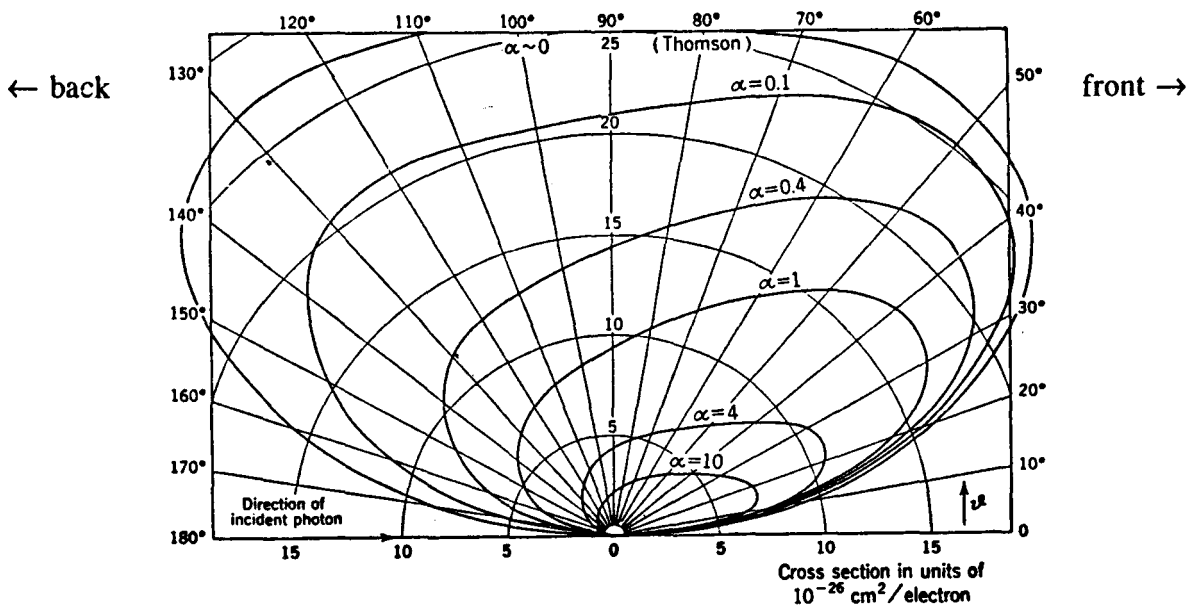

Figure 2.3.4. *Number versus angle distribution ($d\sigma/d\theta$) of the Compton scattered photons.*

2.3.3. It gives the number of scattered photons into a unit solid angle. Figure 2.3.4. shows the distribution of photons scattered between θ and $\theta+d\theta$. This will give information about the number of photons scattered at an angle θ. Figure 2.3.4. shows that the most probable angle of scattering decreases with increasing energy (see also table 2.3.1).

Table 2.3.1. *Most probable angle of Compton scattering versus incident γ-ray energy*

E_γ (MeV)	θ	E_γ (MeV)	θ
0.5	35°	2.0	25°
1.0	30°	5.0	17°

The average range of photons in Ge for hν = 1 MeV is ≈ 30 mm [Sch92a], while the range of 1 MeV electrons is only ≈ 0.7 mm [Eva67]. Most electrons will be stopped in the Ge, so the BGO-veto shield will mainly absorb photons. From figure 2.3.4 can be concluded that most veto-material is needed at the front and at the sides of the Ge-crystal (the front of the Ge-crystal is the incident γ-ray direction: see figure 2.3.3. and 2.3.4). Moreover, for high energetic scattered photons (equation 2.3.2) more BGO is needed to get the same attenuation (equation 2.3.9).

The third interaction mechanism is pair production, where the incident photon creates an electron-positron pair. The photon disappears in this process. This process can only occur if hν is greater than $2m_0c^2$ (= 1.022 MeV). The energy balance of this mechanism is given in equation 2.3.4:

$$h\nu = T_+ + (m_0c^2)_+ + T_- + (m_0c^2)_- \qquad (2.3.4)$$

with: hν = incident photon energy
T_+ = kinetic energy of the positron.
T_- = kinetic energy of the electron.
$(m_0c^2)_+$ = rest mass energy positron = 511 keV.
$(m_0c^2)_-$ = rest mass energy electron = 511 keV.

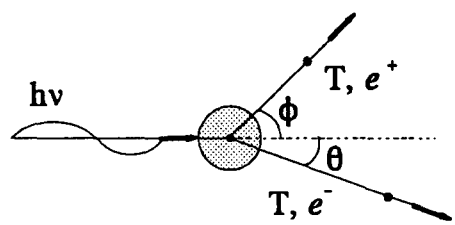

Figure 2.3.5. *Pair-production.*

Linear momentum and energy must be conserved, so this mechanism can only occur in the presence of an atomic nucleus (the recoil energy given to the atom can be neglected).

The relative importance of the above mechanisms depends on the energy of the incident photons and the atomic number (Z) of the absorbing material (Ge, BGO). The region of dominance of each process can be seen in figure 2.3.6.

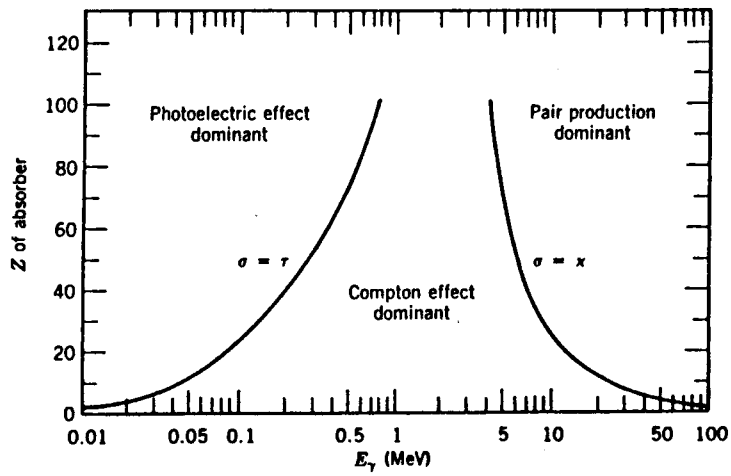

Figure 2.3.6. *The three electromagnetic interaction processes and their regions of dominance.*

The positron will annihilate with an (atomic) electron. It will mostly annihilate when it has virtually no kinetic energy left [Hei57], creating two photons of energy m_0c^2 (= 511 keV) (if the positron still carried some kinetic energy, this energy is distributed to the both photons) (see figure 2.3.7). Naturally, conservation of energy holds (formula 2.3.5):

$$T_+ + (m_0c^2)_+ + (m_0c^2)_- = h\nu_1 + h\nu_2 \qquad (2.3.5)$$

with: $h\nu_1$ = energy first photon.
$h\nu_2$ = energy second photon.

The induced photons are likely to be emitted under an angle of $\theta = 180°$, if the positron has no kinetic energy left [Hei57].

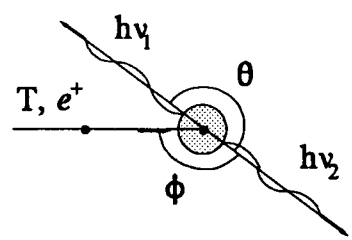

Figure 2.3.7. *Annihilation.*

Finally, the last interaction of importance, bremsstrahlung, occurs when an electron or positron is deflected. The most probable direction of the produced photon is perpendicular to the plane of motion of the electron or positron [Hei57] (see figure 2.3.8).

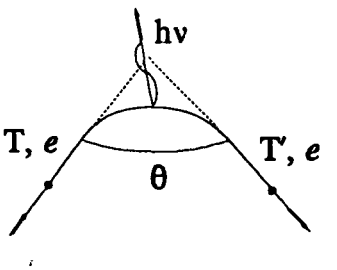

Figure 2.3.8. *Bremsstrahlung.*

For each physical process that can take place, the cross section is calculated by Geant. The cross-sections used are found in [Bru87]. The total cross section for the 5 processes taken into account is given by (equation 2.3.6):

$$\Phi = \Phi_\kappa + \Phi_\sigma + \Phi_\tau + \Phi_a + \Phi_b \qquad (2.3.6)$$

with:
- Φ = total cross section per atom.
- Φ_κ = photo-electrical cross section.
- Φ_σ = Compton scattering cross section.
- Φ_τ = pair-production cross section.
- Φ_b = bremsstrahlung cross section.
- Φ_a = annihilation cross section.

A (pseudo)random number generator is used to decide which interaction will take place. The macroscopic cross-section Σ {cm^{-1}} (also known as linear attenuation coefficient) is related with the total cross section per atom by equation 2.3.7.

$$\Sigma = \frac{N \rho \sum_i p_i \Phi(Z_i, E_\gamma)}{\sum_i p_i A_i} \qquad (2.3.7)$$

with:
- N = Avogadro's number. {mol^{-1}}
- Z_i = atomic number of the i^{th} component of the material.
- A_i = atomic weight of the i^{th} component of the material. {g mol^{-1}}
- ρ = density of the material. {g cm^{-3}}
- Φ = total cross section per atom. {cm^2}
- p_i = proportion by number of the i^{th} element in the material.

The mean free path, λ {cm}, is simply the reciprocal of the macroscopic cross-section Σ (equation 2.3.8).

$$\lambda = \frac{1}{\Sigma} \qquad (2.3.8)$$

The mean free path of Ge respectively BGO versus incident γ-ray energy are shown in

figure 2.3.9 [Scho92a]. The chance that a particle will interact in a piece of material is given by equation 2.3.9.

$$P(x) = 1 - \exp\left(-\frac{x}{\lambda}\right) \qquad (2.3.9)$$

with: P(x) = chance of interaction with the material.
x = thickness of the material {cm}.

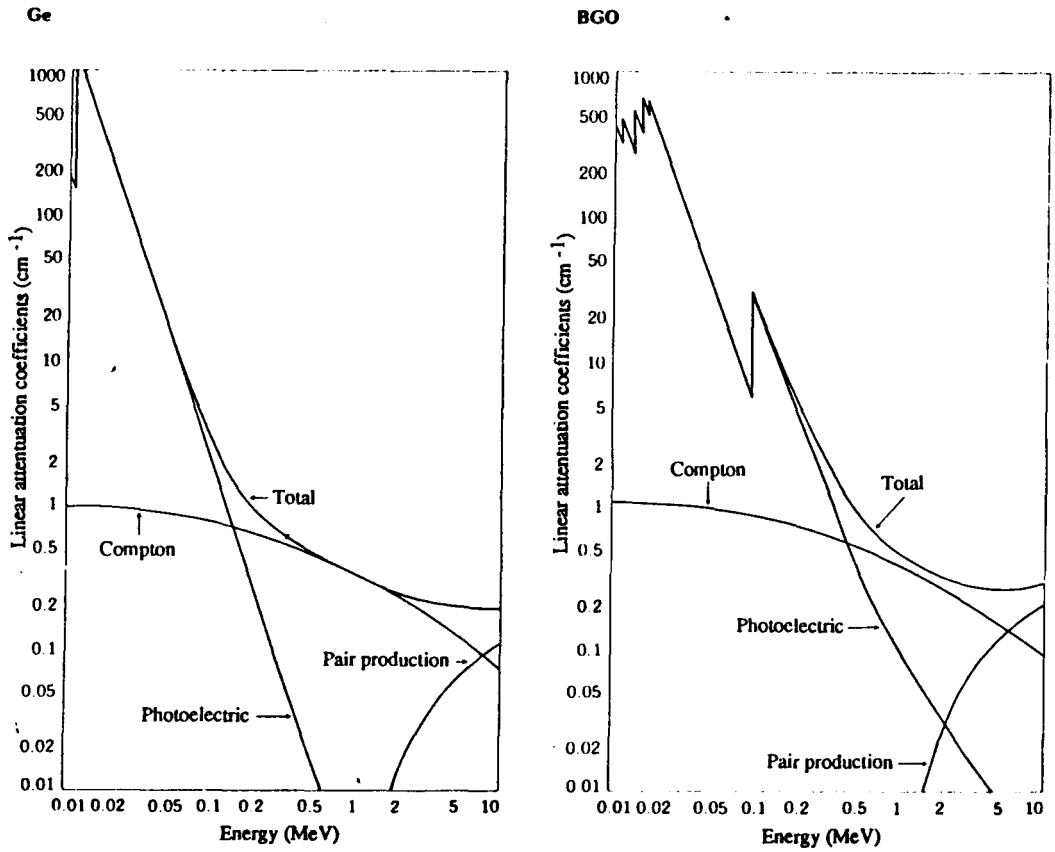

Figure 2.3.9. *The linear attenuation coefficients of Ge (left) and BGO (right).*

§ 2.4 Results obtained with Geant

§§ 2.4.1 Geometrical restrictions

The Monte Carlo calculations used should help us in optimizing the shape of the veto shield in order to get a Peak to Total ratio as high as possible. Of course, there are some restrictions. First the size of the BGO is restricted to an upper limit. Manufacturers (i.e.

Quartz & Silice in our case) are not able to grow BGO crystals with diameter > 106 mm∅ and length (l) > 250 mm. Another restriction is the light-transport through the BGO. The BGO should be tapered, in order to get a light yield as high as possible (See chapter 3). [Ver91] concluded, that material between Ge and BGO should be reduced, in order to get a higher Peak to Total ratio. For this reason there is no material between Ge and BGO. A fourth restriction is of economical nature. Since BGO is quite expensive, we should restrict the amount of BGO as much as possible.

In §§ 2.4.2 we describe the test of the Geant program by comparing our calculations with results using EGS. Optimizing the BGO-shape is discussed in §§ 2.4.3. Finally, using the information acquired in §§ 2.4.3 and Chapter 3 we choose the dimensions of a Ge- and BGO-crystal. Results for these crystals are discussed in more detail in §§ 2.4.4.

§§ 2.4.2 Comparing results obtained by EGS and Geant

To compare the EGS and Geant software packages we repeated the calculations [Ver91] did, but now using Geant. Verhoef investigated the influence of wall- and bottom-thickness of the BGO-suppressor (See figure 2.4.2.1) by varying the bottom-thickness (1 cm ≤ B ≤ 7 cm) while keeping the wall-thickness fixed (W = 2 cm) and varying the wall-thickness (1 cm ≤ W ≤ 5 cm) while keeping the bottom-thickness fixed (B = 4 cm).

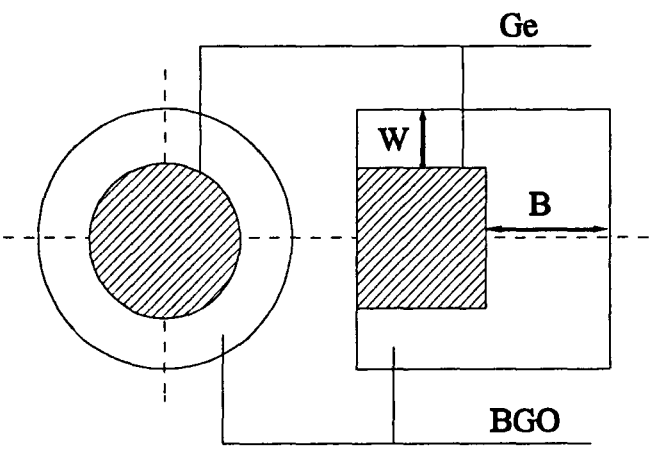

Figure 2.4.2.1. *Setup calculations.*

We repeated these calculations with Geant for an incident γ-energy of E_γ = 662 keV. Comparison of the results [Ver91] with our calculations can be seen in figure 2.4.2.2. We agree with the statement made in [Ver91], that the hollow core of the Ge-detector has minor effects on the Peak to Total ratio. We calculated a decrease of the Peak to Total ratio of 0.9 % for a 1.33 MeV and 1.8 % for a 3.0 MeV incident photon energy compared to a Ge detector without a core hole. We calculated a Peak to Total ratio of 20 % for a bare Ge crystal of ∅ = 50 mm and l = 50 mm, with an incident photon-energy of 1.33 MeV. This is also found experimentally [Ver92]. In contrast with the Geant results [Ver91] calculated

a Peak to Total ratio of 30% for a bare Ge crystal. For suppressed spectra the Geant simulations give Peak to Total ratios which are 1-5 % below those calculated with E.G.S. (See figure 2.4.2.2).

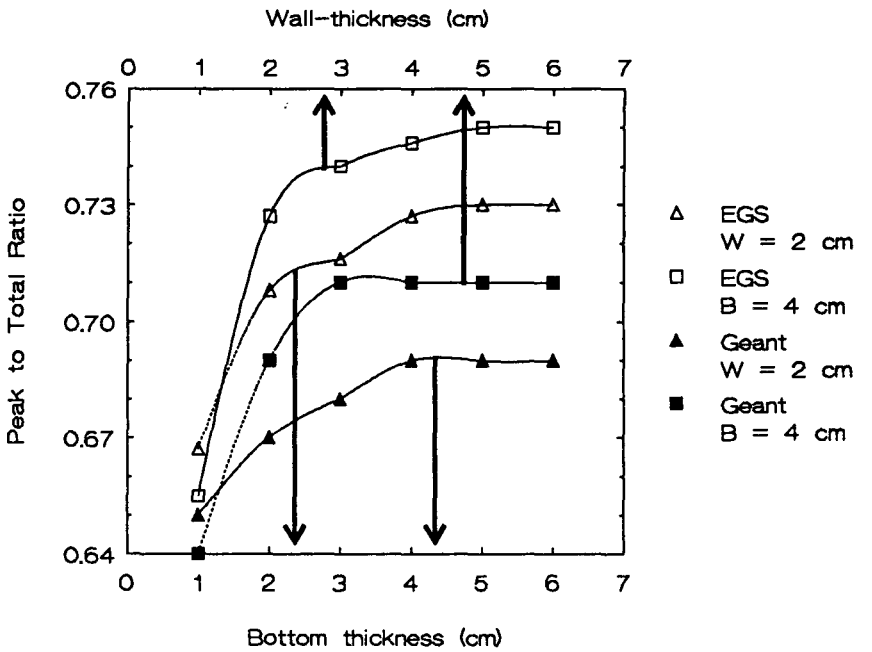

Figure 2.4.2.2. *Comparison of the Peak to Total ratios calculated with EGS and Geant (incident γ-ray energy: E_γ = 662 keV).*

§§ 2.4.3 Optimizing the BGO-crystal shape

In the previous section, the Peak to Total ratio of different Ge-BGO anti-Compton shields was calculated. These Compton shields were tube shaped and had no nose BGO. The simulations discussed in this paragraph have a geometrically more complicated structure. The BGO is made of three pieces: (1) a main BGO (cone), (2) a back BGO (cylindrical) and (3) a nose BGO (cone). Inside the Ge there is a core hole (dimensions hole: diameter = 9 mm∅ and $\text{length}_{\text{hole}} = \text{length}_{\text{Ge}}$ - 15 mm). A setup used for the Monte Carlo simulations is shown in figure 2.4.3.1. The dimensions of the materials used for this setup are shown in table 2.4.3.1.

For all calculations only two restrictions concerning the BGO are made. The main BGO must be tapered in order to acquire a high light collection (See Chapter 3). Therefore the main-BGO is tapered by an angle of 2.0°. Secondly, it must have a wall-thickness of at least 20 mm. This requirement is borne out by figure 2.4.2.2 and figure 2.4.3.2. Figure 2.4.2.2 shows a rapid decrease of the Peak to Total for a wall-thickness less then 20 mm. Figure 2.4.3.2. shows the first interaction of photons versus position inside the BGO (radius (R) and depth (Z): see figure 2.4.3.1).

Table 2.4.3.1. *Setup dimensions used for the Monte Carlo simulations.*

Name	*Shape*	*length (mm)*	*outer radius (mm)*		*inner radius (mm)*	
			top	bottom	top	bottom
Ge	cylindrical	50	25	25	0	0
main-BGO	cone	110	45	53	25	25
back-BGO	cylindrical	50	25	25	0	0
nose-BGO	cone	20	30	45	20	25

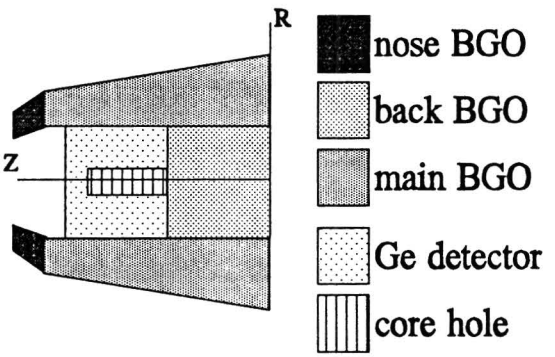

Figure 2.4.3.1. *Setup used for the Monte Carlo simulations.*

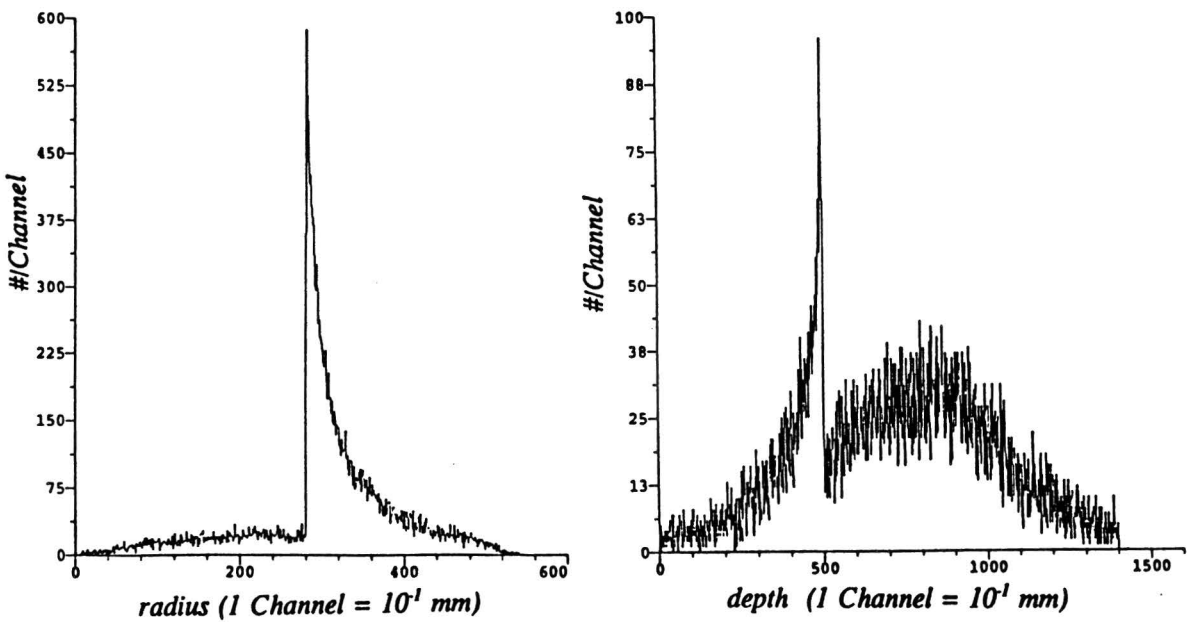

Figure 2.4.3.2. *First interaction of photons versus position inside the BGO; (left: interactions versus radius (R), right: interactions versus depth (Z)).*

The influence of the back-BGO length versus the Peak to Total ratio was tested (figure 2.4.3.3). Together with the results acquired in figure 2.4.2.2, one can conclude that a back-BGO length > 5 cm has minor effects on the Peak to Total ratio.

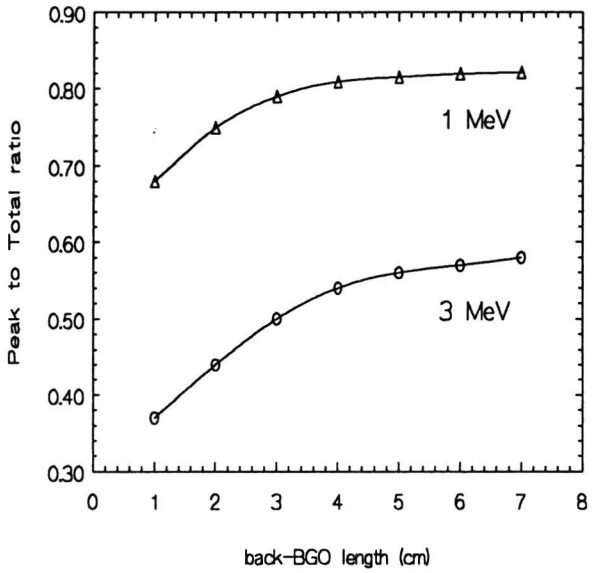

Figure 2.4.3.3. *Peak to Total ratio versus the back-BGO length; The radii of the different BGO pieces were kept constant at the values presented in Table 2.4.3.1.*

The Peak to Total ratio is calculated for three different Ge-detectors. For each detector five different BGO veto shields were tested (see figure 2.4.3.4. and table 2.4.3.2). So, totally 15 different setups were compared.

Table 2.4.3.2. *Dimensions of the different setups.*

Setup I			***Setup II***			***Setup III***		
nr	*lm (mm)*	*nose*	*nr*	*lm (mm)*	*nose*	*nr*	*lm (mm)*	*nose*
1	no suppression		1	no suppression		1	no suppression	
2	100	no	2	110	no	2	120	no
3	100	yes	3	110	yes	3	120	yes
4	110	yes	4	120	yes	4	130	yes
5	120	yes	5	130	yes	5	140	yes

with nr = number of the BGO-configuration.
lm = length of the main BGO.
nose = with (yes) or without (no) nose suppression.

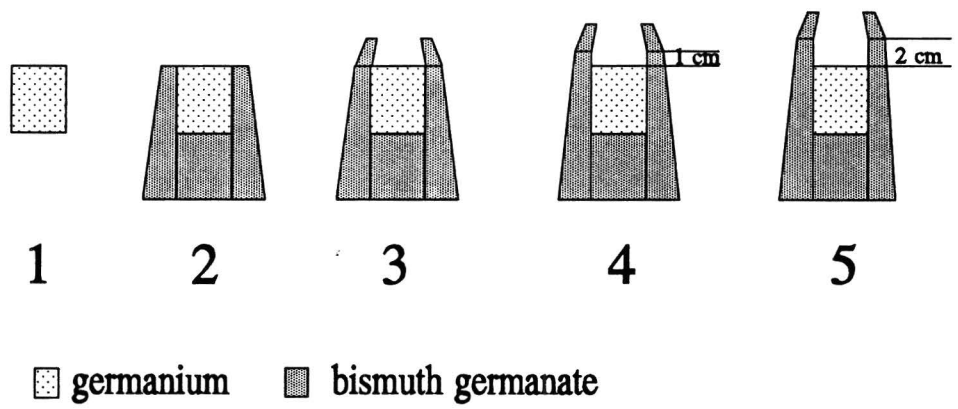

Figure 2.4.3.4. *Cross sections of the five simulated spectrometers*

For all setups the back-BGO had the dimensions 50 mm∅ x 50 mm (diameter x length) and the length of the main-BGO was adapted to the setup used, i.e. the length of the main-BGO was 10 mm and 20 mm longer for setup II respectively setup III compared to setup I. The radii of the different BGO-pieces were kept equal for all simulations (see table 2.4.3.1). If the nose-BGO was used for suppression its dimensions were equal to the nose BGO shown in figure 2.4.3.1. and its dimensions are given in table 2.4.3.1.

Results can be seen in figure 2.4.3.5. (Ge dimensions: 50 mm∅ x 50 mm (diameter x length)), figure 2.4.3.6. (Ge dimensions: 50 mm∅ x 60 mm) and figure 2.4.3.7. (Ge dimensions: 50 mm∅ x 70 mm).

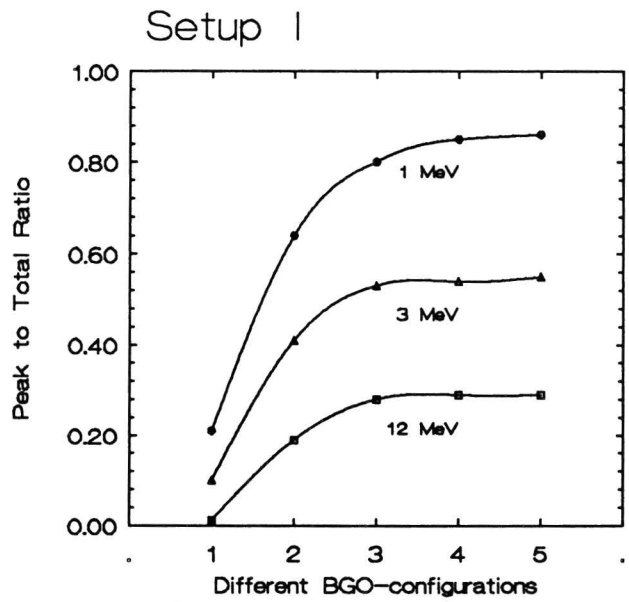

Figure 2.4.3.5. *Peak to Total ratio versus different setups, Ge dimensions: length = 50 mm; diameter = 50 mm∅.*

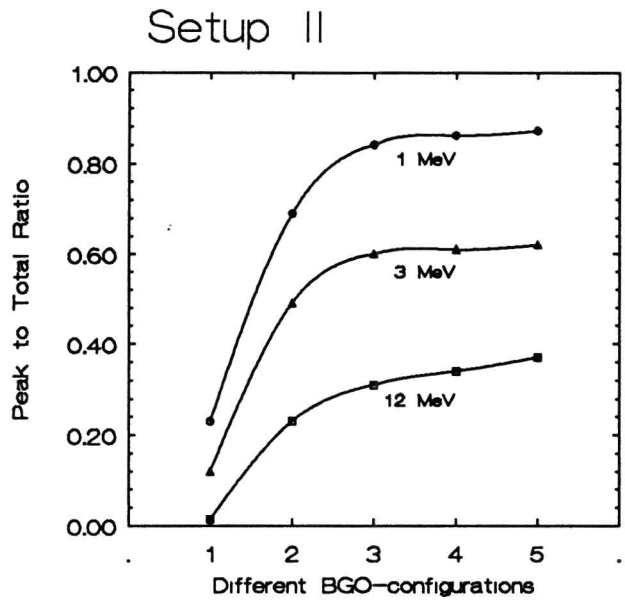

Figure 2.4.3.6. *Peak to Total ratio versus different setups, Ge dimensions: length = 60 mm; diameter = 50 mmØ.*

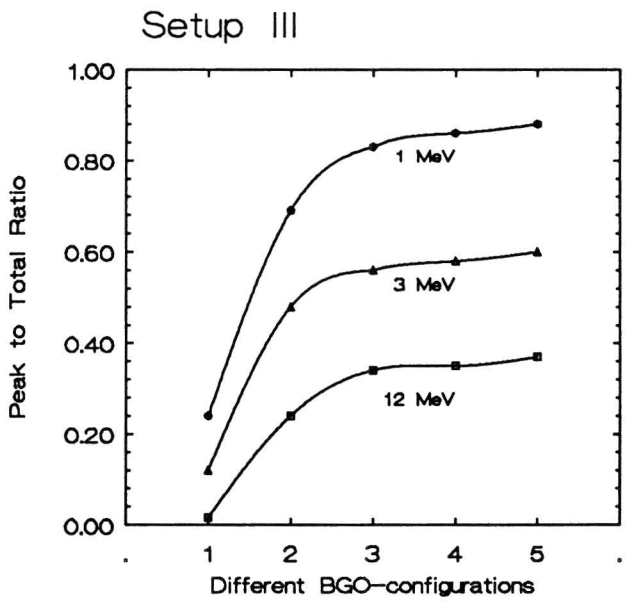

Figure 2.4.3.7. *Peak to Total ratio versus different setups, Ge dimensions: length = 70 mm; diameter = 50 mmØ.*

§§ 2.4.4 The final Ge-BGO configuration

The results shown in figure 2.4.3.4, figure 2.4.3.5. and figure 2.4.3.6. imply that even for high energetic photons (E_γ > 5 MeV) a Ge-crystal with a length > 60 mm will have minor effect for the Peak to Total ratio. Also, the wall-thickness of the BGO-crystal should be > 20 mm at the sides of the Ge-crystal (figure 2.4.2.2. and figure 2.4.3.2.). The radius of the main BGO should be as large as possible, i.e. diameter = 106 mm∅, in order to get a suppression as high as possible. The top (outer) radius should have a diameter which is 10 mm less than the bottom (outer) radius of the main-BGO (crystal should be tapered, angle ≥ 2°). This implies that a Ge-crystal with diameter = 56 mm∅ (= 106 - 10 -2*20 mm) can be used. Mechanical considerations require that the nose-BGO should have an inner diameter > 56 mm∅ (Ge outer radius). The old (Setup A) and new (Setup B) setup are shown in figure 2.4.4.1

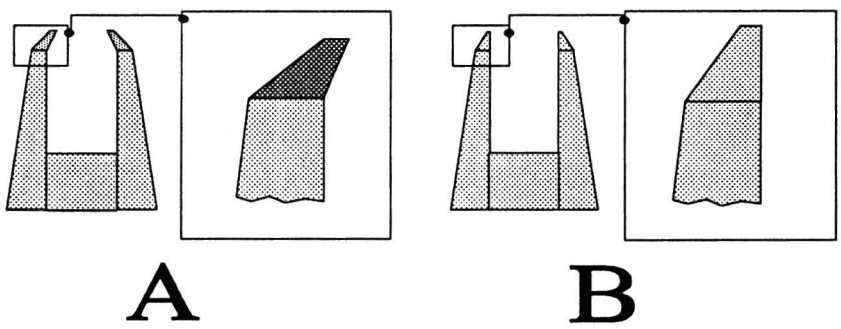

Figure 2.4.4.1. *Configuration of BGO-setups, left: Setup A (old); right: Setup B (new).*

A nose-BGO with an inner diameter < 56 mm∅ (Setup A) can be used, but then the nose-BGO will be a separate crystal. This will give an inferior light yield from the nose-BGO, since a light guide between the main-BGO and the nose-BGO should be applied. Therefore we prefer to have a crystal out of one piece (Setup B). This argument is supported by comparing the Peak to Total ratios for both setups (table 2.4.4.1): there is only a small decrease of the Peak to Total ratio with setup B).

Table 2.4.4.1. *Peak to Total ratio for the old $(P/T)_A$ and new $(P/T)_B$ setup.*

E_γ (MeV)	$(P/T)_A$	$(P/T)_B$
1	0.860	0.846
3	0.600	0.593
12	0.337	0.330

Because a veto-signal from the BGO can only be obtained if enough scintillation photons can be detected (see Chapter 3), the amount of energy deposited inside the BGO is of importance. Below a certain energy threshold no veto-signal is given. In figure 2.4.4.2. the Peak to Total ratio versus BGO-threshold is shown. Introducing a threshold energy for detection has minor effects on the Peak to Total ratio if $E_{threshold} < 100$ keV. Above this value the Peak to Total ratio will decrease rapidly. Fortunately, a BGO-threshold of 50 keV should be achievable, according to [Sch92b].

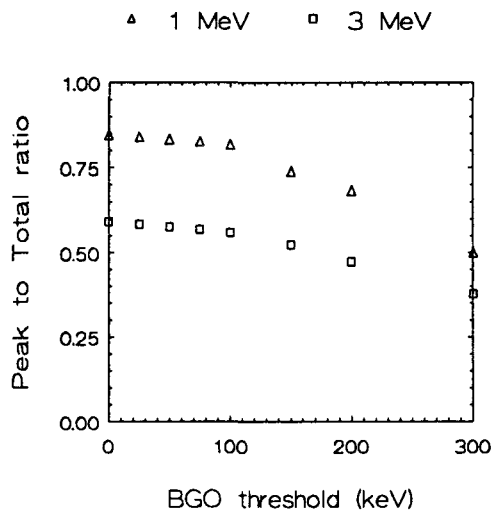

Figure 2.4.4.2. *Peak to Total ratio versus BGO-threshold.*

The Peak to Total for the new setup (Setup B) versus different incident energy can be seen in figure 2.4.4.3.

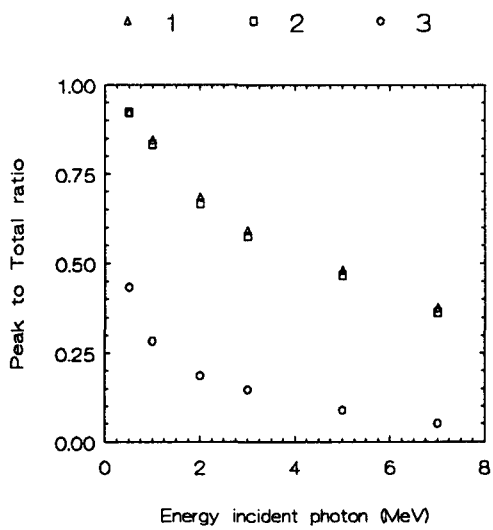

Figure 2.4.4.3. *Peak to Total ratio versus incident photon energy (1: no BGO threshold, 2: BGO threshold 50 keV, 3: no suppression).*

The simulated spectra (suppressed and unsuppressed) of a 1 MeV source are shown in figure 2.4.4.4. In Appendix B all nine parameters (the 2 parameters shown in figure 2.4.4.4. and seven more) obtained by the program are plotted. As expected, near the Compton edge the suppression will be inferior. These are γ-rays which are back-scattered and simply escape, because there is no suppression material at the front window of the Ge- detector.

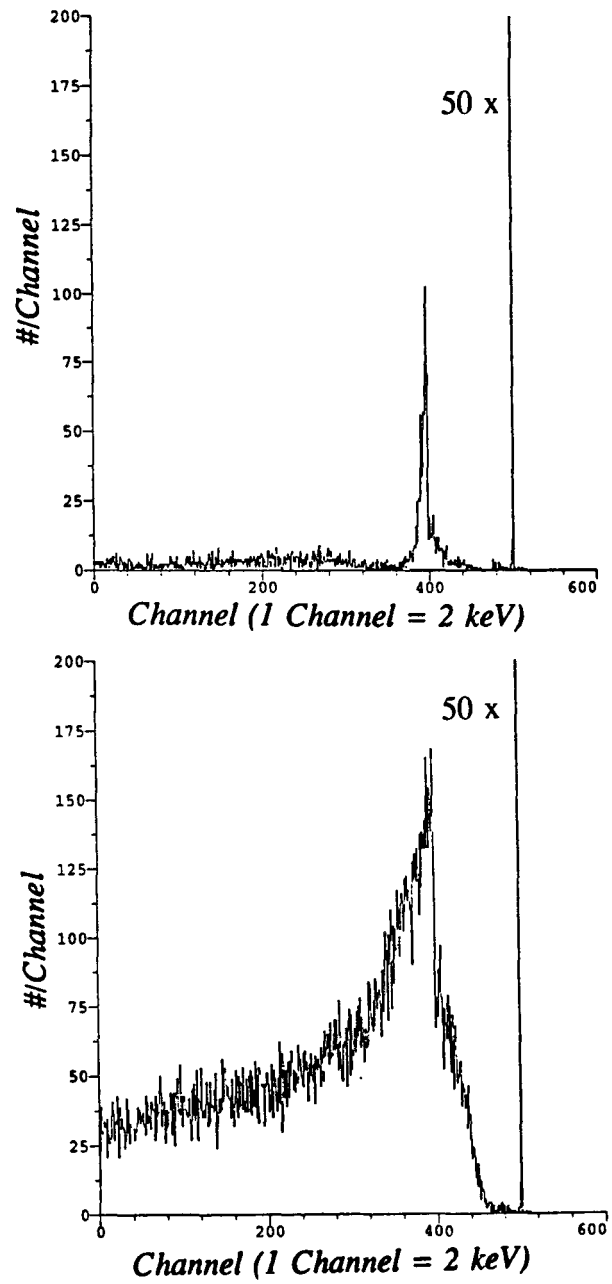

Figure 2.4.4.4. *Simulated spectra of an incident photon: E_γ = 1 MeV: top suppressed spectrum, bottom unsuppressed spectrum.*

§ 2.5 Discussion and conclusions

The Peak to Total ratios are acquired for a simplified geometrical structure. First, the radiation source was a massless, monochromatic point source, which only emitted γ-rays into the part of space occupied by the Ge-crystal. Thus, the effect of photons scattered off material other than the suppressor was not taken into account. Our simulated setup did not consider a collimator in front of the detector. With the collimator more scattered) γ-rays are produced, but it reduces the number of γ-rays directly irradiating the BGO crystal. To reduce the scattering of γ-rays at the collimator we shaped the collimator in a special way (Appendix A).

[Bax92] made the same geometrical simplifications, when calculating the Peak to Total ratio. They report discrepancies of 15% between experimental and calculated results in Peak to Total ratio and introduce a correction factor for this discrepancy (equation 2.5.1).

$$\frac{1}{(P/T)_{est}} = \frac{1}{(P/T)_{cal}} + \frac{b}{P} \qquad (2.5.1)$$

with: $(P/T)_{est}$ = "estimated" experimentally acquired Peak to Total ratio.
$(P/T)_{cal}$ = simulated Peak to Total ratio.
b/P = scattered background.

For the suppressed spectra b/P has a value of 0.22 for the geometrical setup used by [Bax92]. In table 2.5.1. the Peak to Total ratio estimated by equation 2.5.1. and the simulated Peak to Total ratio is presented for different γ-ray energies. In order to calculate the estimated Peak to Total ratio, we used b/P = 0.22.

Table 2.5.1. *The estimated and simulated Peak to Total ratios for different γ-ray energies.*

E_γ (MeV)	$(P/T)_{cal}$	$(P/T)_{est}$
0.551	0.93	0.77
1.00	0.85	0.72
1.33	0.77	0.66
3.00	0.59	0.52

However, we expect a higher $(P/T)_{est}$ then presented in table 2.5.1, because:
(1) we do not have any material (metal) between the Ge and the BGO;
(2) for the Peak to Total ratios reported by [Bax92] only energies depositions above 100 keV are taken into account, while we determined the Peak to Total ratio for the complete spectrum (all energy depositions in the Ge detector, including the 0 keV ≤ E_γ ≤ 100 keV region).

Since the Peak to Total ratios presented in table 2.5.1. already exceed the results of [Bax92] we may be able to achieve also in practice the highest Peak to Total ratio

reported until now (1993).

Since a 50 keV threshold for the BGO was used, the minimum energy deposited in the BGO necessary for detection of the veto-signal was already taken into account. By simulation we found that the Peak to Total ratio hardly differs for $E_{threshold} < 100$ keV. Similar results are reported by [Byr85]. Experimentally, however [Hil86] found that the suppression significantly decreases if the threshold energy was increased from 15 keV to 30 keV. This could mostly be a result of γ-rays which are Compton scattered in the material situated between Ge and BGO, which means that we should have less difficulties with this problem. However, a more detailed discussion of the minimum detectable energy deposition of the cooled BGO in order to acquire a veto signal is found in Chapter 3.

The Peak to Total ratio could be improved by using an active collimator (e.g. BGO) instead of a passive collimator (e.g. lead). Disadvantage is that the acceptable count rate of the spectrometer will drop. Moreover, this could be a problem since the acceptable count rate for cooled BGO is lower than for BGO at room temperature (at room temperature the count rate could be as high as 10^6 (when a passive collimator is used), while if the crystal is cooled it would be 10^5).

Chapter 3

Collection of the light in BGO-crystals

§ 3.1 Use of bismuth germanate as a veto shield

Recently, a large influence of Ge-BGO Compton suppression spectrometers in experimental arrangements in nuclear spectroscopy can be observed. The high attenuation of BGO for γ-rays allows the building of anti-Compton spectrometers with a small external diameter. We developed a Ge-BGO Compton suppression spectrometer that also fits in the Eurogam project [Bea92].

A problem with the used or proposed configuration of BGO suppression shields is to achieve the rejection factor based on the attenuation of BGO. Present calculations suggest higher suppression factors than acquired by experiments [Bax92,Bea92, Hil86]. Very seldom however, it is considered that the detection efficiency not only depends on the attenuation of the scintillator, but also on the fact that the energy deposition of the γ-quantum should result in a proper electrical pulse at the output of a photomultiplier or a photodiode. This was not a major problem for NaI(Tl) Compton suppression shields because of the high light output of this type of crystal. However, the light output of a BGO crystal only amounts to 7-15 % of that of a NaI(Tl) crystal [Tak81,Hol88], depending on the crystal quality of the BGO. Since the BGO is only used to acquire a veto signal, often crystals of minor quality are used (crystals of minor quality are yellowish and contain layers of voids [Kob84,Gra84,Unr84]), which results in an inferior photon collection.

In the past, several people have investigated the light collection efficiency from scintillation crystals [Hil89,Lun88,Car90a,Ish86]. Mostly Monte Carlo simulations have been used to study the light transport in scintillators [Der81,Der82,Car90b]. This approach records the fate of individual scintillation photons after following them in every physical process in which they are involved. We use a Monte Carlo simulation program, named LGUIDE [Mic92a], to determine the light output of scintillation crystals. This program is used to simulate the influence of the geometry of the crystal as well as the influence of different surface treatments on the light yield.

In this chapter we discuss the light collection in scintillators in general and bismuth germanate in particular. In § 3.2 the physical description of light transport inside scintillators is presented. The advantages of the program LGUIDE with respect to the program used by [Ver91] are discussed in § 3.3. In § 3.4 we tested the Monte Carlo simulation program by comparing experimental and simulated results. For this purpose a long rectangular BGO crystal is used. Firstly, we measured the light yield versus width of the air gap (between the scintillator and the photomultiplier tube). Secondly we examined the influence of the source position which irradiates the crystal. For the BGO crystal, which will serve as veto shield surrounding the Ge detector, we first optimized the light output (§ 3.5). This is done by comparison of the photon collection for different surface treatments of the crystal. Secondly, the influence of crystal quality is simulated by varying the attenuation length of the scintillation photons. Finally, the minimum energy needed in order to detect a veto signal is determined. The chapter is concluded with is a short discussion and some recommendations (§ 3.6).

§ 3.2 Theory of light transport

In order to get a light yield as high as possible the surfaces of the scintillation crystal need to be treated. Firstly, light impinging on the read-out surface should be transmitted to the photomultiplier tube or photodiode. Secondly, the other surfaces should have a reflectivity as high as possible, so that the photon impinging on a non read-out surface still can be detected after one or more reflections. Therefore non read-out surfaces are covered with reflector materials, which should increase the light yield by reflecting photons which are transmitted through the crystal surface via the reflection material back into the crystal.

Surfaces can either be polished or rough. Crystal surfaces which are rough (diffuse) can only be applied to non read-out surfaces, because of their high reflectivity. Commonly, diffuse surfaces are covered with MgO, AlO or reflective tape. Reflection of an incident photon at a diffuse interface is shown in figure 3.2.1.

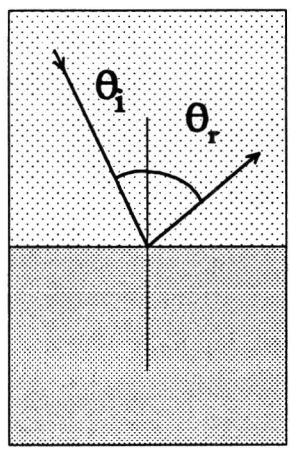

Figure 3.2.1. *Diffuse surface reflection.*

Reflection on diffuse reflectors is described by Lambert's law stating that the reflectivity is independent of the incident angle (see also figure 3.2.1) and that the angular distribution after reflection follows a cosine law per unit solid angle (equation 3.2.1).

$$\frac{I(\theta_r)}{I_0} = \cos\theta_r \qquad (3.2.1)$$

with: I_0 = incoming light intensity $\{W.m^{-2}.sr^{-1}\}$.
$I(\theta_r)$ = reflected light intensity at angle θ_r $\{W.m^{-2}.sr^{-1}\}$.
θ_r = reflection angle.

The reflectivity of a diffuse surface covered with reflective teflon tape amounts to $R = 0.97 \pm 0.01$ [Mic92d,Ver91,Car90a,Sch92a].

A specular or polished surface can either be a non read-out or a read-out surface. A read-out surface should have a transmissivity as high as possible, while a non read-out surface should

have a reflectivity as high as possible. The difference between the both surfaces is that the non read-out surface will be covered by reflector material. For both surfaces Snell's law describes the relation between incident, reflected and transmitted photons. Equation 3.2.2a. gives the relationship between incident and reflected photons, while equation 3.2.2b. gives the relationship between incident and transmitted photons.

$$\theta_i = \theta_r \tag{3.2.2a}$$

$$n_i \sin\theta_i = n_t \sin\theta_t \tag{3.2.2b}$$

with: n_i = refraction index valid for incident photon.
n_t = refraction index valid for transmitted photon.
θ_i = angle of incidence.
θ_t = angle of transmission.
θ_r = angle of reflection.

The angle of reflection as well as the angle of transmission are dependent on the angle of incidence. For incident photon angles greater than the critical angle total internal reflection occurs (see figure 3.2.2). The critical angle θ_c can be calculated using formula 3.2.3.

$$\theta_c = \arcsin\left(\frac{n_t}{n_i}\right) \tag{3.2.3}$$

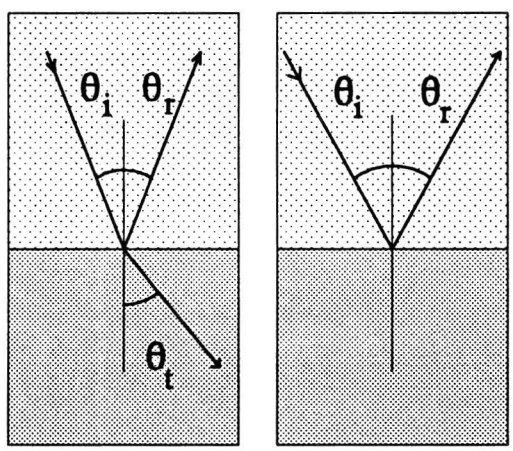

Figure 3.2.2. *Specular reflection, left:* $\theta_i < \theta_c$ *(part of the photons is reflected, part is transmitted); right:* $\theta_i > \theta_c$ *(total internal reflection).*

The reflectivity (R) at an interface can be calculated if the angle of incidence and both refraction indices are known (equation 3.2.4)[Hec87,Bor70]. Photons can either be absorbed, reflected or transmitted. Absorption of photons at the read-out surface is negligible, so the transmission (T) is given by formula 3.2.5.

$$R = \frac{1}{2}\left[\frac{\tan^2(\theta_i - \theta_t)}{\tan^2(\theta_i + \theta_t)} + \frac{\sin^2(\theta_i - \theta_t)}{\sin^2(\theta_i + \theta_t)}\right] \qquad (3.2.4)$$

$$T = 1 - R \qquad (3.2.5)$$

The transmission at the read-out surface should be as high as possible. Therefore it is desirable to have a light guide material, which couples the scintillator to the read-out device. The light guide material should have a refraction index n_{lg} between the refraction index of the scintillator material and that of the photodiode or photomultiplier tube. In our setup BGO is used as a scintillatoion crystal and a PMT as detection device. Since $n_{BGO} = 2.15$ and $n_{PMT} = 1.6$ the light guide material (normally coupling grease) should have a refraction index of $1.6 \leq n_{lg} \leq 2.15$. However, in our setup the BGO is cooled and in vacuum (air: pressure 10^{-5}-10^{-6} mbar), so application of a light guide material is not possible. Instead we will employ an air (vacuum) gap ($n_{air} = 1.0$) between the scintillation crystal and the PMT. In figure 3.2.3. the reflectivity at a BGO-air interface is compared with the reflectivity at a BGO-coupling grease ($n_{grease} = 1.5$) interface for various angles of incidence. Note that the reflectivity becomes unity for $\theta_i > \theta_c$.

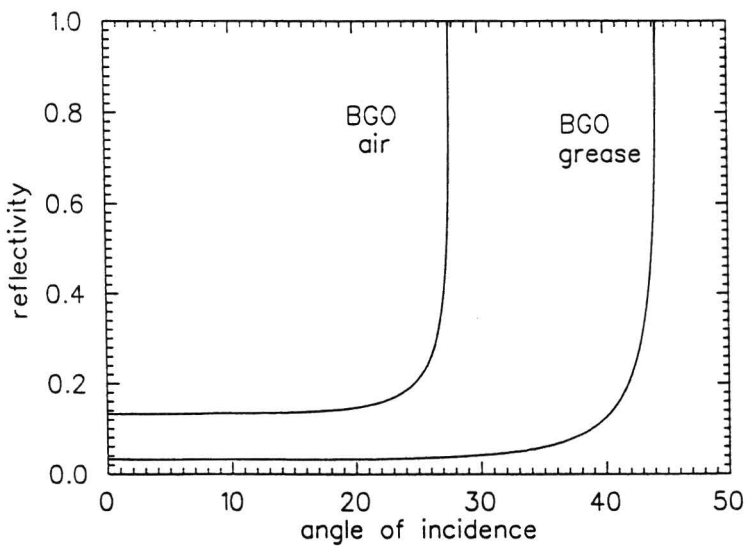

Figure 3.2.3. *Reflectivity versus angle of incidence for a BGO-air and a BGO-grease interface.*

In order to keep the cryostat vacuum tight, a quartz (glass) window is situated between the BGO and the photomuliplier tube (see figure 3.2.4). The probability that a photon which reaches the BGO read-out surface is transmitted to the photomultiplier is deduced in Appendix C. The transmission probability of a photon as a function of its angle of incidence on the BGO read-out surface is shown in figure 3.2.5. and compared to the transmission

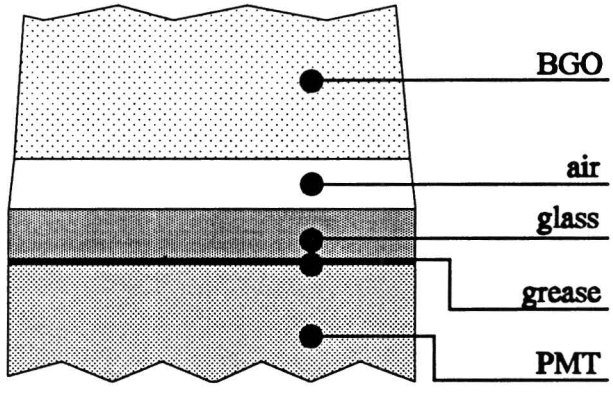

Figure 3.2.4. *Read-out of scintillation photons.*

possibility of a photon impinging on the BGO read-out surface, but now only transmission of a BGO-air-PMT interface is considered. Figure 3.2.5. points out that the application of a glass window and coupling grease will not result in a major light yield reduction.

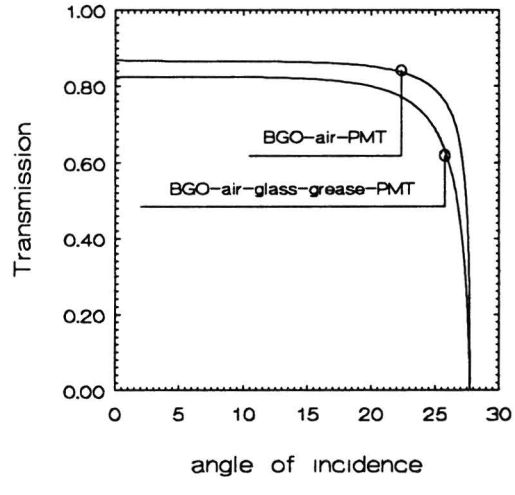

Figure 3.2.5. *Transmission of scintillation photons versus angle of incidence on the BGO read-out surface.*

Self absorption in the BGO crystal also causes a decrease of the light yield. The probability of a scintillation photon to be absorbed inside the crystal is given by equation 3.2.6.

$$P(L) = 1 - \exp\left(-\frac{\lambda}{L}\right) \qquad (3.2.6)$$

with: P(L) = chance of absorption for a distance L.
L = distance traversed by a photon through the crystal {mm}.
λ = attenuation length {mm}.

For high quality BGO crystals the attenuation length amounts to: $\lambda = \approx 300$ mm [Mic92d]. Crystals of lower quality will have an attenuation length of: 150 mm $\leq \lambda \leq$ 250 mm [Mic92d]. For large crystals absorption of photons inside the crystal can cause a major reduction of the light yield.

The influence of polarisation of the scintillation photons was tested by simulation. The induced photons are simulated to be emitted in a random direction with a random polarisation. Transmissivity and reflectivity differ for photons with different polarisation [Hec87,Bor70], but the influence of polarisation is found negligible for the light output of scintillation crystals. Similar results were found by [Ver91,Car90a].

§ 3.3 The Monte Carlo simulation program

To determine the light output of a scintillation crystal, a Monte Carlo simulation program, named LGUIDE [Mic92a], is used. The irradiation of the scintillator is simulated by generation of randomly chosen point sources within the crystal volume. The point sources will emit photons isotropically. By keeping the number of photons from each point source equal, the light yield acquired from different positions inside the crystal can be calculated. The light yield will vary with position due to optical self absorption, absorption at a non read-out surface and losses at the read-out surface (see § 3.2).

A more detailed description of the program, including flow chart, can be found in [Ver91]. The program we use nowadays, LGUIDE, is more advanced. Advantages of LGUIDE with respect to the program used by [Ver91] are:

(1) Besides the crystal volume, also the shape of the light guide can be included.

(2) One or more detection devices can be simulated. Although, at present it is not yet possible to include different detection devices (photomultipliers and photodiodes) for one crystal geometry.

(3) The program now has the possibility not only to simulate diffuse, but also specular surfaces. Even the light yield of crystals with diffuse as well as specular surfaces can be calculated.

(4) The normalisation factor, due to the conversion of γ-ray energy into scintillation photons and the transparency of the coupling grease, present in the old program [Ver91], has been removed. Present calculations give the percentage of scintillation photons detected, instead of the energy deposited in the detection device.

(5) The program is more convenient in use. Crystal shapes can be seen on a monitor, and adapted to one's needs by using a mouse. After a program run, shape and results can be seen simultaneously in different windows on the monitor.

(6) From the program a geometrical more advanced program EURO[1] [Mic92b] is deduced. With the program EURO we can simulate all shapes, while with the program LGUIDE only cylindrically symmetric shapes can be simulated. Physical parameters are equal to the LGUIDE program. Disadvantage of the program EURO is that crystal

[1] The program EURO is specially written to determine the light collection of the BGO crystals used in the cluster structure of the EUROBALL-project.

shapes can not be visualized.

(7) The program LGUIDE as well as the program EURO can be operated in a MS-WINDOWS environment. This enables us to "run" more applications at once.

The program LGUIDE gives us the possibility to optimize the light output by varying crystal shape as well as surface treatments. Results acquired using the program are discussed in the next sections and compared with experimental results.

§ 3.4 The rectangular BGO crystal

In order to investigate the decrease of the light yield when an air gap between the photomultiplier and the BGO crystal is applied, a test experiment is built (see figure 3.4.1). The scintillation crystal is a long rectangular BGO crystal, read out by a photomultiplier tube.

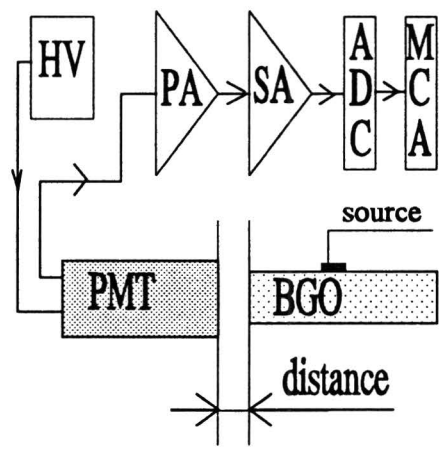

Figure 3.4.1. *Test setup to determine the influence of the width of an air gap between BGO and PMT on the light yield.*

BGO	bismuth germanate crystal (lxbxh: 120x19x18 mm^3)
PMT	Hamamatsu photomultiplier tube R434
PA	Ortec VT120 preamplifier
SA	Canberra 2020 spectroscopy amplifier
ADC	Canberra 8075 analog digital converter
MCA	Canberra S100 multi channel analyzer cartridge
HV	Ortec 456 high voltage power supply

To induce scintillation photons inside the BGO, we used a ^{137}Cs γ-ray source (E_γ = 662 keV), which was attached at the middle of the crystal. Directly or via one or more reflections the photons can reach the read-out surface, where a certain fraction of the photons will be transmitted to the PMT. The signal of the PMT is amplified and fed to an ADC. The digital signal coming from the ADC is connected to a MCA, which generates spectra.

Firstly, we investigated the reduction of the light yield if an air gap is introduced instead of a coupling grease. Comparison gives experimentally a yield reduction of 66% in case of an air gap, while simulations predict a decrease of 71%. The discrepancy between experiment and simulation can be a consequence of the fact that the refraction index of the coupling grease is not exactly known (variation in refraction index amounts to $1.4 \leq n_g \leq 1.6$ [Sch92b, Car90a,Mic92d]).

Secondly, we varied the distance between BGO and PMT (without the application of a coupling grease). We expect a light yield reduction if the distance between scintillator and photomultiplier is increased. Results can be seen in figure 3.4.2, where experimental results as well as results obtained using the Monte-Carlo simulation program are shown. Calculated and experimental results are in agreement.

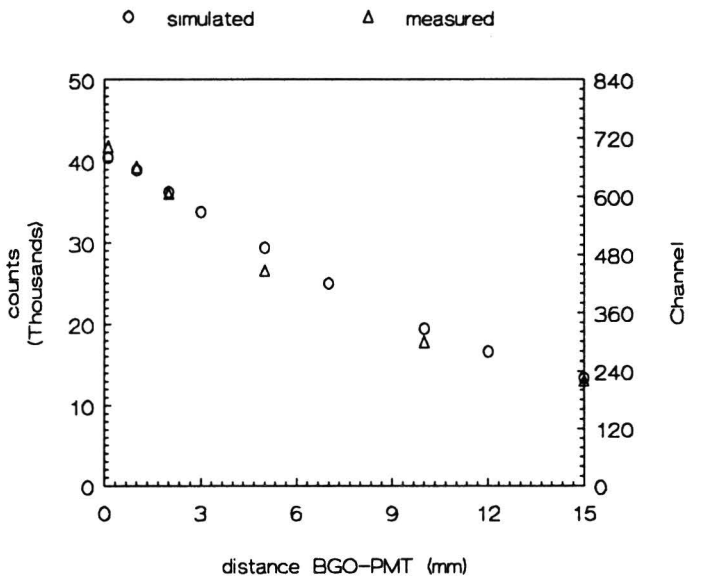

Figure 3.4.2. *Light yield versus PMT-BGO distance; left axis: the number of photons detected according to the simulations; right axis: the channel number of the peak in the measured spectrum (proportional detected number of photons). In the calculations we induced 10^6 photons, so ≈ 4% of the light will reach the photomultiplier, if an air gap of 0.1 mm is present.*

The influence of the position of the γ-ray source irradiating the BGO is tested. The experimental setup is similar to the setup shown in figure 3.4.1, but now the position of the γ-ray source is varied, while the distance between PMT and BGO is kept constant. A perfect crystal should give a high light output which is equal for all source positions. However, absorption of photons inside the crystal or at surfaces is ineluctable. For a rectangular crystal we therefore expect a higher light output if the source position is closer to the photo multiplier tube. Monte Carlo simulations confirm this statement. However, experimentally obtained results do not agree (figure 3.4.3).

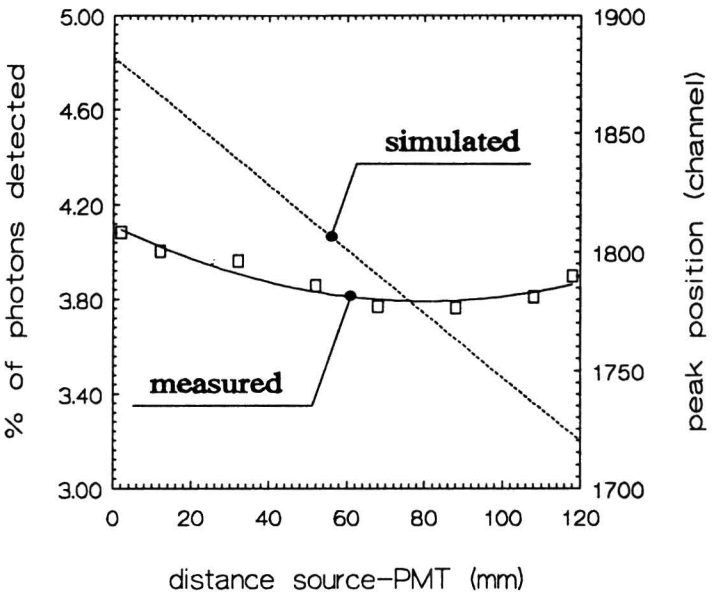

Figure 3.4.3. *Light yield versus source position; left axis: simulated results (percentage of photons collected); right axis: the measured peak position (channel).*

Several reasons could cause the disagreement between experiment and simulation.

(1) In the experiments we do not have a point source, like in the simulations. The γ-ray source was collimated to a diameter of 5 mm∅.

(2) A γ-ray which is Compton scattered within the crystal deposits its energy at different positions inside the crystal.

(3) Temperature could change during the experiments. At room temperature a temperature increase of 1 kelvin causes the light yield to drop ≈ 1% [Zuc89,Zha90,Lor84]. However, during the measurements temperature fluctuations larger than 1 kelvin did not occur.

(4) In the simulation we assume a reflectivity R = 0.97 and an attenuation length λ = 300 mm as "overall" properties of the crystal [Mic92d].

(5) Crystal properties vary with position in the crystal.

(6) The simulation program does not describe the transport of scintillation photons properly.

Argument (1) and (2) can explain why the experimentally acquired photon collection does not drop as quick as the simulated yield versus position inside the crystal. However, the experiments show an increasing yield if the source is positioned at the ends of the BGO crystal. The above reasons do not involve a physical explanation for this phenomenon. However, similar experimental results also performed with rectangular BGO crystals are acquired by [Man92b,Cur92].

The influence of the reflectivity at a surface as well as the attenuation length of scintillation photons on the light output is examined using the Monte Carlo simulation program. From figure 3.4.4. it can be seen that for the long rectangular crystal (120 x 18 x 19 mm^3) it is more important to have a good crystal than to have a high reflectivity. (A crystal with

R = 0.96 will have twice the amount of photons lost at surfaces compared to a crystal with R = 0.98, while the light yield only increases ≈ 3%. However, if the attenuation length is increased from 150 mm to 300 mm the light yield increases by ≈ 23%).

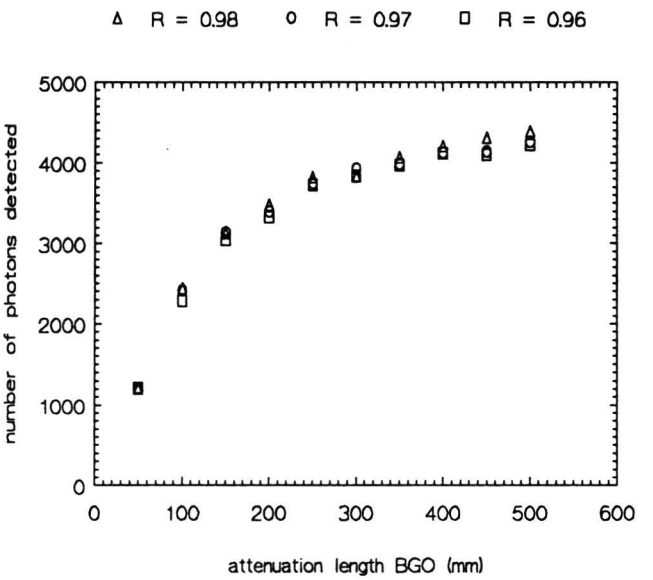

Figure 3.4.4. *The light output (percentage of photons detected) versus attenuation length for different reflectivities.*

We conclude that for long rectangular crystals with specular surfaces the attenuation length is of larger importance than the surface reflectivity. Similar results are reported by [Car90a, Mic92c].

§ 3.5 The BGO veto shield

This section is subdivided in four subsections. The first subsection comprises information concerning the light output coming from tapered crystals. In the second (§§ 3.5.2) we optimized the photon collection of the BGO veto shield by comparing the light output of the crystal for different surface treatments. The influence of crystal quality is determined in the third subsection. Finally, in §§ 3.5.4. we calculated the minimum energy deposition necessary to acquire a veto signal.

§§ 3.5.1 Tapered BGO crystals

In chapter 2 we already mentioned that the BGO veto shield was conically shaped, which provides a superior light output. This was already found by [Ver91,Hil86]. According to [Car90b,Der82,Mic92d] long crystals should have specular surfaces to provide a high light output. [Mic92c] showed that for long crystals with specular surfaces, conical shaping results in a higher light output (figure 3.5.1.1. and figure 3.5.1.2).

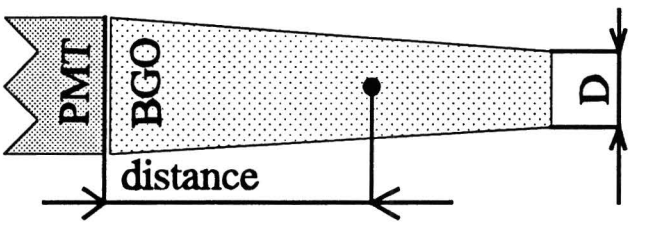

Figure 3.5.1.1. *Lay out of scintillation crystal and photomultiplier used in simulations by [Mic92c]. The dimensions of the BGO crystal are: length: 240 mm, diameter: back 20 mm, top D mm.*

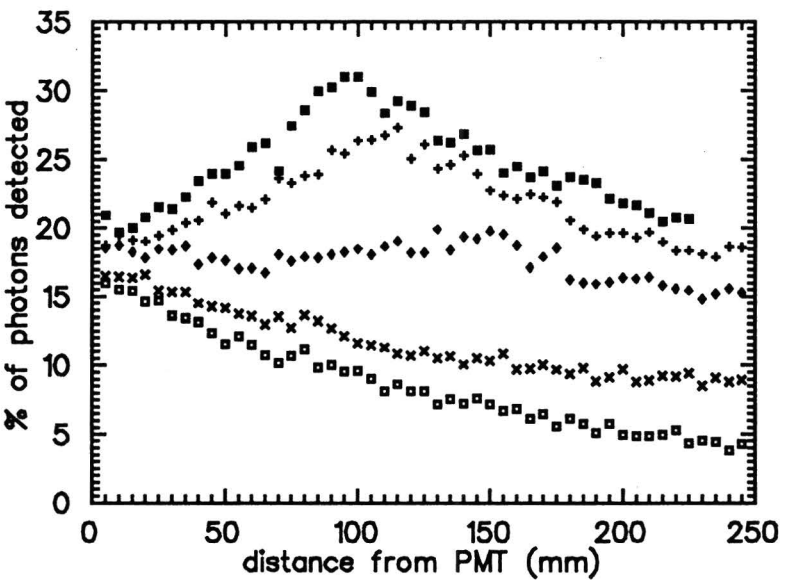

Figure 3.5.1.2. *The light yield versus distance simulated point source-PMT, for differently tapered BGO crystals [Mic92c]; ■: D = 4 mm, +: D = 6 mm, ◆: D = 10 mm, x: D = 16 mm, □: D = 20 mm. The simulations used an attenuation length of λ = 200 mm and a reflectivity of R = 0.9.*

For the heavily tapered crystal (D = 4 mm) a maximal light output occurs for a point source positioned at 100 mm distance from the PMT. Tapering results in an increasing light output for larger source PMT distances, because tapered crystals internally reflect the light towards the photomultiplier tubes. However, if the distance source-PMT becomes large compared to the attenuation length of the BGO crystal, losses occur due to optical self absorption. From figure 3.5.1.2. it can also be seen that appropriate tapering of crystals can result in a uniform light output (◆: D = 10 mm).

γ-rays which are back scattered are less energetic and induce less light. We therefore want

to acquire the highest light output coming from the top of the BGO crystal. From figure 3.5.1.2. one can conclude that tapering of the crystal will increase the light yield. However, the tapering angle is restricted by the maximal outer diameter of a bare BGO crystal (diameter $\leq$ 106 mm$\varnothing$) and the minimum BGO wall thickness ($d_w \geq 20$ mm) needed for sufficient suppression. Only BGO situated in front of the Ge detector, which should suppress γ-rays scattered backwards can have a wall thickness $d_w < 20$ mm. Since the Ge detector's dimensions amount to: length = 60 mm; diameter: 56 mm$\varnothing$; the Compton suppression shield's shape is restricted. Only the nose part (see also Chapter 2) can be adapted. Since we want to get a high light output from the top of the crystal (nose part) we tapered it heavily. This results in a BGO shape shown in figure 3.5.1.3. A more detailed drawing of the BGO Compton suppression shield can be found in Appendix A.

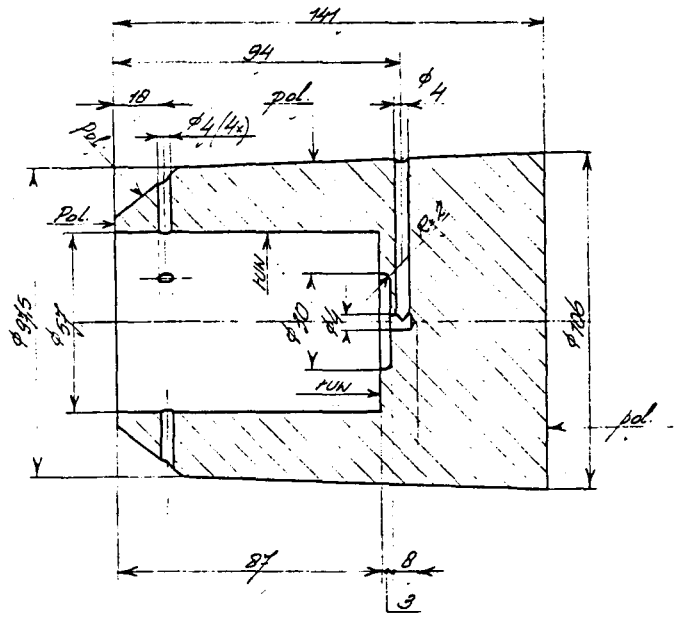

Figure 3.5.1.3. *Cross section of the BGO veto shield.*

§§ 3.5.2 Surface treatments

The influence of surface treatments on the light yield is simulated for the BGO veto shield. Firstly, we require a high "overall" photon light collection. Secondly, as mentioned before, we want to get the highest light output from the top of the crystal. The irradiation of the crystal is simulated by 1000 point sources, randomly distributed over the crystal volume. Each point source emits 1000 photons isotropically. The percentage of the detected photons is stored for each position of the point source. Three crystals with different surface treatments are compared. The percentage of detected photons is shown for different heights of the point source in the crystals in figure 3.5.2.1, which subsist different surface treatments. In table 3.5.2.1. the average percentage of detected photons is presented including its variance in yield, and provides good inside in the overall performance of the crystal.

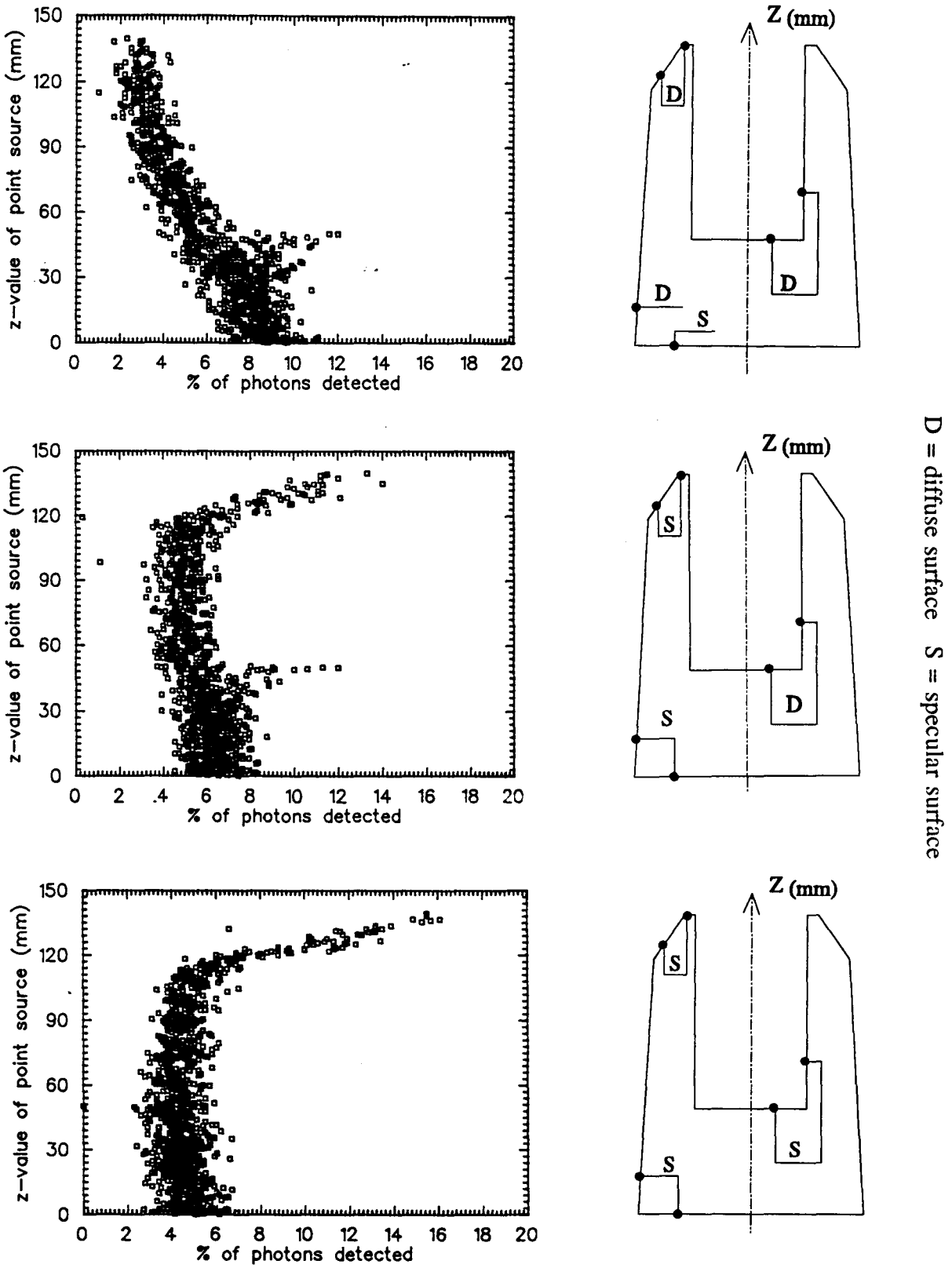

Figure 3.5.2.1. *Light yield for different surface treatments as indicated, left: percentage of photons detected versus height in BGO crystal, right: cross section of the BGO crystal (including surface treatments).*

Table 3.5.2.1. *Light collected for crystals with different surface treatments; Average percentage of photons collected (ε_Y).*

Surface treatment	ε_Y
Diffuse	5.7 ± 3.7
Diffuse & specular	5.8 ± 1.7
Specular	4.5 ± 1.2

Although the mean yield (table 3.5.2.1) of the crystal with diffuse non read-out surfaces hardly differs from the crystal which consists of diffuse as well as specular surfaces, we prefer a crystal which subsists of specular as well as diffuse surfaces, because:

(1) a superior light collection coming from the top of the crystal (see figure 3.5.2.1) (top of crystal: 120 mm ≤ z ≤ 140 mm).

(2) smaller variance in collection efficiency.

§§ 3.5.3 Crystal quality

Crystal quality largely determines the attenuation length. Results of a BGO crystal with λ = 200 mm and λ = 300 mm are shown in figure 3.5.3.1. Simulated results of other attenuation lengths are reported in table 3.5.3.1.

Table 3.5.3.1. *Average percentage of light collected of the veto shield for different attenuation lengths.*

λ (mm)	Yield (%)
150	4.7 ± 2.0
200	5.8 ± 1.7
250	7.1 ± 1.6
300	9.2 ± 2.2
350	9.0 ± 1.9
400	9.4 ± 2.3

Note that improvement of the attenuation length above λ = 300 mm does not result in a higher light output. The calculations confirm our statement that application of a high quality crystal (λ = 300 mm) gives rise to a higher light collection with respect to the crystal of which the attenuation length amounts to: λ = 200 mm (5.8% → 9.2%; increase of 59%).

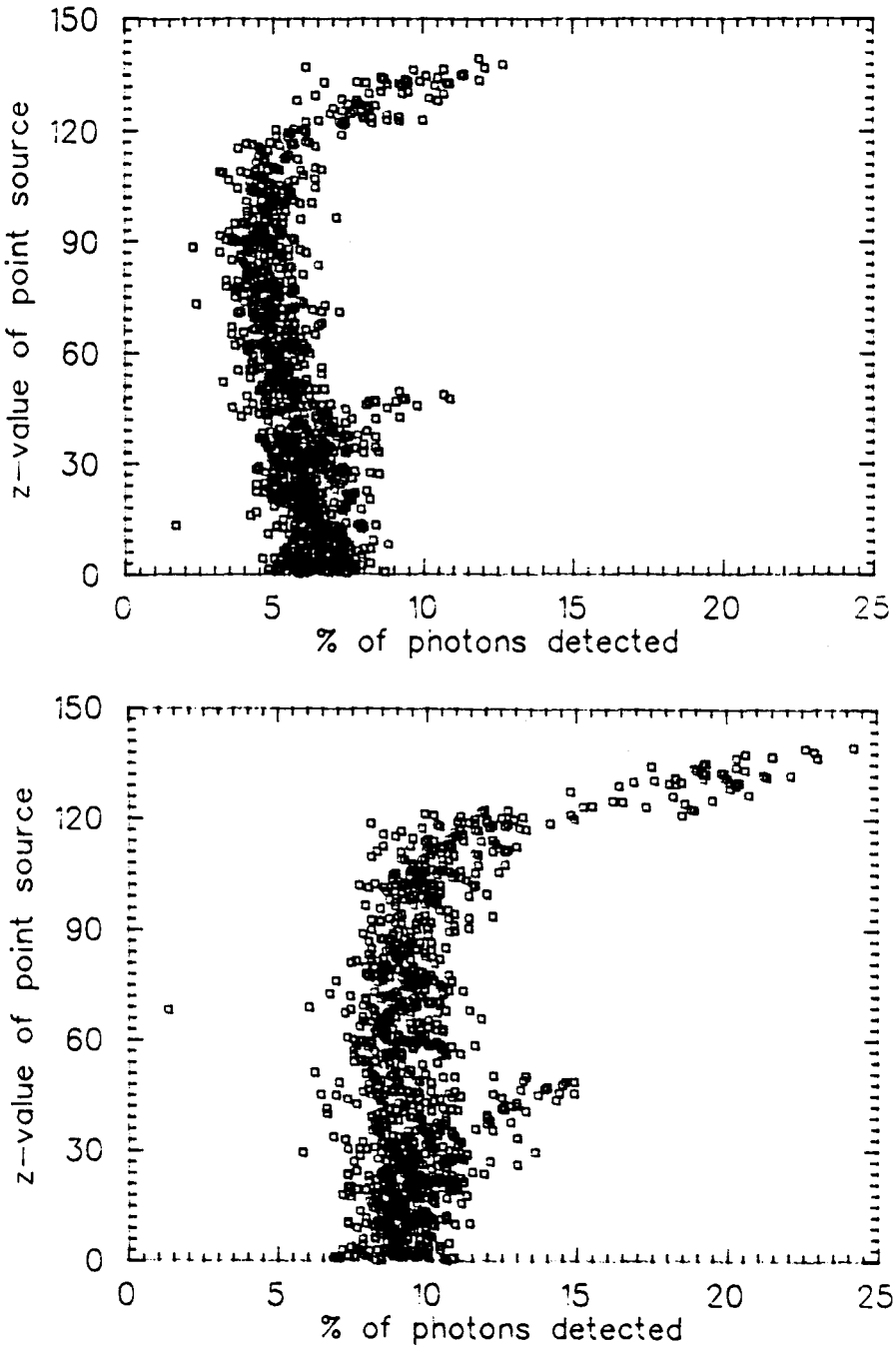

Figure 3.5.3.1. *% of photons detected versus position inside the crystal: top: λ = 200 mm, bottom: λ = 300 mm.*

§§ 3.5.4 Minimum detectable energy

Finally, we want to determine the minimum energy deposition in the BGO crystal which still leads to a veto signal. Firstly, we need to calculate the number of induced (photo)electrons inside the photomultiplier for an arbitrary energy deposition (equation 3.5.4.1. and 3.5.4.2).

$$N = \Delta E \cdot \frac{\Delta P}{\Delta E} \cdot \epsilon_Y \cdot \epsilon_{PMT} \cdot \epsilon_{BD} \qquad (3.5.4.1)$$

$$\epsilon_{BD} = \frac{\int_0^t \exp(-t'/\tau)\, dt'}{\int_0^\infty \exp(-t'/\tau)\, dt'} = [1 - \exp(-t/\tau)] \qquad (3.5.4.2)$$

with:
- N = number of (photo)electrons induced inside the photomultiplier.
- ΔE = energy deposited inside the crystal {keV}
- ΔP/ΔE = conversion factor (number of scintillation photons per unit energy deposition) {keV^{-1}}
- ϵ_Y = relative yield (number of photons which reaches the photomultiplier to the number of induced photons).
- ϵ_{PMT} = quantum efficiency of the photomultiplier.
- ϵ_{BD} = ballistic deficit.
- τ = decay time of the BGO crystal {s}.
- t = collection time {s}.

The noise equivalent level of a photomultiplier is estimated as one (photo)-electron (N_{noise} = 1). Normally, the energy threshold of a BGO veto crystal is set just above the noise equivalent level. For a crystal which is coupled to a photomultiplier by a grease the threshold energy amounts to $\Delta E_{noise} \approx 10$ keV [Bax92,Bea92], while equation 3.5.1 and 3.5.2. result in a noise equivalent energy of $\Delta E_{noise} = 7.5$ keV (N_{noise} = 1; ΔP/ΔE = 9 keV^{-1}; $\epsilon_Y = 0.1$; $\epsilon_{PMT} = 0.15$; $\epsilon_{BD} = 0.99$). Signals are considered to be detectable, when they exceed $3 \cdot \Delta E_{noise}$, so the minimum energy deposition ΔE of a γ-ray to result in a veto signal amounts to: ΔE ≈ 23 keV. In our setup, however we expect a reduction of the light yield due to:

(1) The long decay time of BGO at low temperatures (τ increases → ϵ_{BD} decreases).
(2) The air gap between the BGO crystal and the PMT causes internal trapping of the scintillation photons (ϵ_Y decreases)
(3) An increasing collection time (t), which results in an increased number of "noise" electrons (N_{noise}) per collection of one energy deposition.

On the other hand, we expect an increasing photon collection, due to:

(1) An increasing conversion factor (ΔP/ΔE), because the BGO crystal is cooled [Zuc89,Web73].
(2) The cooling of the BGO reduces the number of after glow photons in the crystal, which results in a decreasing number of noise electrons (N_{noise}) per unit of time.

Again using equation 3.5.4.1. and 3.5.4.2. we find a noise equivalent energy value of $\Delta E_{noise} \approx 5.0$ keV (N_{noise} = 1; ΔP/ΔE = 33 keV^{-1}; $\epsilon_Y = 0.05$; $\epsilon_{PMT} = 0.20$; $\epsilon_{BD} = 0.6$), which means that we can detect a energy deposition of ΔE ≈ 15 keV.

Note that the shaping time of a BGO crystal operated at room temperature will be 1 μs (while its decay time amounts to 0.3 μs), while the shaping time of a cooled crystal amounts to 10 μs (decay time 10 μs).

§ 3.6 Conclusions and discussion

The results presented in this chapter are principally acquired by computer simulation. Agreement between experiment and simulation is found. However, a simulation is an idealized reality. Even high quality crystals contain some layers of voids, mostly situated in the middle of a large crystal. Our simulations make use of "overall" properties of a crystal and do not possess the possibility to include position dependent crystal properties.

In Chapter 2 we assumed that the minimum detectable energy deposition inside the BGO amount to: $\Delta E = 50$ keV. Although the calculated minimum energy deposition amounts to: $\Delta E = 15$ keV, the peak to total ratios acquired in Chapter 2 are valid, because we have shown that the simulated peak to total ratio hardly differs for $\Delta E < 100$ keV.

However, [Hil86] reports experimentally a significant reduction of the suppression if the BGO threshold is increased from $\Delta E = 15$ keV to $\Delta E = 30$ keV, while calculations showed little variation of the peak to total ratio for BGO thresholds below $\Delta E < 100$ keV, similar to our simulated results.

Chapter 4

Cooling of the Ge and BGO crystals

§ 4.1 Cooling of the Compton suppression spectrometer

In order to get a high energy resolution, the Ge crystal has to be cooled below 110 kelvin. In our setup the Ge crystal is cooled through the BGO crystal. The setup is cooled with a copper rod attached at one end to the BGO and at the other end to a dewar filled with liquid nitrogen (77 kelvin) (figure 4.1.1). In this chapter will be discussed whether the needed Ge temperature will be reached for the designed setup and how much time it will take before the detector can be operated.

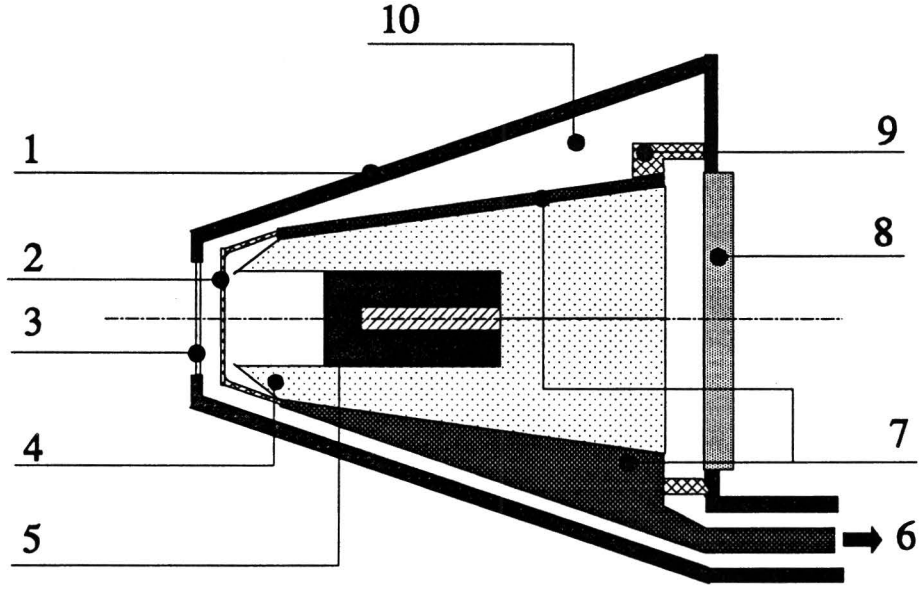

Figure 4.1.1. *Cross section of the spectrometer.*

1:	AL ENDCAP	6:	TO DEWAR
2:	IR-SHIELD	7:	CU COOLING ATTACHMENT
3:	BE WINDOW	8:	QUARTZ GLASS
4:	BGO CRYSTAL	9:	KEL-F SPACER
5:	GE DETECTOR	10:	VACUUM

The first problem is to calculate the temperature of the BGO and Ge when equilibrium is reached (§ 4.2). For this the temperature increase due to heat conduction through air and spacers as well as heat radiation are taken into account. The second problem is to estimate the time needed to cool the Ge and BGO crystals below 110 kelvin and the thermal conductance needed to transport the heat (§ 4.3). We use the cooling down time of an existing setup to estimate the time needed to cool the spectrometer. Experimentally, this theory is verified using a test setup. Finally, in § 4.4 the expansion of solids (BGO, Ge and Cu) with increasing temperature is discussed and tested.

§ 4.2 Calculation of the temperature at equilibrium

All bodies at temperature above absolute zero emit thermal radiation [Kre86,Gra74], and consequently lose energy. Thermal radiation occurs in the 1 μm ≤ λ ≤ 1000 μm region (for our temperature region of interest: see also figure 4.2.1). When radiation falls upon a body, a fraction is absorbed (α), a fraction is reflected (ρ) and the remainder is transmitted (τ) through the body (equation 4.2.1):

$$\alpha + \rho + \tau = 1 \qquad (4.2.1)$$

For most solid materials all radiation is absorbed within a very thin surface layer (thickness layer less than 10 nm [Hec87]), so $\tau \approx 0$.

First consider a black body, which has the property that it absorbs all incident radiation ($\alpha = 1$, so $\rho = 0$ and $\tau = 0$). A black body also radiates the maximum emissive power (E_b) with respect to its temperature. The rate at which the energy is radiated from a black body is given by the Stefan-Boltzmann formula (equation 4.2.2):

$$E_b = \sigma T^4 \qquad (4.2.2)$$

with: E_b = rate at which energy is radiated from a unit area of the surface of a black body {$W.m^{-2}$}.
σ = Stefan-Boltzmann constant {$W.m^{-2}.K^{-4}$} = $5.7\ 10^{-8}\ W.m^{-2}.K^{-4}$.
T = temperature of the black body {K}.

Using equation 4.2.2 we can calculate the energy emitted by a black body. But if a black body is surrounded by other black bodies of the same temperature, all bodies do not change temperature. In this case all bodies will absorb and emit the same amount of energy. This principle is called Prevost's principle of exchange. The Stefan-Boltzmann formula gives the total amount of energy emitted by a black body. The thermal radiation spectrum changes with the temperature of the black body [Kre86,Eng72]. The wavelength distributions for black bodies of different temperatures can be seen in figure 4.2.1.[Kre86].

To relate the intensity of radiation to the emissive power (E_b), we simply determine the energy from a surface radiation into a hemispherical enclosure placed above (see figure 4.2.2). Since the hemisphere will intercept all the radiant rays emanating from the surface, the total amount of radiation passing through the hemispherical surface equals the emissive power. The rate of radiation emitted from dA_1 passing through dA_n is given by equation 4.2.3:

$$\frac{dq_r}{dA_1} = I_b(\theta,\phi)\cos\theta\, d\omega \qquad d\omega = \sin\theta\, d\theta\, d\phi \qquad (4.2.3)$$

with: dq_r = radiation energy coming from surface dA_1 per unit of time {W}.
dA_1 = radiating surface area {m^2}.
$I_b(\theta,\phi)$ = radiation intensity {$W.m^{-2}.sr^{-1}$}.
$d\omega$ = radiation solid angle {sr}.

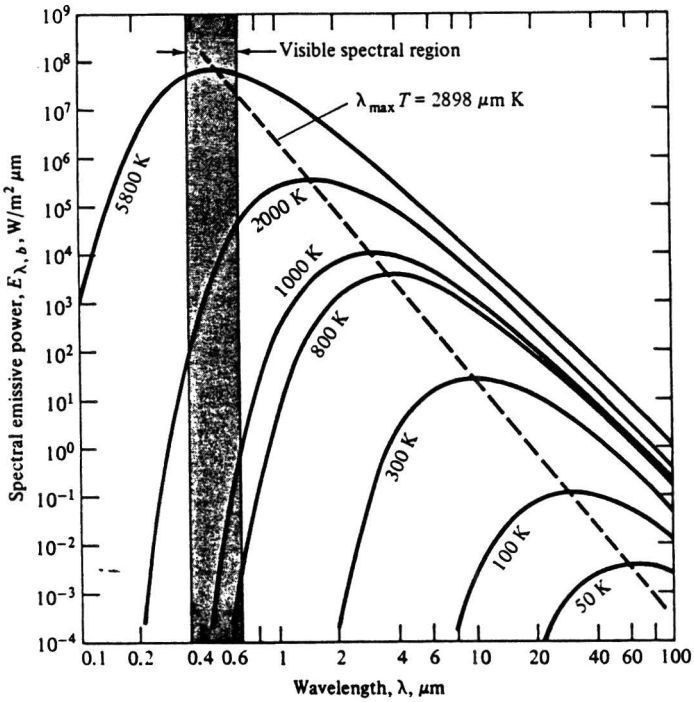

Figure 4.2.1. *Wavelength distribution of thermal radiation for different temperatures.*

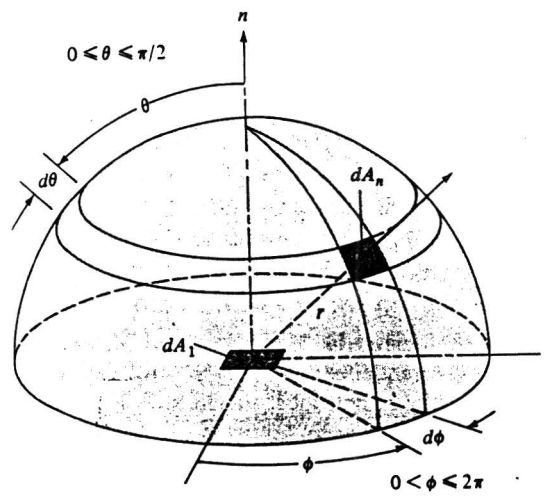

Figure 4.2.2. *Radiation from a differential area dA_1 into surrounding hemisphere centred at dA_1.*

Black body radiation is perfectly diffuse[1]. If the radiation intensity from a surface is independent of direction, it is said to conform to Lambert's cosine law (equation 4.2.3). Integration of equation 4.2.3. over all angles gives the relationship between the emissive power and radiation intensity (equation 4.2.4).

$$\left(\frac{q}{A}\right)_r = E_b = \pi I_b \qquad (4.2.4)$$

with: E_b = emissive power of the black body {$W.m^{-2}$}.
q = radiation energy of the black body per unit of time {W}.
A = surface area of the black body {m^2}.
I_b = radiation intensity of the black body {$W.m^{-2}.sr^{-1}$}
π = radiation solid angle {sr}.

If the body can not considered to be black the analysis becomes more difficult and the absorptivity as well as the reflectivity and transmissivity have a wavelength, temperature and angle of incidence dependence (formula 4.2.5):

$$\alpha = \alpha(\lambda,\theta,T) \quad \rho = \rho(\lambda,\theta,T) \quad \tau = \tau(\lambda,\theta,T) \qquad (4.2.5)$$

The emissivity of a body is usually defined as the ratio of the radiative flux emitted by the body to that of a black body at the same temperature. In the grey body approximation, the emissivity is a constant over the whole temperature region and for all wavelengths. A real body will have a emissivity which has got a temperature and wavelength dependence, but for most solid materials the grey body approximation will describe the system sufficiently. The energy radiated from a grey body is then given by formula 4.2.6:

$$E = \epsilon \sigma T^4 = \epsilon E_b \qquad (4.2.6)$$

with: E = radiative flux emitted by a real body {$W.m^{-2}$}.
E_b = radiative flux emitted by a black body {$W.m^{-2}$}.
ϵ = emissivity.
σ = Stefan-Boltzmann constant {$W.m^{-2}.K^{-4}$}.
T = temperature of the grey body {K}.

An example of a grey body approximation can be seen in figure 4.2.3. Consider a body in temperature equilibrium within a black body enclosure. Even if the temperature of the body is not equal to the black body temperature the emitted energy is equal to the absorbed radiation. This is called Kirchhoff's law (equation 4.2.7):

$$\epsilon = \alpha \qquad (4.2.7)$$

with: α = absorptivity.
ϵ = emissivity.

[1] Industrial rough surfaces approach diffuse characteristics.

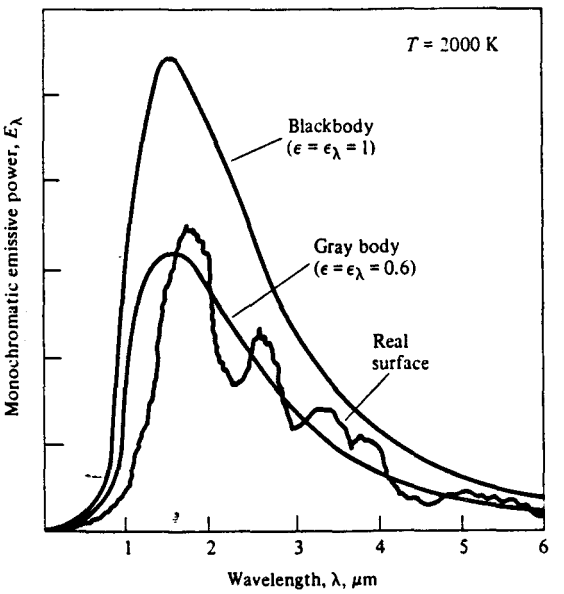

Figure 4.2.3. *Comparison of hemispherical monochromatic emission for a black, a grey and a real surface.*

Grey bodies will obey Kirchhoff's and Lambert's law. The radiation from grey surfaces can be considered in terms of radiosity, which is defined as the rate at which radiation leaves a given surface per unit area. For most solids no transmission [Hec87] will occur and radiosity will obey formula 4.2.8:

$$J_i = \rho_i G_i + \epsilon_i E_{bi} \qquad (4.2.8)$$

with: J_i = radiosity {W.m^{-2}}.
G_i = irradiation or radiation incident on a unit surface area per unit of time {W.m^{-2}}.
E_{bi} = black body emissive power {W.m^{-2}}.
ρ_i = reflectivity.
ε_i = emissivity.
i = surface index.

To keep a surface at an equilibrium temperature an amount of energy must be supplied. The net rate of heat transfer from a surface by radiation is equal to the difference between the outgoing and incoming radiation (formula 4.2.9):

$$q_i = A_i (J_i - G_i) \qquad (4.2.9)$$

with: q_i = energy difference between absorbed and emitted radiation of a body per unit of time {W}.
A_i = surface {m^2}.
J_i = radiosity {W.m^{-2}}
G_i = irradiation or radiation per unit of time incident on a unit surface area {W.m^{-2}}.
i = surface index.

For most solids is valid: $\rho_i + \varepsilon_i = 1$. Combining equation 4.2.8 and equation 4.2.9 gives formula 4.2.10:

$$q_i = A_i \left[\frac{\epsilon_i}{\rho_i} (E_{bi} - J_i) \right] = \frac{A_i \epsilon_i}{1 - \epsilon_i} [E_{bi} - J_i] \qquad (4.2.10)$$

The different surfaces will irradiate each other. The ratio of emitted radiation from one surface (A_i) which will hit another surface (A_j) to the total emitted radiation of surface (A_i) is called the view factor F_{ij}. Because in our setup the distances between the surfaces which irradiate each other are very small compared to the length and width of the surfaces (Appendix A and figure 4.1.1) the view factors are approximately unity (see figure 4.2.5).

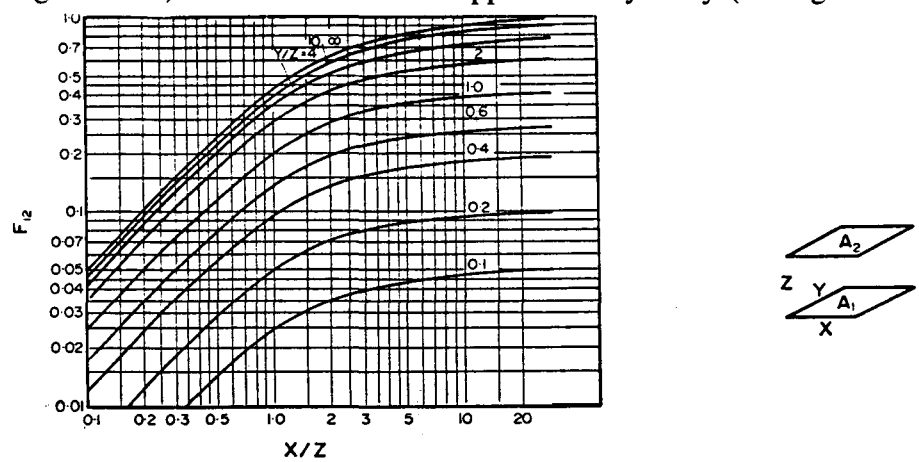

Figure 4.2.2. *View factors for two parallel plates versus their distance; the parameters X and Z are illustrated on the right hand.*

Since our setup is cylindrically symmetric the heat necessary to keep a surface at equilibrium temperature can be calculated more exactly by (formula 4.2.11) [Kre86]:

$$q_i = \frac{A_i \sigma (T_i^4 - T_j^4)}{\frac{1}{\epsilon_i} + \frac{A_i}{A_j} \left[\frac{1 - \epsilon_j}{\epsilon_j} \right]} \qquad (4.2.11)$$

with:
- q_i = energy difference between absorbed and emitted radiation per unit of time {W}.
- σ = Stefan-Boltzmann constant {$W.m^{-2}.K^{-4}$}.
- T_i = temperature of the cooled body {K}.
- T_j = temperature of the body at room temperature {K} ≈ 293 K.
- A_i = surface of the cooled body {m^2}.
- A_j = surface of the viewed body {m^2}.
- ε_i = emissivity of the cooled body.
- ε_j = emissivity of the viewed body.

Whenever a temperature gradient exists in a solid medium, heat will flow from a warmer to a colder part. The rate at which heat is transferred by conduction is given in equation 4.2.12. [Sch90].

$$q_k = -k(T)\, S \frac{dT}{dx} \qquad (4.2.12)$$

with: q_k = rate of heat transfer due to conduction {W}.
k = thermal conductivity {$W.m^{-1}.K^{-1}$}.
S = surface area perpendicular to the conduction direction {m^2}.
x = conduction direction {m}.

The thermal conductivity is a material property, which is temperature dependent. Since we only want to make an estimate of the temperature of the detector, our calculations make use of an "overall" thermal conductivity, which is the averaged thermal conductivity of the temperature region of interest.

Temperature increase due to heat conduction can occur through spacer material or through air. Since the spectrometer is situated in high vacuum conduction through air is negligible compared to heat conduction through spacer material. In our setup the main contribution to heat conduction will be through the Kel-F spacer, which holds the BGO-crystal in position (see Appendix A and figure 4.1.1). The conduction length through the Kel-F is: $d_s = 20 \pm 3$ mm, while the conduction surface amounts to: $S = (2.3 \pm 0.2)\ 10^3$ mm^2. The heat conduction through the spacer material is given by equation 4.2.13.

$$q_s = k_s \frac{S\,(T_i - T_j)}{d_s} \qquad (4.2.13)$$

with: q_s = energy lost by conduction through spacer material per unit of time {W}.
k_s = conductivity of the spacer material {$W.m^{-1}.K^{-1}$}.
S = surface perpendicular to the conduction direction of the spacer material {m^2}.
T_i = temperature of the cooled body {K}.
T_j = temperature of the viewed body {K} ≈ 293 K.
d_s = conduction length through the spacers {m}.

There will be an equilibrium temperature for the setup which is calculated, due to heat transfer through a copper rod. The conducted heat will depend on the equilibrium temperature (formula 4.2.14).

$$q_c = k_c \frac{S\,(T_c - T_i)}{d_c} \qquad (4.2.14)$$

with: q_c = amount of energy per unit of time supplied by the copper cooling rod {W}.
k_c = conductivity of the copper {$W.m^{-1}.K^{-1}$}.
S = area perpendicular to the cooling direction in the copper {m^2}.
d_c = length of the copper rod {m}.
T_i = equilibrium temperature {K} = temperature of the cooled body {K}.
T_c = liquid nitrogen temperature {K} ≈ 77 K.

If all contributions of heat lost are taken into account (in our setup dominated by conduction through spacers and heat radiation), the equilibrium temperature can be calculated using equation 4.2.15:

$$q_c = q_i + q_s \qquad (4.2.15)$$

with: q_c = energy supplied through the copper rod per unit of time {W}.
q_s = energy lost by conduction through spacer material per unit of time {W}.
q_i = energy lost by radiation per unit of time {W}.

For different values of the emissivity the equilibrium temperature (T_i) has been calculated with equation 4.2.15. The equilibrium temperature has been calculated. For typical emission coefficients of Cu, Al and glass (see table 4.2.1. [Kre86]) the emission coefficient of BGO is varied (because emission coefficients of BGO are not reported in literature).

Table 4.2.1. *Emissivity of different materials.*

Material		Emissivity
Copper:	*polished*	0.04
	oxidized	0.87
Aluminium:	*polished*	0.04
	anodized	0.94
Steel:	*polished*	0.07
	oxidized	0.80
Quartz Glass		0.40
		0.95

This results in a calculated equilibrium temperature of $T_i = 100 \pm 1$ kelvin (all metals polished; $\varepsilon_{BGO} = 0.5$; quartz window). Although we applied polished metals and a quartz window instead of glass, heat radiation largely determines the equilibrium temperature we can achieve. We need an equilibrium temperature $T_i \leq 110$ kelvin in order to operate the Ge detector properly. However, it is favourable to acquire a temperature $T_i \leq 100$ kelvin.

According to the calculations this should be possible. If experiments should show that we can not obtain temperatures $T_i \leq 100$ kelvin, we could consider the application of a IR filter, which possesses a high transmission ($T > 0.9$) for scintillation photons of the BGO ($400 \text{ nm} \leq \lambda \leq 550 \text{ nm}$) and high reflectivity ($R \approx 0.98$) for thermal radiation wavelengths (the IR-filter should be placed between the BGO and the quartz window). Calculations with an IR filter ($\varepsilon_{ir} = 0.02$) show a further drop in equilibrium temperature of 9 kelvin (table 4.2.2).

Calculations reveal that our dewar (contents: 7.5 dm^3) must be filled with liquid nitrogen every 3 days after equilibrium is reached, according to the energy needed per unit of time given in table 4.2.2.

Table 4.2.2. *Equilibrium temperature for different material emissivities.*

Surface of metals	ε_{BGO}	IR-filter	q_c (W)	q_i (W)	q_s (W)	T_{equi}(K)
Polished	0.5	no	3.69	2.82	0.87	100 ± 1
Polished	1.0	no	4.32	3.47	0.85	104 ± 1
Oxidized/Anodized	0.5	no	23.7	23.4	0.3	225 ± 2
Polished	0.5	yes	2.19	1.28	0.91	91 ± 1
Polished	1.0	yes	2.19	1.28	0.91	91 ± 1

§ 4.3 Calculation of the cooling down time

The time needed to cool the Ge and BGO can be estimated using equation 4.3.1. [Kre86, Gra74,Car59]. This equation describes conduction in solids. It is considered that heat radiation is a second order influence when cooling down. The equation can be solved if the boundary and start conditions are known. In cylindrical coordinates (r,θ,z) the heat equation 4.3.1. transfers into formula 4.3.2.

$$\rho c_p \frac{\partial T}{\partial t} = k\nabla^2 T = k\left(\frac{\partial^2 T}{\partial x^2} + \frac{\partial^2 T}{\partial y^2} + \frac{\partial^2 T}{\partial z^2}\right) \qquad (4.3.1)$$

$$\kappa\left(\frac{\partial^2 T}{\partial z^2} + \frac{\partial^2 T}{\partial r^2} + \frac{1}{r}\frac{\partial T}{\partial r} + \frac{1}{r^2}\frac{\partial^2 T}{\partial \theta^2}\right) = \frac{\partial T}{\partial t} \qquad (4.3.2)$$

$$\kappa = \frac{k}{\rho c_p} \qquad (4.3.3)$$

with: ρ = density {g.cm^{-3}}.
c_p = specific heat {J.g^{-1}.K^{-1}}.
k = thermal conductivity {W.cm^{-1}.K^{-1}}.
T = temperature {K}.
κ = diffusivity {cm^2.s^{-1}}.
t = time {m}.

In the case of a long copper rod the ratio of the heat transfer in radial (in air) to axial (in copper) direction will be almost zero because the heat conductivity in high vacuum (10^{-4}-10^{-5} mbar) is much smaller than in copper. This will simplify the heat equation even more (formula 4.3.4) (the z-direction is chosen to be the heat transfer direction)
Equation 4.3.4. can be separated in time (Θ(t)) depending and position (L(z)) depending parts (formula 4.3.5). Solutions of the time depending part (Θ(t)) will be of the form (formula 4.3.6), if an "overall" diffusivity is used for the temperature region of interest.

$$\kappa \frac{\partial^2 T(z,t)}{\partial z^2} = \frac{\partial T(z,t)}{\partial t} \tag{4.3.4}$$

$$\kappa \frac{1}{L(z)} \frac{\partial^2 L(z)}{\partial z^2} = \frac{1}{\Theta(t)} \frac{\partial \Theta(t)}{\partial t} \tag{4.3.5}$$

$$T_k - T_i = (T_j - T_i) \exp -\left(\frac{\kappa t}{l^2}\right) = (T_j - T_i) \exp -\left(\frac{t}{\tau}\right) \tag{4.3.6}$$

with: T_k = temperature at time t {K}.
T_j = start temperature (normally room temperature ≈ 293 K) {K}.
T_i = equilibrium temperature {K}.
κ = diffusivity of the material {$m^2.s^{-1}$}.
l = conduction length through the material {m}.
τ = time constant of the material {s}.

Formula 4.3.6. will be used to make an estimation of the time needed to cool the new setup (the Ge-BGO Compton suppression spectrometer) by using the time needed to cool the old setup (Ge detector). The old setup has a temperature below 100 K within 4 ± 1 hours of cooling [Ver92]. Using equation 4.3.6. will give the time constant of the old setup (T_k = 100 K; T_i = 83 K; T_j = 293 K) which amounts to: τ_o = 1.5 ± 0.4 hours.

Because our setups consist of different materials, we introduce an average diffusivity, which is valid for the total setup. We make the assumption that temperature drops between interfaces of different materials are negligible. The average diffusivity is given by equation 4.3.7.

$$\frac{1}{\kappa_t} = \frac{\sum_i (l_i / \kappa_i)}{\sum_i l_i} = \frac{\sum_i (l_i / \kappa_i)}{L} \tag{4.3.7}$$

with: κ_t = average diffusivity {$m^2.s^{-1}$}.
κ_i = diffusivity of the i^{th} material {$m^2.s^{-1}$}.
l_i = cooling length through the i^{th} material {m}
L = total cooling length of the different materials {m}.

By measuring the cooling distances through the several materials the average diffusivity can be calculated. If the time constant of an existing (old) setup is known, the time constant of a new setup can be calculated using equation 4.3.8.
Equation 4.3.6. then gives the minimum cooling down time for the new setup. Since we assumed that the temperature drops between interfaces of materials are negligible, a test setup is built (§§ 4.3.1) to determine the applicability of this theory.

$$\frac{\tau_n}{\tau_o} = \frac{(L_n^2 / \kappa_{t,n})}{(L_o^2 / \kappa_{t,o})} \qquad (4.3.8)$$

with: $\tau_{o/n}$ = time constant of a setup {s}.
$\kappa_{t,o/n}$ = average diffusivity {$m^2.s^{-1}$}.
$L_{o/n}$ = total cooling length {m}.
o/n = setup index (o = old, n = new).

We also want to be sure that the used copper rod is able to transport the required heat necessary to cool the rod itself, the BGO and the Ge. The heat transferred through the copper rod is given by equation 4.3.9.

$$q_c = k_c \frac{S\,(T_k - T_c)}{d_c} \qquad (4.3.9)$$

with: q_c = amount of energy per unit of time supplied by the copper cooling rod {W}.
k_c = conductivity of the copper {$W.m^{-1}.K^{-1}$}.
S = area perpendicular to the cooling direction in the copper {m^2}.
d_c = length of the copper rod {m}.
T_k = temperature at time t {K} = temperature of the cooled body at time t {K}.
T_c = liquid nitrogen temperature {K} ≈ 77 K.

The maximum energy rate transferred through the copper rod is when the cooling down process starts, because $T_k = T_j \approx 293$ kelvin. Let us calculate the total amount of energy (Q_c) the copper rod can transfer (equation 4.3.10) by using equation 4.3.6. This amount of energy will be transferred in τ seconds if the temperature difference would not change (τ is the time constant of the setup).

$$Q_c = \int dQ_c = \int_0^{\infty} \frac{k_c\,(T_k - T_i)\,S}{d_c}\,dt = \qquad (4.3.10)$$

$$= -\frac{k_c\,S\,(T_i - T_j)}{d_c} \int_0^{\infty} e^{-(\frac{t}{\tau})}\,dt = \frac{-k_c\,S\,(T_i - T_j)\,\tau}{d_c}$$

The amount of energy needed to cool the total setup can be calculated by equation 4.3.11. To satisfy our condition (the copper rod must be able to transfer the required heat at all times) the copper rod which would be used, must satisfy equation 4.3.12.

$$Q_n = (T_i - T_j) \sum_i (c_{p_i} \rho_i V_i) \qquad (4.3.11)$$

with: Q_n = total amount of energy needed to cool the setup {J}.
T_i = equilibrium temperature of the cooled body {K} ≈ 100 K.
T_j = start temperature {K} ≈ 293 K.
$c_{p,i}$ = specific heat of the i-th material of the cooled body {J.kg^{-1}.K^{-1}}.
ρ_i = density of the i-th material of the cooled body {kg.m^{-3}}.
V_i = volume of the i-th material of the cooled body {m^3}.

$$Q_c \geq Q_n \qquad (4.3.12a)$$

$$\frac{S}{d_c} \geq \frac{Q_n}{k_c (T_i - T_j) \tau} \qquad (4.3.12b)$$

In §§ 4.3.2 the time constant of the new setup is calculated (τ_n = 21 ± 5 hours). Density and specific heat of copper, germanium [Tol70-4] and bismuth germanate [Xi 89] are reported in literature. It appears that the copper rod used in the new setup (dimensions: length = 75 cm; diameter: 2 cm∅) satisfies this condition (equation 4.3.12).

§§ 4.3.1 Cooling down time of a test setup

In order to estimate the cooling down time of a setup, we introduced an average diffusivity of a setup (equation 4.3.7), while neglecting temperature drops at interfaces of materials. Although temperature does drop at interfaces, we want to show that equations 4.3.7. and 4.3.8. can be used to make an estimate of the cooling down time of an unknown system. For this we built a test setup, which is presented in figure 4.3.1.1. We already indicated the positions where we measured the temperature.

In order to acquire the temperature at the indicated positions, we used a temperature dependent resistor (PT-100) and a stable current supply (I = 100.20 ± 0.02 μA), and measured the voltage over the PT-100 resistor (figure 4.3.1.2).

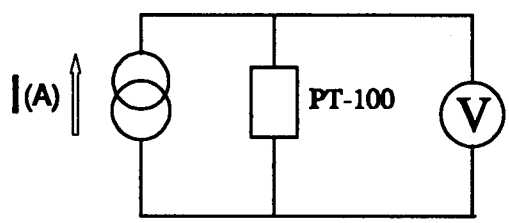

Figure 4.3.1.2. *Electrical setup for temperature measurements.*

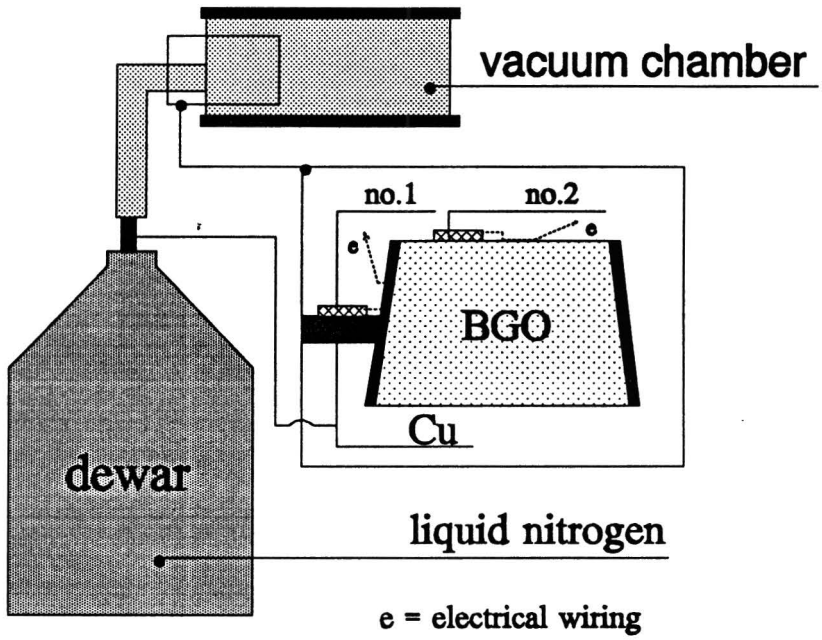

Figure 4.3.1.1. *Test setup with measure points 1 and 2.*

The resistors are thermally connected to the BGO and copper (figure 4.3.1.1) at the indicated measure points with a glue which has a high thermal conductivity. In order to decrease the heat conduction the wires to the resistors are made of thin stainless steel, which have a low thermal conductivity. The wires are thermally connected to the BGO and the copper to avoid electrical heating of the PT-100 resistors. Cooling distances through the copper and the bismuth germanate are given in table 4.3.1.1.

Table 4.3.1.1. *Cooling distances of the test setup.*

Material	PT100-no. 1	PT100-no.2
Cu	36 ± 2 cm	39 ± 2 cm
BGO	-	2.0 ± 0.5 cm

Using the information of table 4.3.1.1. the ratio of the time constants of the two measure points (PT100-no.1 and PT100-no.2) can be calculated (formula 4.3.7. and 4.3.8) and amounts to: $\tau_1/\tau_2 = 7 \pm 2$. In figure 4.3.1.3 we show the measured temperature of PT100-no.1 and PT100-no.2 versus cooling time. From figure 4.3.1.3. the time constants can be obtained using equation 4.3.1.1.

$$\frac{\tau_2}{\tau_1} = \frac{\tan(\alpha_1)}{\tan(\alpha_2)} \qquad \textbf{(4.3.1.1)}$$

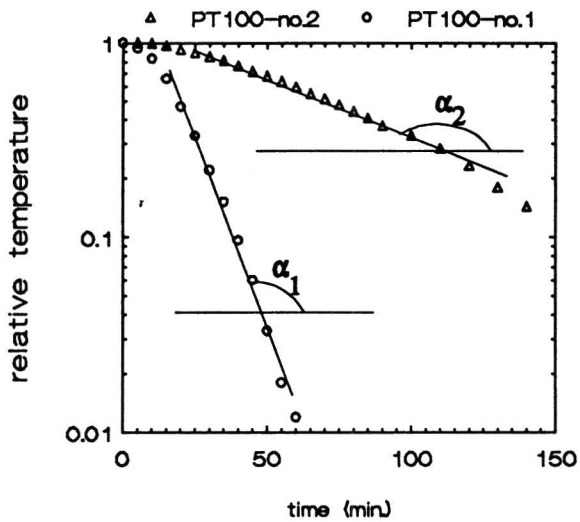

Figure 4.3.1.3. *Cooling down time of the test setup versus relative temperature; relative temperature is defined as* $(T - T_i)/(T_j - T_i)$.

The experimentally acquired ratio of time constants amounts to: $\tau_2/\tau_1 = 9 \pm 4$. Since our first goal was to get an idea of the order of cooling time, it seems that the theory presented in § 4.3 can be used to give a rough estimate of the cooling down time needed for the Ge-BGO Compton suppression spectrometer.

§§ 4.3.2 Cooling down time of the Ge-BGO spectrometer

To determine the cooling down time of the Ge-BGO Compton suppression spectrometer we need to known the cooling distances through the materials of the old as well as the new setup (table 4.3.2.1).

Table 4.3.2.1. *Conduction distances through several materials for the old and new setup.*

Material	Old Setup (mm)	New Setup (mm)
Copper	200 ± 20	750 ± 20
Ge	25 ± 1	27 ± 1
BGO	-	23 ± 1
Teflon	1.0 ± 0.2	-

The information of table 4.3.2.1. results in a time constant ratio of: $\tau_n/\tau_o = 16 \pm 4$ (equation 4.3.7 and 4.3.8). Knowing the time constant of the old setup ($\tau_o = 1.5 \pm 0.4$ hours) results in a time constant of the new setup of: $\tau_n = 21 \pm 5$ hours. The cooling down time can be calculated by equation 4.3.6. and is presented for several temperatures and configurations in table 4.3.2.2. According to these calculations the spectrometer can be operated after 2-4 days of cooling, which is acceptable.

Note that application of an IR-filter has two advantages: (1) a lower equilibrium temperature, which is favourable for operating the Ge-detector (see § 4.2); (2) a shorter cooling time.

Table 4.3.2.2. *Cooling down time of the Ge-BGO Compton suppression spectrometer for different equilibrium temperatures and different maximum operating temperatures.*

T(max)(K)	IR-filter	T_{equi}(K)	time (hours)
105	no	100	77 ± 18
110	no	100	62 ± 15
95	yes	91	82 ± 20
100	yes	91	65 ± 15
110	yes	91	50 ± 12

Experiments must be done to verify the correctness of the calculations. Since the Ge is very vulnerable, the temperature could be measured by putting in a dummy material (e.g. copper) at the position of the Ge.

§ 4.4 Linear expansion of Cu, Ge and BGO

It is well known that most solid objects will expand when the temperature increases. Different materials have different expansion coefficients. In our setup we have to be sure that the copper will not crush the BGO and/or the BGO will not crush the Ge-crystal. So, the influence of expansion of solids has to be investigated. For small temperature differences one can use a linear approximation (formula 4.4.1).

$$L_i(T) = L_i(T_0) + \alpha_i(T)\,\Delta T \qquad (4.4.1)$$

with: $L_i(T)$ = length of the i-th material at temperature T {m}.
$L_i(T_0)$ = length of the i-th material at reference temperature {m}.
$\alpha_i(T)$ = expansion coefficient {$m.K^{-1}$}.
ΔT = temperature difference between material and reference temperature {K}.

However, in our case the temperature difference will be ≈ 200 K. It is more accurate to use a polynomial function, which describes the expansion (equation 4.4.2):

$$L_i(T-T_0) = a_{0,i} + a_{1,i}(T-T_0) + a_{2,i}(T-T_0)^2 + a_{3,i}(T-T_0)^3 + O(\geq(T-T_0)^4) \qquad (4.4.2)$$

For our calculations the expansion coefficients for BGO where taken from [Jun84,Xi 89] and for Ge and Cu from [Tou75-13]. The data were fitted with the coefficients of the polynomial function up to the third order. Using this gives the following results:

(1) By cooling down the copper with inner diameter of ≈ 106 mm∅ it will shrink 0.39 ± 0.01 mm, while the experimentally determined shrinkage amounts to 0.36 ± 0.02 mm.

(2) By cooling down the BGO the outer diameter of ≈ 106 mm∅ will shrink 0.1 ± 0.02 mm, while the inner diameter of the BGO (≈ 57 mm∅) will shrink 0.05 ± 0.01 mm. [2]

(3) By cooling down the Ge the outer diameter of ≈ 56 mm∅ will shrink 0.013 ± 0.002 mm.

From these data one can conclude that the Cu cylinder should have an inner diameter which is 0.3 mm larger than that of the BGO at room temperature. The BGO should have an inner diameter which is 0.1 mm larger than that of Ge at room temperature.

However, experiments done with the test setup discussed in §§ 4.3.1. showed that the BGO outer diameter and the Cu cylinder its inner diameter can neatly fit at room temperature (no spacing) as long as the thickness of the copper surrounding the BGO does not exceed 2 mm. In the Ge-BGO spectrometer we will surround the BGO with copper which has got a thickness of 2 mm.

Ge crystals should be treated very carefully, since they are easily damaged. Moreover they are never perfectly cylindrical. We therefore prefer a space of 1 mm between the Ge and the BGO. This has also the advantage that the Ge crystal is more easily put in and out of the setup.

[2] Expansion coefficients of BGO below 140 Kelvin are not reported in literature. In the lower temperature region we extrapolated the expansion coefficients.

Chapter 5

Construction of the Ge-BGO Compton suppression spectrometer

§ 5.1 Design considerations

Compton suppression spectrometers build up to now all subsist of a Ge detector in a cryostat (made of metal) surrounded by a scintillator veto shield (figure 5.1.1), e.g. [Bea92,Mic86].

← back

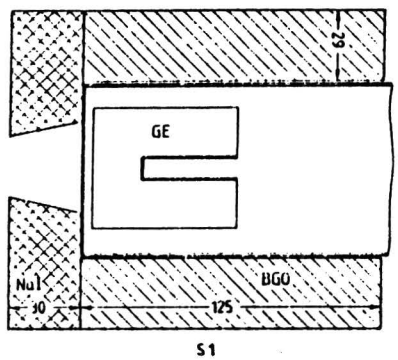

front →

Figure 5.3.1. *Layout of a Compton suppression spectrometer; a symmetric BGO shield is coupled to a backscatter NaI crystal [Mic86].*

In Chapter 2 we have shown that veto material is most effective in forward direction (the direction of the incident γ-rays). Therefore a second Ge crystal is often placed in front of the high resolution Ge crystal and is used as veto detector. Since this crystal is only needed to veto scattered γ-rays its energy resolution may be inferior to the first Ge crystal (see figure 5.1.2). The second Ge crystal could also be replaced by a BGO scintillation crystal, read out by photodiodes (figure 5.1.2, see also [Ver91]).

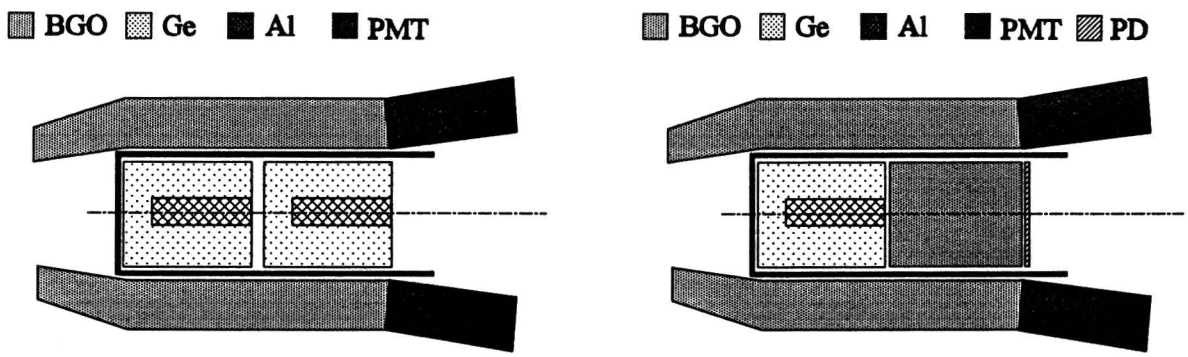

Figure 5.1.2. *Layout of Compton suppression spectrometers with front direction veto material; left: a second Ge crystal; right: a cooled BGO crystal read out by photodiodes.*

Moreover, [Eml86,Mic86] also place a thin Ge crystal at the back of the first Ge crystal in order to suppress the back scattered γ-rays (figure 5.1.3). This setup subsists a 4π surrounding of veto material. Disadvantage is the strong attenuation of low energy γ-rays in the Ge crystal placed at the back of the first Ge crystal.

← back

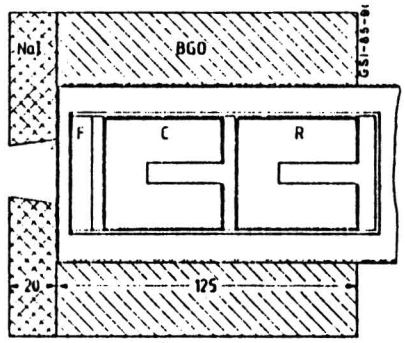

front →

Figure 5.1.3. *Layout of a Compton suppression spectrometer [Eml86]; in the front direction a second Ge crystal is added, while at the back of the high resolution Ge a third (thin) Ge crystal is used to acquire a 4π veto shield.*

All the detector configurations discussed above have got a Ge detector in a cryostat surrounded by a veto shield. The material situated between the Ge and the veto shield causes attenuation of scattered γ-rays which results in a suppression reduction (Chapter 2). We therefore developed a unique detector, where the Ge and the BGO veto shield are together in one cryostat, so that material between the crystals is avoided (figure 5.1.4).

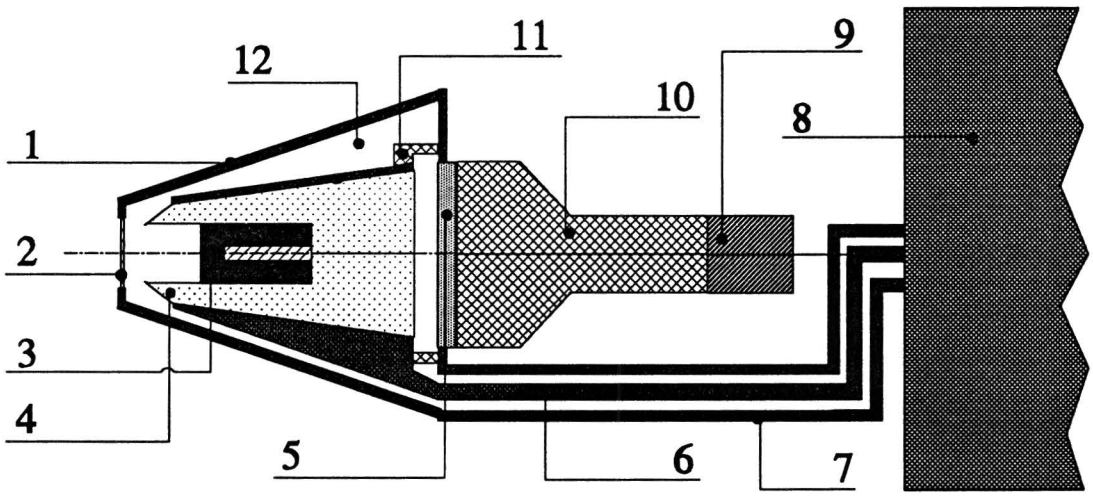

Figure 5.1.4. *Cross section of the Ge-BGO Compton suppression spectrometer; the Ge and BGO are within one cryostat (drawing is not to scale).*

1:	AL ENDCAP	5:	QUARTZ WINDOW	9:	RESISTOR BRIDGE
2:	BE WINDOW	6:	CU COOLING ROD	10:	PHOTOMULTIPLIER
3:	GE CRYSTAL	7:	STEEL COOLING ROD SURROUNDING	11:	KEL-F
4:	BGO CRYSTAL	8:	DEWAR	12:	VACUUM

Disadvantage is that this design requires a much more complicated cryostat. However, simulations have shown that the light yield of the BGO crystal is higher with respect to the photon collection of BGO veto shields operated in common Compton suppression spectrometers (Chapter 3).

§ 5.2 Electrical restrictions

The Compton suppression spectrometer subsists of a Ge crystal and a BGO veto shield. In order to collect the information carriers (electrons/holes) a high voltage (≈ 4.5 kV) will be applied to the Ge crystal. For detection of the scintillation photons of the BGO a photomultiplier tube will be used (see figure 5.2.1).

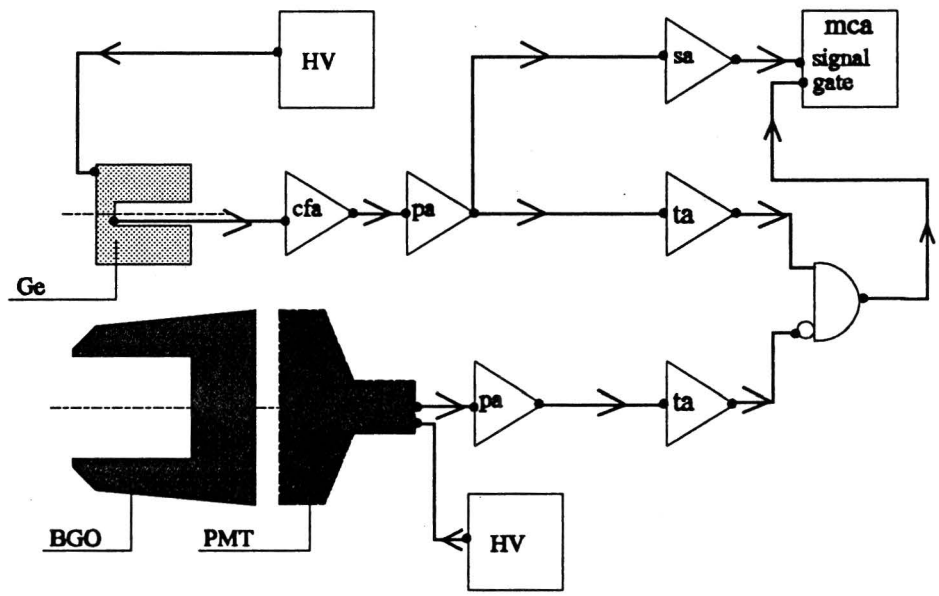

Figure 5.2.1. *Electrical setup of the Compton suppression spectrometer.*

HV	:	HIGH VOLTAGE	CFA	:	COLD FET ASSEMBLY
PA	:	PREAMPLIFIER	TA	:	TIMING AMPLIFIER
SA	:	SPECTROSCOPY AMPLIFIER	MCA	:	MULTI CHANNEL ANALYZER

The signals of the Ge and the PMT are amplified and fed to an anti-coincidence circuit. If a γ-ray is scattered and deposits energy in the Ge as well as the BGO the event can be rejected.

We use a high voltage to operate the Ge detector. Therefore the Ge crystal needs to be electrically isolated. Normally teflon is used for this. However, application of teflon would increase the cooling down time (1 mm teflon between the Ge and the BGO increases the cooling down time by approximately 40%). According to [Ver92] the Ge crystal is electrically isolated if the material which surrounds the detector has got an electrical resistivity more than 10^{12} Ω.cm. Therefore we determined the electrical resistivity of the BGO experimentally. First, we checked if the BGO blows out when a high voltage is used. No blow out occurred

up to 10 kV. Secondly, the electrical resistance of BGO is measured for several BGO crystals with different thicknesses. Results are presented in table 5.2.1.

Table 5.2.1. *Electrical resistance of several BGO pieces with different thicknesses (d).*

d (mm)	resistance (Ω)
5	$2 \pm 1\ 10^{13}$ Ω
10	$4 \pm 1\ 10^{13}$ Ω
20	$7 \pm 2\ 10^{13}$ Ω

The data presented in table 5.2.1. show that application of teflon or other electrically isolating material is not necessary (electrical resistivity of the BGO amounts to $(4 \pm 1)\ 10^{13}$ Ω.cm).

In order to get a good charge collection in the Ge crystal a high voltage must be applied, which is supplied through a copper rod, connected to a Cu ring (figure 5.2.3). The copper ring is firmly pressed by 3 screws, which should result in: (1) the steady positioning of the Ge crystal in the BGO scintillator; (2) a good electrical contact of the copper ring to the Ge detector. To improve the electrical contact a thin indium foil between the copper ring and the Ge crystal is used.

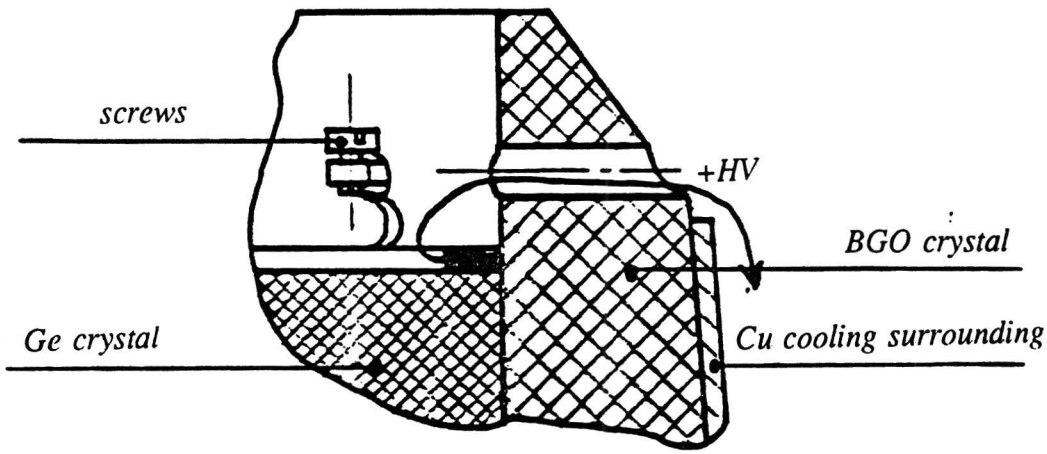

Figure 5.2.3. *Connection between the high voltage and the Ge crystal.*

§ 5.3 Mechanical construction

Since the detector among other applications must also fit as a segment of the Eurogam cluster detector, its dimensions are restricted. The outer dimensions of the detector configuration presently used for the Eurogam detectors are shown in figure 5.3.1. [Bea92].

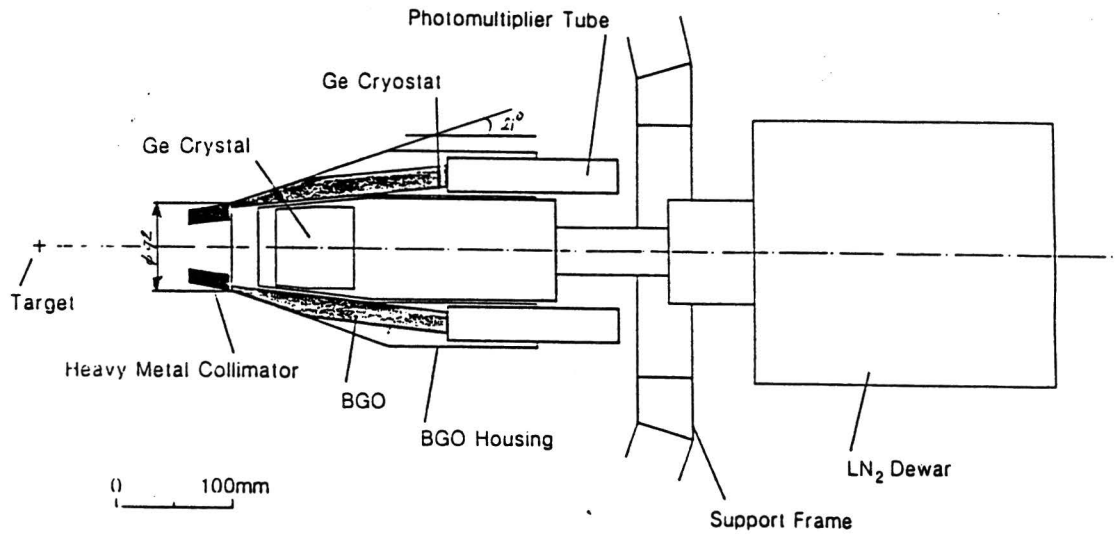

Figure 5.3.1. *A schematic diagram of the Eurogam detector module showing the Ge and BGO detectors, the heavy metal collimator and part of the support frame. The distance of the target to the detector cryostat is 189.1 mm, while the tapering angle amounts to 21° and the entrance window has a diameter of 92 mmØ.*

The complete drawing of the compact Compton suppression spectrometer is given in figure 5.3.2. (the corresponding names and drawings of the different parts are given in Appendix A). Figure 5.3.2. shows that the maximum dimensions of the spectrometer are equal to the outer dimensions of the spectrometer used in the Eurogam project. We aligned the spectrometer at one axis (so it is cylindrically symmetric), which should result in a more compact spectrometer and thus is easier to handle. Several parts of the spectrometer will be discussed in more detail.

Part no. 3 is the lead collimator, which is used to attenuate γ-rays which directly irradiate the BGO crystal. Application of the collimator will increase the maximum tolerable count rate of the spectrometer. Disadvantage is the increased number of Compton scattered γ-rays entering the Ge crystal. We shaped the collimator in such a way that number of scattered γ-rays which leave the collimator and enter the Ge detector is reduced, while the attenuation factor of the collimator hardly decreases. This is done by changing the inner diameter of the collimator in 5 steps, instead of continuously. This has the advantage that incident γ-rays "see" less lead (see figure 5.3.3).

For the entrance window of the spectrometer we replaced the Al (endcap material) by a Be window because: (1) Be is stronger than Al, which means that a thinner entrance window can be used; (2) the atomic number and density of Al is higher than the atomic number and density of Be. (1) and (2) result in less attenuation of γ-rays in the entrance material of the cryostat.

In order to keep the Ge-BGO Compton suppression detector in position we have to attach the spectrometer to the cryostat. Since the cryostat is at room temperature the attachment should have a low heat conductivity. Moreover, the detector must be operated in high vacuum. Therefore the material should not gas out. Finally, the material must be mechanically stable in order to hold the spectrometer (mass ≈ 8 kg) at its place. The most suitable material for our demands appears to be Kel-F (a teflon alike, but mechanically stable material).

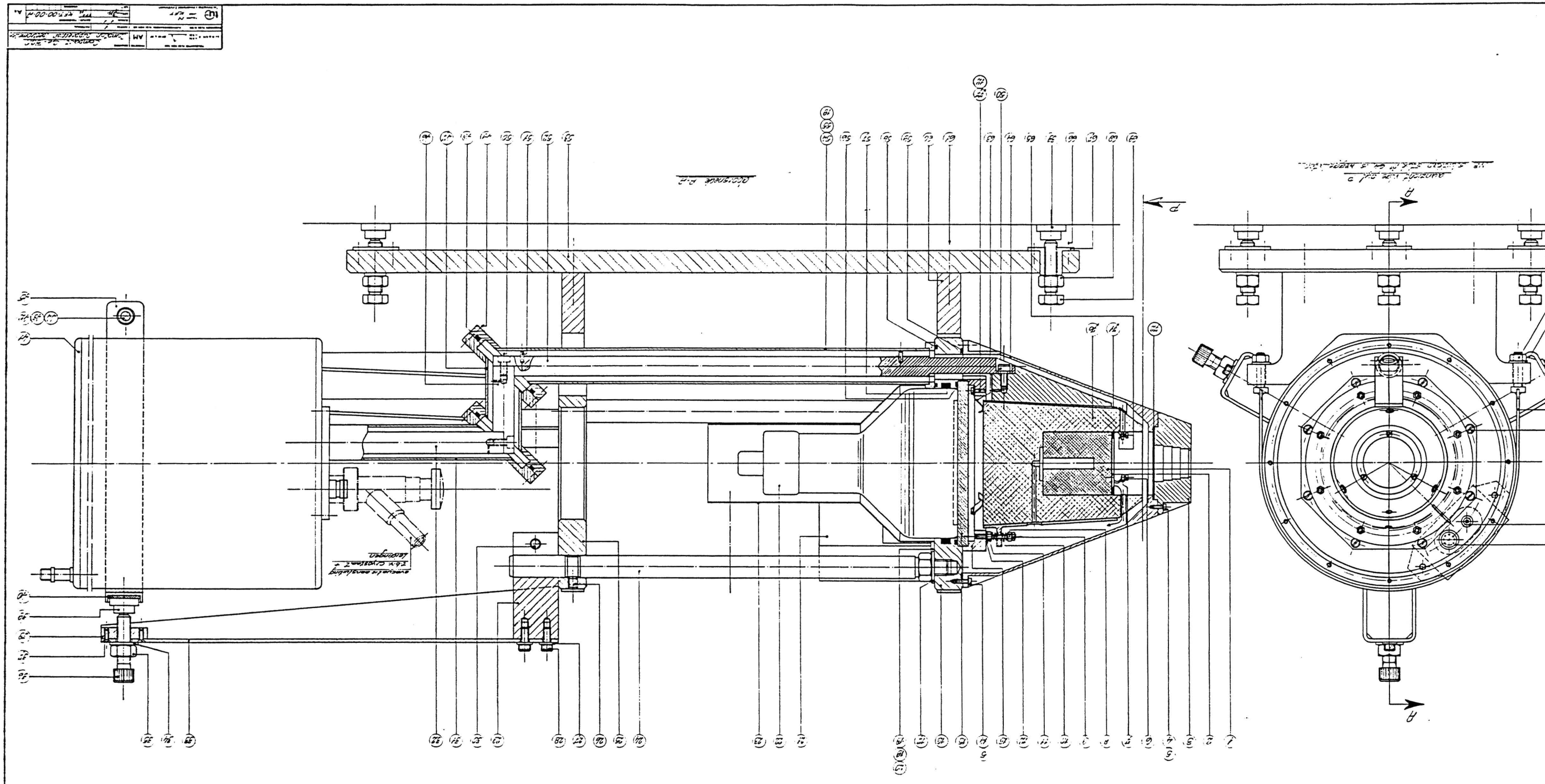

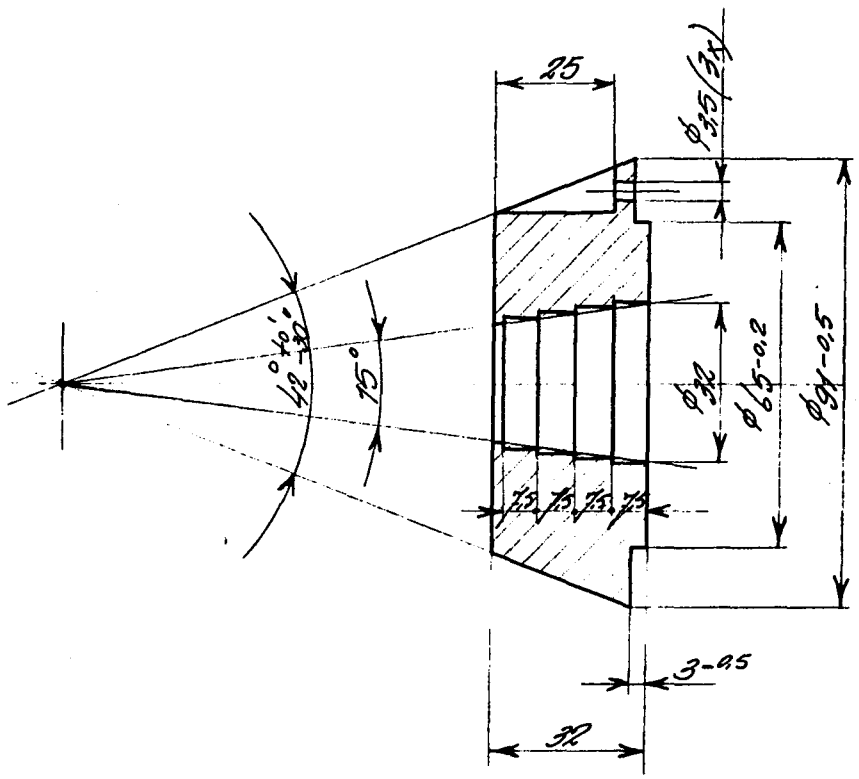

Figure 5.3.3. *Lead collimator. The collimator is shaped in such a way that the γ-rays only see a small scatter surface.*

In order to avoid vibrations, which can result in a worsening of the energy resolution of the Ge, the spectrometer is attached to a flexible suspension (figure 5.3.3).

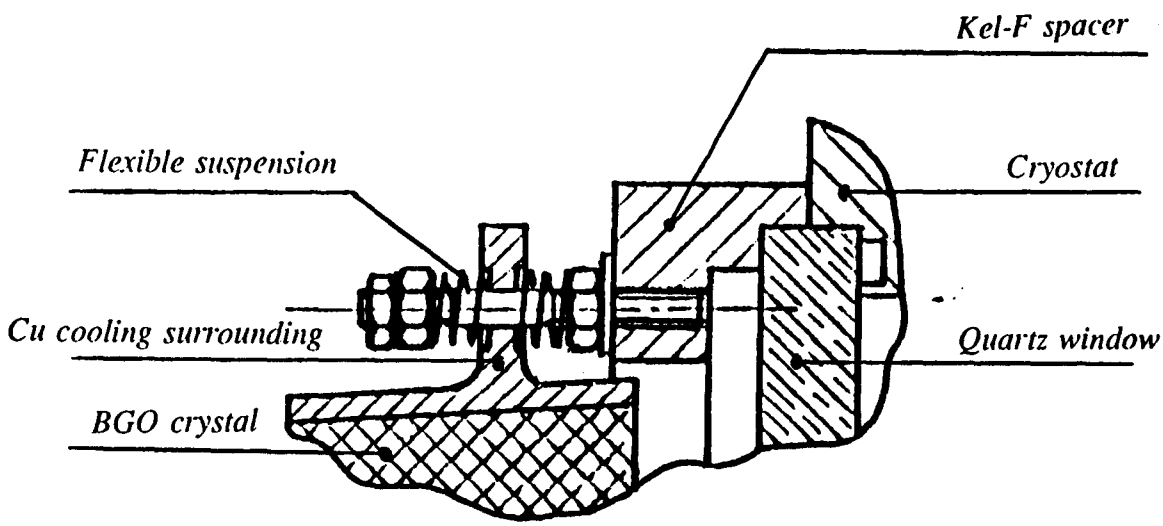

Figure 5.3.3. *The flexible suspension of the Ge-BGO spectrometer. The Kel-F spacer connects the cooled part (T ≈ 100 K) to the cryostat (T ≈ 293 K).*

Conclusions

We used Monte Carlo simulations to optimize the Peak to Total ratio as well as the light yield of the Ge-BGO Compton suppression spectrometer. Calculations of the Peak to Total reveal that:

(1) The wall thickness of the surrounding BGO should be at least 20 mm in order to get sufficient suppression.

(2) Application of a nose BGO is necessary to acquire a high Peak to Total ratio and sufficient suppression of back scattered γ-rays.

(3) The final Ge-BGO configuration has the highest simulated Peak to Total ratio (E_γ = 1.33 MeV; P/T = 0.77) reported until now (1993).

(4) The experimental Peak to Total ratios can be estimated using a correction factor [Bax92]. The estimated "experimental" Peak to Total ratio could even be higher, because we do not have any material between Ge and BGO, although the estimated Peak to Total ratio already exceeds the results acquired by [Bax92]. Therefore, we may be able to achieve also in practice the highest Peak to Total ratio reported until now (1993).

In the determination of the Peak to Total ratio we assumed that the minimum detectable energy deposition inside the BGO amounts to: ΔE = 50 keV. Although the minimum energy deposition may differ from ΔE = 50 keV, the Peak to Total ratios acquired by simulation show no significant variance in Peak to Total ratio for BGO thresholds of: $\Delta E < 100$ keV. Therefore the simulated Peak to Total ratios are valid.

To improve the Peak to Total ratio, we could consider to use an active collimator (scintillator) instead of a passive one (lead). An active collimator will predominantly improve the suppression of back scattered γ-rays, while the acceptable count rate of the spectrometer will decrease. This active collimator should be read out by photodiodes, because of their small size with respect to photomultiplier tubes.

The light yield of the BGO is simulated with a program named LGUIDE, which has got the possibility to simulate crystals with various sizes and different surface treatments.

(5) Comparison between simulations and experiments done for a long rectangular crystal show good agreement if "overall" performances of the crystal are concerned. Therefore, the program LGUIDE may be used to optimize the light yield.

(6) Disadvantage of the program is that it can only describe scintillation crystals with "overall" properties. Since crystals are never homogeneous crystal properties vary with position in the crystal. Disagreement is found between experiments and simulations, when the rectangular crystal is irradiated at different positions, probably caused by the inhomogeneity of the crystal.

(7) For long crystals with specular surfaces the attenuation length of the scintillation photons is of more importance than the surface reflectivity. Since backscattered γ-rays are less energetic, the tapering angle of the nose BGO is larger with respect to the tapering angle of the main BGO in order to acquire an increased light output from the top of the crystal (nose BGO).

(8) Tapering of crystals with specular surfaces results in a higher light output. Tapering can also be used to acquire an uniform light yield from every position within the scintillator.

(9) Crystals with different surface treatments give rise to different light yields. For our BGO veto shield the photon collection of a crystal consisting of specular as well as diffuse surfaces is the best solution.

(10) Differences of crystal quality are simulated by different attenuation lengths of the scintillation photons. For our veto shield the photon collection is largely determined by the attenuation length up to $\lambda = 300$ mm. For attenuation lengths above $\lambda = 300$ mm the light output of our scintillation crystal hardly differs.

(11) The minimum detectable energy deposition in the BGO veto shield amounts to: $\Delta E = 15$ keV.

[Hil86] reports experimentally a significant reduction of the suppression if the BGO threshold is increased from $\Delta E = 15$ keV to $\Delta E = 30$ keV, while calculations showed little variation of the Peak to Total ratio for BGO thresholds below $\Delta E < 100$ keV [Byr85], similar to our simulated results. This reveals the large influence of γ-rays scattered in non detection material. Moreover, it emphasis the importance of the avoided material between Ge and BGO and the minimum detectable energy of $\Delta E = 15$ keV of the BGO veto shield.

The Ge and BGO crystals are within one cryostat. Since the Ge crystal must be operated at temperatures below 110 kelvin, both crystals are cooled. Calculations reveal that:

(12) Polishing of the cryostat materials largely influences the equilibrium temperature which can be reached after long cooling.

(13) We can acquire an equilibrium temperature of 100 kelvin.

(14) The cooling down time needed to operate the Ge crystal amounts to 2-3 days.

(15) The copper cone, which surrounds the BGO crystal may fit exactly around the BGO crystal at room temperature, provided that the thickness of the cone is less than 2 mm.

If experiments show that we are not able to acquire an equilibrium temperature at which the Ge detector can be operated, the application of a IR-filter between BGO and PMT could be considered. According to the calculations this should result in a drop of the equilibrium temperature by 9 kelvin.

References

[Bax92] A.M. Baxter et. al.: *Compton suppression tests on Ge and BGO prototype detectors for GAMMASPHERE* - N.I.M. A317 (1992) 101-110

[Bea92] C.W. Beausang et. al.: *Measurements on prototype Ge and BGO detectors for the Eurogam array* - N.I.M. A313 (1992) 37-49

[Bru87] R. Brun et. al.: *Geant3 User's Guide* - CERN Report No. DD/EE/84-1 - 1987

[Bur92] P. Burger: *Canberra, Olen (Belgium); private communications* - 1992

[Byr85] A.P. Byrne and G.D. Dracoulis: *Monte Carlo calculations for asymmetric NaI(Tl) and BGO Compton suppression shields* - N.I.M. A234 (1985) 281-287

[Bor70] M. Born and E. Wolf: *Principles of optics* - Pergamon press - Oxford (1970)

[Car59] M.S. Carslaw and J.C. Jaeger: *Conduction of Heat in Solids* - Second Edition - Oxford University Press - Great Britain (1959)

[Car90a] C. Carrier and R. Lecomte: *Theoretical modelling of light transport in rectangular parallelepipedic scintillators* - N.I.M. A292 (1990) 685-692

[Car90b] C. Carrier and R. Lecomte: *Effect of geometrical modifications and crystal defects on light collection in ideal rectangular parallelepipedic BGO scintillators* - N.I.M. A294 (1990) 355-364

[Cur92] D. Curien: *Discussion at the Euroball meeting in Simonskall 20-21 march 1992* - CRN Strasbourg

[Der81] S.E. Derenzo: *Monte Carlo calculation of the detection efficiency of arrays of NaI(Tl), BGO, CsF, Ge and plastic detectors for 511 keV photons* - IEEE, Vol NS-28 No. 1 (1981) 131-136

[Der82] S.E. Derenzo and J.K. Riles: *Monte Carlo calculations of the optical coupling between bismuth germanate crystals and photomultiplier tubes* - IEEE Vol. NS-29 No. 1 (1982) 191-195

[Ebe92] Ebert et. al.: *Information presented during Euroball meeting in Simonskall 20-21 march 1992* - Universität of Köln

[Eji89] H. Ejiri and M.J.A. de Voigt: *Gamma-ray and electron spectroscopy in Nuclear Physics* - Pergamon press - Oxford (1989)

[Eks92] L.P. Ekström and A. Nordlund: *Gamma-gamma correlations with detector arrays* - N.I.M. A313 (1992) 421-428

[Eng72] Enge, Wehr and Richards: *Introduction to Atomic Physics* - Addison-Wesley Publishing company, Inc. (1972)

[Eva67] R.D. Evans: *The atomic nucleus* - McGraw-Hill - New York (1967)

[For85] R.L. Ford and W.R. Nelson: *The EGS code system* - SLAC-report No. 210 - Stanford, CA (1985)

[Gra84] B.C. Grabmaier: *Crystal scintillators* - IEEE, Vol NS-31, No. 1 (1984) 372-376

[Gra74] W.A. Gray & R. Müller: *Engineering calculations in radiative heat transfer* - First edition - Pergamon Press Oxford (1974)

[Hec87] E. Hecht: *Optics* - second edition - Addison-Wesley Publishing company Inc. (1987)

[Hei57] W. Heitler: *Quantum theory of radiation* - Third edition - Clarendon Press - Oxford (1957)

[Hil86] L. Hildingsson et. al.: *Transverse BGO Compton suppression shield* - N.I.M. A252 (1986) 91-94

[Hil89] S.K.Hilal et. al.: *Improvement of light coupling in BGO detector module by optimization of the crystal shape* - IEEE Vol. NS 36 No. 1 (1989) 1043-1046

[Hol88] I. Holl et. al.: *A measurement of the light yield of common inorganic scintillators* - IEEE Vol. NS 35 No.1 (1988) 105-109

[Ish86] H. Ishibashi et. al.: *Effect of surface toughness and crystal shape on performance of bismuth germanate scintillators* - Japanese Journal of Applied Physics Vol.25, No. 9 (1986) 1435-1438

[Jun84] A. Junod and C. Roulet: *Heat capacity and thermal conductivity of Bismuth Germanate* ($Bi_4Ge_3O_{12}$) -Journal of Crystal Growth 69 (1984) 138-140

[Kre86] F. Kreith and M.S. Bohn: *Principles of Heat Transfer* - Fourth Edition -Harper & Row Publishers, Inc - New York (1986)

[Kob84] M. Kobayashi et. al.: *Improvement of the longitudinal uniformity in the response of long BGO detectors* - N.I.M. 222 (1984) 458-462

[Kno79] G.F. Knoll: *Radiation detection and measurement* - John Wiley and Sons - New York (1979)

[Kra88] K.S. Krane: *Introductory Nuclear Physics* - Wiley - New York (1988)

[Kut92] D. Kutchin, R.M. Lieder and W. Gast: *The Clover and the Cluster: a simulation calculation to compare their performances* - to be published (1992)

[Leo87] W.R. Leo: *Techniques for nuclear and particle physics experiments (a how to approach)* - Springe-Verlag - Berlin (1987)

[Lie84] R.M. Lieder et. al.: *Design of a Bismuth Germanate anti-Compton spectrometer and its use in nuclear spectroscopy* - N.I.M. 220 (1984) 363-370

[Lor84] Eckart Lorenz: *Recent progress in BGO-development for high resolution calorimetry* - communications with the Max-Planck Institut fuer Physik und Astrophysik - München (1984)

[Los87] Los Alamos Monte Carlo Group: *MCNP* - Los Alamos National Laboratory (1987) report LA-7396-M(rev.)

[Lun88] N. Lund and S. Chang-Quan: *Experiments with light collection from BGO crystals* - unpublished (1988)

[Man92] A. Mangnus: *Eindhoven, University of Technology: measurements done with a long rectangular BGO crystal* - 1992

[Man92a] A. Mangnus: *Eindhoven, University of Technology: internal communications* - 1992

[Mic67] W. Michaelis and H. Küpfer: *A high resolution Ge(Li) Anti-Compton spectrometer for radiative neutron capture spectroscopy* - N.I.M. 56 (1967) 181-188

[Mic86] C. Michel et. al.: *Monte Carlo simulation of complex Gerrmanium detector systems and Compton suppression spectrometers* - N.I.M. A251 (1986) 119-133

[Mic92a] S.L. Micek: *Eindhoven, University of Technology: the program LGUIDE* - 1992

[Mic92b] S.L. Micek: *Eindhoven, University of Technology: the program EURO* - 1992

[Mic92c] S.L. Micek: *Eindhoven, University of Technology: calculation of the light yield versus source position in a long tapered bismuth germanate crystal* - 1992

[Mic92d] S.L. Micek: *Eindhoven, University of Technology: internal communications* - 1992

[Nol85] P.J. Nolan and D.W. Gifford: *The performance of a bismuth germanate escape suppressed spectrometer* -N.I.M. A236 (1985) 95-99

[Nyh85] L. Nyhoff and S. Leestma: *Fortran 77 for Engineers and Scientists* - 2nd edition - Macmillan Publishing Company - New York (1985)

[Pey90] A. von Pey: *Temperature behaviour of a hybride preamplifier* - internal document of the Eindhoven, University of Technology (1990)

[Pil79] H.V. Piltingsrud: *The low-temperature scintillation properties of bismuth germanate and its application to high energy gamma radiation imaging devices* - Journal of Nuclear Medicine 20 (1979) 1279-1285

[Sch90] P. Schram and F. van Ooldenhoven: *Compendium FTV II* - notes reached out during course - Eindhoven, University of Technology (1990)

[Sch92a] P. Schotanus et. al.: *Harshaw QS Scintillation Detectors* - Catalogue (1992)

[Sch92b] P. Schotanus: *Quartz & Silice, de Meern; private communications* - 1992

[Tab87] S.L. Tabor: *BGO suppressed Gamma detector arrays* - N.I.M. B24/25 (1987) 1031-1034

[Tak81] K. Takagi et. al.: *Improvement in the scintillation conversion efficiency of $Bi_4Ge_3O_{12}$ single crystals* - Journal of Crystal Growth 52 (1981) 584-587

[Tou70-1] Y.S. Touloukian et. al.: *Thermophysical properties of matter - Vol. 1 - Thermal conductivity - metallic elements and alloys* - IFI/Penum - New York (1970)

[Tou70-3] Y.S. Touloukian et. al.: *Thermophysical properties of matter - Vol. 3 - Thermal conductivity - non -metallic liquids and gases* - IFI/Penum - New York (1970)

[Tou70-4] Y.S. Touloukian et. al.: *Thermophysical properties of matter - Vol. 4 - Specific Heat - metallic elements and alloys* - IFI/Penum - New York (1970)

[Tou75-10] Y.S. Touloukian et. al.: *Thermophysical properties of matter - Vol. 10 - Thermal diffusivity* - IFI/Penum - New York (1970/1975)

[Tou75-13] Y.S. Touloukian et. al.: *Thermophysical properties of matter - Vol. 13 - Thermal expansion - metallic elements and alloys* - IFI/Penum - New York (1975)

[Unr84] W.P. Unruh and R.A. Murray: *Light scattering from the substructure of Bismuth Germate* - IEEE Vol NS-31 No.1 (1984) 377-380

[Ver91] B.A.W. Verhoef: *Development of a compact anti-Compton spectrometer* - report on graduate study at the Eindhoven, University of Technology (1991)

[Ver92] P. Vermeulen: *Canberra, Olen (Belgium); private communications* - 1992

[Wea88] Robert C. Weast, Ph.D.: *CRC Handbook of Chemistry and Physics* - First student edition - Boca Raton (1988)

[Web73] M.J. Weber, R.R. Monchamp: *Luminescence of $Bi_4Ge_3O_{12}$: Spectral and decay properties* - Journal of Applied Physics Vol. 44 No 12 (1973) 5495-5499

[Xi 89] T.G. Xi et. al.: *Thermal properties of bismuth germanate $Bi_4Ge_3O_{12}$* - Journal of material science letters 8 (1989) 1317-1319

[Zha90] N. Zhang et. al.: *Study of a large BGO crystal in a charged particle beam* - IEEE Vol. NS-37, No. 2 (1990) 216-219

[Zuc89] A. Zuchiatti et. al.: *Temperature behaviour of a BGO prototype for use on a 4π high energy spectrometer* - N.I.M. A281 (1989) 341-345

Abbreviations

N.I.M.	Nuclear Intruments and Methods in Physics Research
IEEE	IEEE Transactions on Nuclear Science

Appendix A Drawings of the Compton suppression spectrometer

pos. nr.	aantal	benaming	materiaal	tekeningnr.	opmerkingen
35	3	moer zesk. M12	St vern.		
34	3	sluitring M12	St. vern.		
33	3	arm		KFT-00-24-A2	
32	1	Cry-geleider		KFT-00-18-A3	
31	1	vacuumleiding		KFT-00-23-A2	
30	3	inbusbout M8×30	St.		
29	3	klemblok		KFT-00-06-A4	
28	6	inbusbout M6×15	St		
27	6	sluitring M6	St. vern.		
26	3	stelschroef M8×8	St.		
25	1	draagring II		KFT-00-22-A2	
24	3	koppelstang		KFT-00-21-A2	
23	1	magnetic shield			
22	1	Photomultiplier tube			
21	1	versterker			
20	2	cil. kopschr. M5×10	St.vern.		
19	4	sluitring M5	St.vern.		
18	1	flens		KFT-00-05-A4	
17	3	sluitring M14	St. vern.		
16	1	draagring I		KFT-00-30-A1	
15	1	venster		KFT-00-17-A3	
14	12	cil. kopschr. M3×12	r.v.s.		
13	1	isolator		KFT-00-20-A2	
12	13	sluitring M4	r.v.s.		
11	8	stelstift		KFT-00-04-A4	
10	16	drukveer	St.	D11650 TEVEMA	in sectie aanw.
9	8	moer zesk. M3	r.v.s.		
8	8	stelmoer		KFT-00-03-A4	
7	3	cil. kopschr. M2×5	r.v.s.		
6	1	stelring			
5	11	sluitring M3	r.v.s.		
4	3	cil. kopschr. M3×8	r.v.s.		
3	1	collimator		KFT-00-16-A3	
2	1	contactring			
1	1	Ge. detector			

Stuklijst voor: Compact Ge-BGO Compton Suppression Spectrometer

Technische Hogeschool Eindhoven Faculteit: N Groep: KFT	36l. 61 Get. Jm. Gec.	Datum 27-8-92	Tekeningnr. KFT-00-00 Wijziging	Formaat A4

NDC 881114

pos. nr.	aantal	benaming	materiaal	tekeningnr.	opmerkingen
70	1	Compton shield			
69	3	stelschroef		KFT-00-15-A4	
68	3	borgmoer		KFT-00-14-A4	
67	3	draadbus		KFT-00-13-A4	
66	12	verz. kopscht. M3x6	st. verz.		
65	3	bladveer			
64	1	sluitkap		KFT-00-33-A1	
63	4	bladveer		KFT-00-12-A4	
62	1	inbusbout M6x25	f.v.s.		
61	4	inbusbout M8x20	st.		
60	2	steunplaat		KFT-00-28-A2	
59	1	O-ring MRC 265	VITON	ERIKS	in sectie aanw.
58	1	O-ring MRC 123	VITON	ERIKS	in sectie aanw.
57	1	quadring MRC 4431	BUNA	ERIKS	in sectie aanw.
56	1	O-ring MRC. 253	VITON	ERIKS	in sectie aanw.
55	2	inbusbout M6x15	st.		
54	1	vacuumleiding		KFT-00-32-A1	
53	1	grondplaat		KFT-00-31-A1	
52	1	Cry. geleider		KFT-00-35-A2	
51	6	spacer		KFT-00-11-A4	
50	3	inbusbout M6x15	f.v.s.		
49	12	cil. kopscht. M3x20	f.v.s.		
48	2	O-ring MRC 230	VITON	ERIKS	in sectie aanw.
47	1	vacuumleiding		KFT-00-26-A2	
46	1	Cryo-geleider		KFT-00-10-A4	
45	1	klemband		KFT-00-25-A2	
44	4	sluitring M8	st. vern.		
43	4	moer zesk. M8	st. vern.		
42	1	inbusbout M8x35	st		
41	1	dewar		Canberra	
40	3	drukschijf		KFT-00-09-A4	
39	6	drukstuk 5-25	st.	DIN 6371	
38	3	draadplaat		KFT-00-08-A4	
37	6	verz. kopscht. M4x10	st. vern.		
36	3	stelbout		KFT-00-07-A4	

Stuklijst: Compact Ge-BGO Compton Suppression Spectrometer

Technische Hogeschool Eindhoven Faculteit: N Groep: KFT	36 bl. 2	Datum 27/1/92	Tekeningnr. KFT-00-00	Formaat A4
	Get. GM.			
	Gec.		Wijziging	

NDC 881114

pos. nr.	aantal	benaming	materiaal	tekeningnr.	opmerkingen
79	4	cil. kopschr. M4x6	r.v.s.		
78	2	sluiting M6	r.v.s.		
77	1	Cryo-koppeling	Cu.	canberra	in groep KFT aanw.
76	1	meetdoorvoer			
75	1	HV doorvoer			
74	8	cil. kopschr. M4x20	r.v.s.		
73	2	klemband		KFT-00-29-A2	
72	1	Be. Venster			
71	1	BGO-houder			

Stuklijst voor: Compact Ge-BGO Compton Suppression Spectrometer

Technische Hogeschool Eindhoven
Faculteit: N
Groep: KFT

36 bl. bl.3 | Datum 27/8/92 | Tekeningnr. KFT-00-00 | Formaat A4
Get.: JM
Gec.:
Wijziging

NDC 881114

The drawings of the seperate parts can be retrieved from P. Magendans: tel. 040- 474095

Appendix B The program GeBGO.for

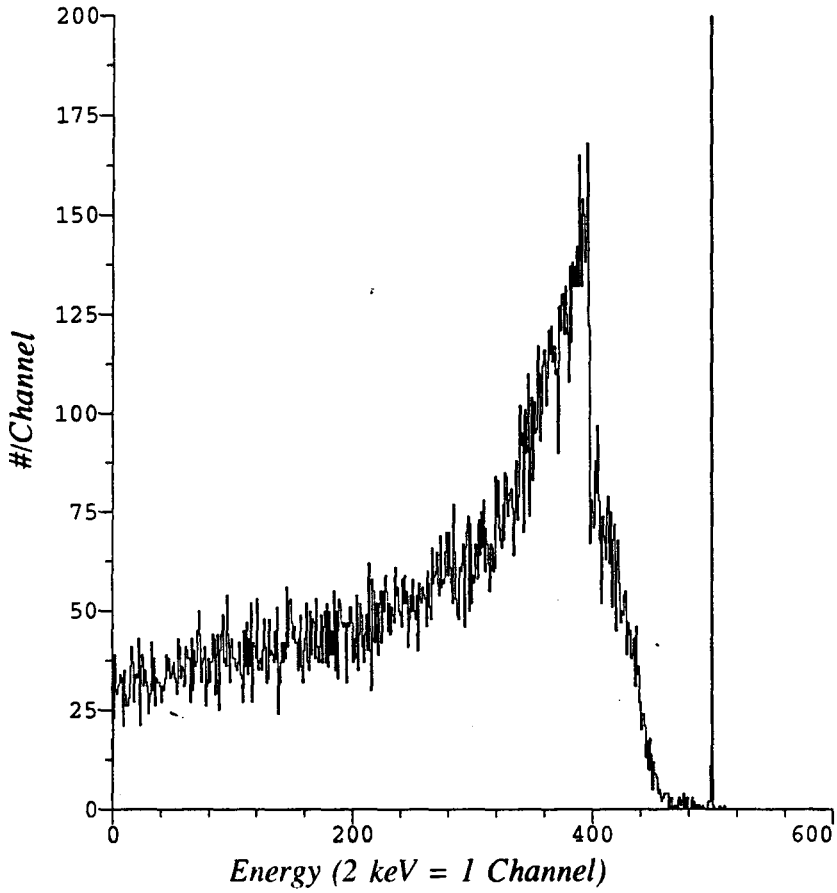

Figure B.1. *Unsuppressed spectrum.*

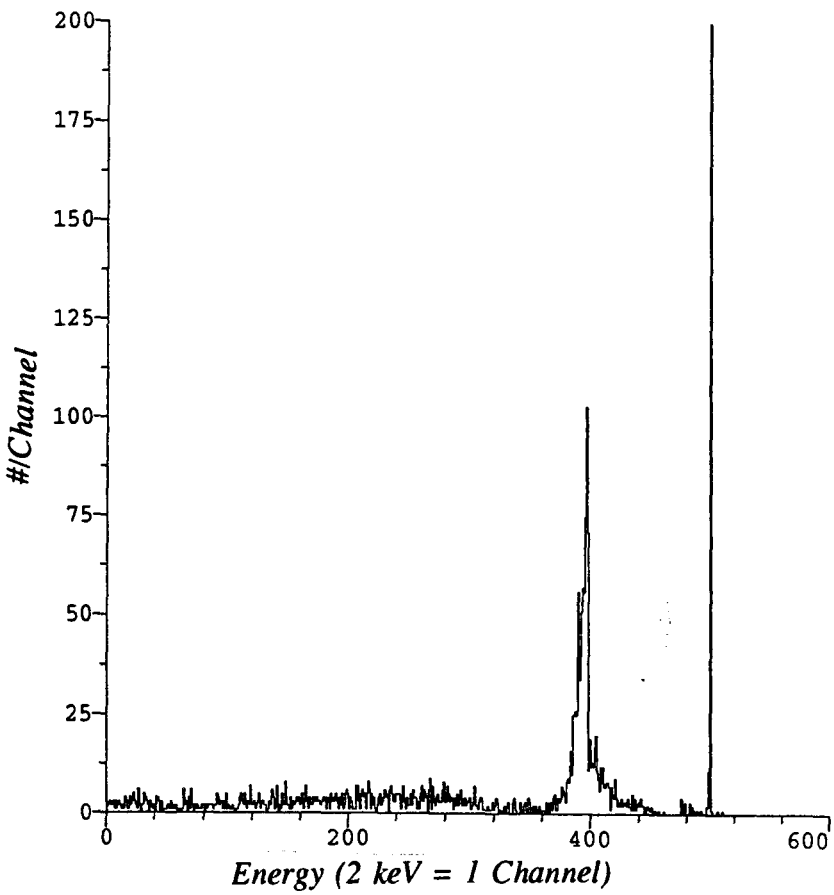

Figure B.2. *Suppressed spectrum.*

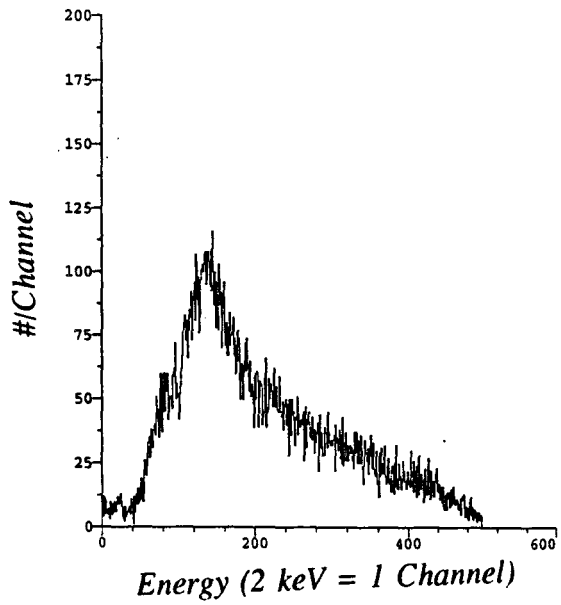

Figure B.3. *Energy spectrum of the main BGO.*

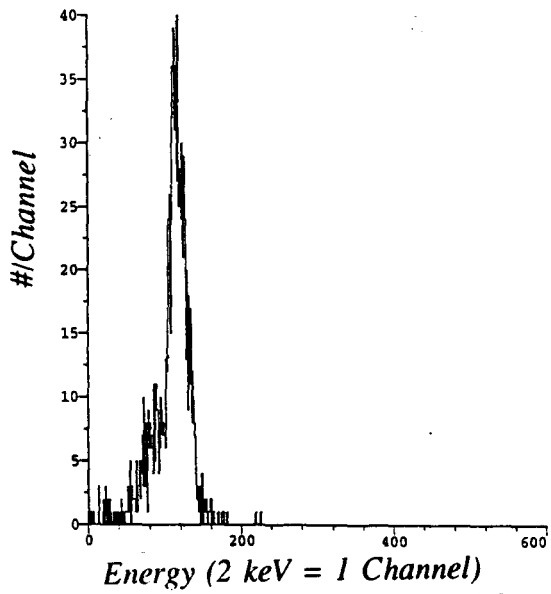

Figure B.4. *Energy spectrum of the nose BGO.*

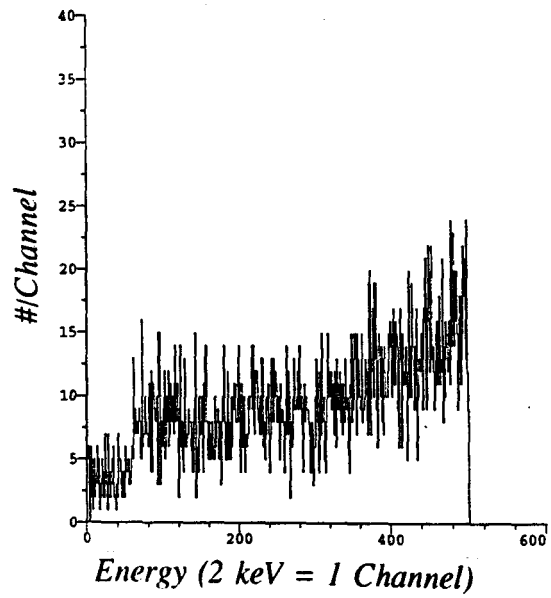

Figure B.5. *Energy spectrum of the back BGO.*

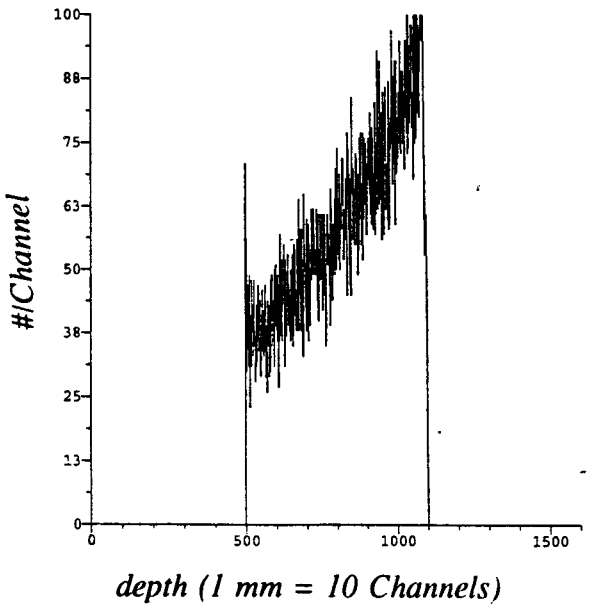

Figure B.6. *First interaction versus depth in the Ge crystal.*

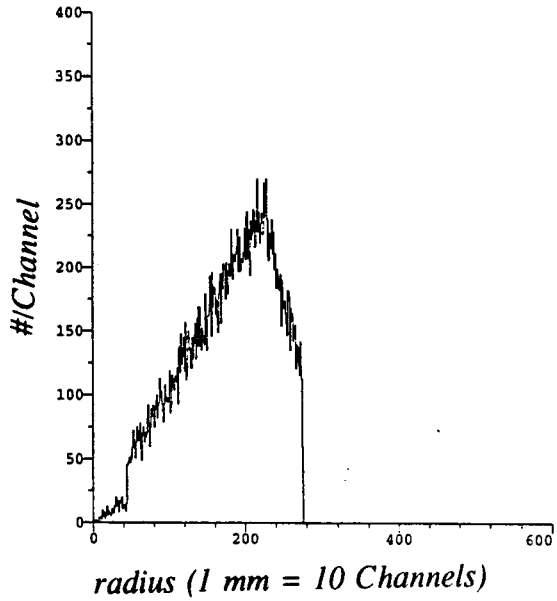

Figure B.7. *First interaction versus radius in the Ge crystal.*

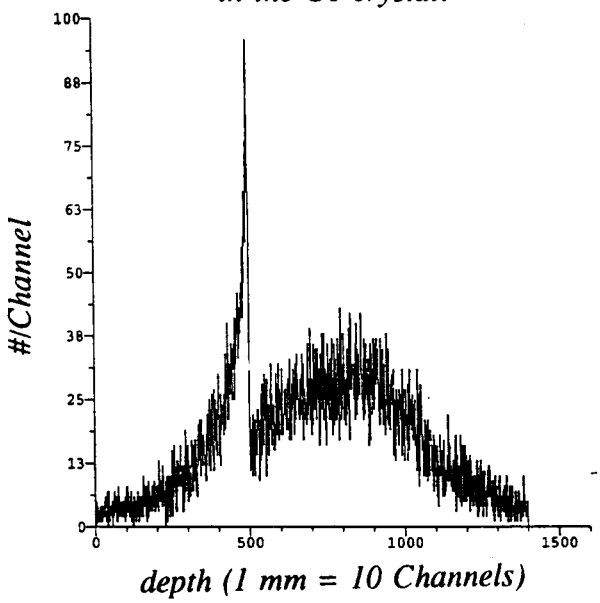

Figure B.8. *First interaction versus depth in the BGO crystal.*

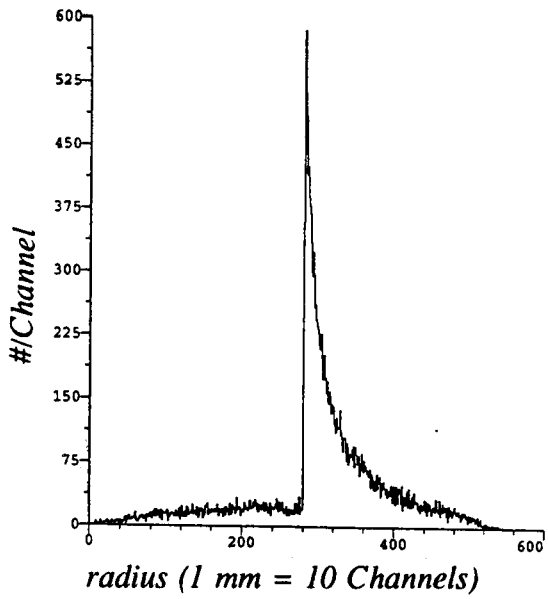

Figure B.9. *First interaction versus radius in the BGO crystal.*

```
C-----------------------------------------------------------------------
C    I ---- Program GEBGO-----                                        I
C    I Program to calculate response of Ge+BGO composite detector:      I
C    I - one Ge cristal ('tube' shape, inner radius = 0.0) with a       I
C        core hole of vacuum;                                          I
C    I - two BGO cristals :                                            I
C    I   - first: 'main' ('conical' shape);                            I
C    I   - second: 'back' ('tube' shape);                              I
C    I   - third: 'nose' ('tube' shape);                               I
C    I - point-like source of different source of radiation            I
C    I   (default: gammas) with defined energy & width (gaussian shape); I
C    I - all secondaries particles included !!!!!!                     I
C    I - results written in PAX-format event file ( 10 descriptors):   I
C    I    - 1: energy deposit in Ge cristal (max.  16.382 MeV),        I
C    I    - 2: energy deposit in BGO-main   (max.  16.382 MeV),        I
C    I    - 3: energy deposit in BGO-back   (max.  16.382 MeV),        I
C    I    - 4: energy deposit in BGO-nose   (max.  16.382 MeV),        I
C    I    - 5: first interaction in Ge  - radius  (max. 81.91 cm ),    I
C    I    - 6: first interaction in Ge  - zet     (max. 81.91 cm ),    I
C    I    - 7: first interaction in BGO - radius  (max. 81.91 cm ),    I
C    I    - 8: first interaction in BGO - zet     (max. 81.91 cm ),    I
C    I    - 9: escape - radius  (max. 81.91 cm ),                      I
C    I    -10: escape - zet     (max. 81.91 cm ),                      I
C    I                                                                 I
C    I Author: Antek Buda, KVI - Groningen / IBJ - Swierk              I
C    I Version: 27-02-1992                                             I
C    I Revised: 06-05-1992       Yves Wintraecken, Cyclotron, TUE      I
C    I                                                                 I
C    -----------------------------------------------------------------
     PROGRAM MAIN
C
     REAL*4 ETRAN,WIDTH,DIST,RILU,GERA,GELE,BMTI,BMTO,
    *       BMBI,BMBO,BMLE,BBRA,BBLE,BNTI,BNTO,BNBI,BNBO,BNLE,
    *       AIRA,AILE
     INTEGER*4 IPAR,MONO,IPLA,IAS,IMAG,IFIE,ITWI,IHIT,ONLY,IRIN
     PARAMETER (NG=100000,NH=10000)
     DIMENSION NHIT(6)
     COMMON//H(NH)
     COMMON/GCBANK/Q(NG)
     COMMON /USER/ ETRAN,WIDTH,DIST,RILU,GERA,GELE,BMTI,BMTO,
    *              BMBI,BMBO,BMLE,BBRA,BBLE,BNTI,BNTO,AIRA,AILE
     COMMON /CONTROL/ IPAR,MONO,IPLA,IAS,IMAG,IFIE,ITWI,IHIT,ONLY,IRIN
C
C    ALLOCATE MEMORY FOR ZEBRA
     CALL GZEBRA(NG)
C
C    INITIALIZATION PHASE
```

```
      CALL UGINIT
C
C     PROCESSING PHASE
      CALL GRUN
C
C     TERMINATION PHASE
      CALL UGLAST
C
      STOP
      END
C
      SUBROUTINE UGINIT
C.    ------------------------------------------------------------------
C.    I                                                                I
C.    I     i n i t i a l i s a t i o n                                I
C.    I                                                                I
C.    ------------------------------------------------------------------
C
      IMPLICIT NONE
      INCLUDE 'CERN_GEANT:GEANT (GCLIST)'
      INCLUDE 'CERN_GEANT:GEANT (GCPHYS)'
      INCLUDE 'CERN_GEANT:GEANT (GCCUTS)'
      CHARACTER*20 FNAME,FILE,STRING
      INTEGER   M,CONTEXT,PUTEVENT_OPEN
      INTEGER*4 IPAR,SEED,NE,NTH,NX,NY,NZ,IAS,IMAG,IFIE,ITWI,I,J,K,L,
     *          MONO,IPLA,IHIT,ONLY,IRIN
      REAL*4 ETRAN,WIDTH,DIST,RILU,GERA,GELE,BMTI,BMTO,
     *       BMBI,BMBO,BMLE,BBRA,BBLE,BNTI,BNTO,BNBI,BNBO,BNLE,
     *       AIRA,AILE,TIMER
      COMMON /USER/ ETRAN,WIDTH,DIST,RILU,GERA,GELE,BMTI,BMTO,
     *              BMBI,BMBO,BMLE,BBRA,BBLE,BNTI,BNTO,BNBI,BNBO,BNLE,
     *              AIRA,AILE
      COMMON /CONTROL/ IPAR,MONO,IPLA,IAS,IMAG,IFIE,ITWI,IHIT,ONLY,IRIN
      COMMON /FILE/ FILE,CONTEXT
      COMMON /SEED/ SEED
C             initialize variables
      CALL GINIT
      SEED=SECNDS(TIMER)
C
C
      write(*,*) 'Event Output File :'
      read(*,'(a)') file
      write(*,'(a)') file
C
      M = PUTEVENT_OPEN(CONTEXT,4096,FILE)
      IF (.NOT.M) CALL LIB$SIGNAL(%VAL(M))
c
```

```
C         output header,  information about user cards
      WRITE (*,1000)
      WRITE (*,1001)
C
C         energy cuts for tracking
      CUTGAM=0.000011          ! kinetic energy cut for gammas (11keV)
      CUTELE=0.000011          ! kinetic energy cut for electrons (11keV)
C         define user data cards, read data cards
      CALL GUFFGO
      CALL GFFGO
C
C         information about user cards values used in run
      WRITE (*,1000)
      WRITE (*,1003) IPAR,ETRAN,WIDTH,DIST,RILU,GERA,GELE,
     +               BMTI,BMTO,BMBI,BMBO,BMLE,BBRA,BBLE,
     +               BNTI,BNTO,BNBI,BNBO,BNLE,AIRA,AILE
      ETRAN = ETRAN*1.0E-03                    ! from MeV to GeV
      WIDTH = WIDTH*1.0E-02                    ! from % to absolute
      WIDTH = WIDTH/(2.0*SQRT(2.0*ALOG(2.0)))  ! from FWHM to sigma
C
      GELE = GELE/2.0
      BMLE = BMLE/2.0
      BBLE = BBLE/2.0
      BNLE = BNLE/2.0
      AILE = AILE/2.0
C
C         initialize data structures
      CALL GZINIT
C
C
C  define particles, materials, tracking media, geometry, detectors ...
      CALL GPART
      CALL GUMATE
      CALL GUGEOM
      CALL GPHYSI
      CALL GDINIT
C
      IF (LPRIN(1) .NE. 0) THEN
C       CALL GPRINT ('VOLU',0)
C       CALL GPRINT ('ROTM',0)
C       CALL GPRINT ('MATE',0)
C       CALL GPRINT ('TMED',0)
        CALL GPPART(IPAR)
      ENDIF
C
C
      RETURN
```

```
 1000 FORMAT
     +(' GEANT ================================================== T',/)
 1001 FORMAT (/,' Following user cards are defined:    /default/',/
     +,' PART  - particle type /1=gamma/',/
     +,' ETRA  - energy of the particle [MeV]  /1.173/',/
     +,' FWHM  - energy width (DE/E) [%]  /0.0/',/
     +,' DIST  - distance to the front face of Ge /15.0/',/
     +,' RILU  - radius of illuminated area on Ge surface',/
     +,'         (if RILU=0 then GERA) /0.0/',/
     +,' GERA  - radius of Ge cristal /2.5/',/
     +,' GELE  - length of Ge cristal /5.0/',/
     +,' BMTI  - inner radius (at the top) of main BGO /2.5/',/
     +,' BMTO  - outer radius (at the top) of main BGO /4.5/',/
     +,' BMBI  - inner radius (at the bottom) of main BGO /2.5/',/
     +,' BMBO  - outer radius (at the bottom) of main BGO /4.5/',/
     +,' BMLE  - length of main BGO /10.0/',/
     +,' BBRA  - radius of back BGO /2.5/',/
     +,' BBLE  - length of back BGO /5.0/',/
     +,' BNTI  - inner radius (at the top) of nose BGO /2.0/',/
     +,' BNTO  - outer radius (at the top) of nose BGO /2.0/',/
     +,' BNBI  - inner radius (at the bottom) of nose BGO /2.0/',/
     +,' BNBO  - outer radius (at the bottom) of nose BGO /3.5/',/
     +,' BNLE  - length of nose BGO /2.0/',/
     +,' AIRA  - radius of air core inside Ge /0.9/',/
     +,' AILE  - length of air core inside Ge /3.5/',/)
C
 1002 FORMAT(10(1X,F5.2))
 1003 FORMAT (/,' User cards used in this run:',/
     +,' PART = ',I2,/
     +,' ETRA = ',F6.3,/
     +,' FWHM = ',F6.2,/
     +,' DIST = ',F5.1,/
     +,' RILU = ',F4.1,/
     +,' GERA = ',F4.1,/
     +,' GELE = ',F4.1,/
     +,' BMTI = ',F4.1,/
     +,' BMTO = ',F4.1,/
     +,' BMBI = ',F4.1,/
     +,' BMBO = ',F4.1,/
     +,' BMLE = ',F4.1,/
     +,' BBRA = ',F4.1,/
     +,' BBLE = ',F4.1,/
     +,' BNTI = ',F4.1,/
     +,' BNTO = ',F4.1,/
     +,' BNBI = ',F4.1,/
     +,' BNBO = ',F4.1,/
     +,' BNLE = ',F4.1,/
```

```
     +,' AIRA = ',F4.1,/
     +,' AILE = ',F4.1,/)
      END
C=====================================================================
C
C
       SUBROUTINE UGLAST
C.    7------------------------------------------------------------------
C.    I                                                          I
C.    I    user-supplied termination routine                        I
C.    I                                                          I
C.    ------------------------------------------------------------------
C
C                 standard termination routine
      IMPLICIT NONE
      CHARACTER*20 FILE
      INTEGER M,CONTEXT,PUTEVENT_CLOSE
      INTEGER*4 MINY
      COMMON /FILE/ FILE,CONTEXT
C
      CALL GLAST
C
      M = PUTEVENT_CLOSE(CONTEXT)
      IF(.NOT.M) CALL LIB$SIGNAL(%VAL(M))
      RETURN
      END
C=====================================================================
C
      SUBROUTINE GUFFGO
C.    7------------------------------------------------------------------
C.    I                                                          I
C.    I  Define user steering cards                               I
C.    I                                                          I
C.    ------------------------------------------------------------------
C
      IMPLICIT NONE
      INTEGER*4 IPAR,IAS,IMAG,IFIE,ITWI,MONO,IPLA,IHIT,ONLY,IRIN
      REAL*4 ETRAN,WIDTH,DIST,RILU,GERA,GELE,BMTI,BMTO,
     *       BMBI,BMBO,BMLE,BBRA,BBLE,BNTI,BNTO,BNBI,BNBO,BNLE,
     *       AIRA,AILE
      COMMON /USER/ ETRAN,WIDTH,DIST,RILU,GERA,GELE,BMTI,BMTO,
     *              BMBI,BMBO,BMLE,BBRA,BBLE,BNTI,BNTO,BNBI,BNBO,BNLE,
     *              AIRA,AILE
      COMMON /CONTROL/ IPAR,MONO,IPLA,IAS,IMAG,IFIE,ITWI,IHIT,ONLY,IRIN
      DATA IPAR    /1/
      DATA ETRAN   /1.173/
      DATA WIDTH   /0.0/
```

```
      DATA DIST   /15.0/
      DATA RILU   /0.0/
      DATA GERA   /2.5/
      DATA GELE   /5.0/
      DATA BMTI   /2.5/
      DATA BMTO   /5.0/
      DATA BMBI   /2.5/
      DATA BMBO   /5.0/
      DATA BMLE   /10.0/
      DATA BBRA   /2.5/
      DATA BBLE   /5.0/
      DATA BNTI   /2.0/
      DATA BNTO   /2.0/
      DATA BNBI   /2.0/
      DATA BNBO   /3.5/
      DATA BNLE   /2.0/
      DATA AIRA   /0.9/
      DATA AILE   /3.5/
C
      CALL FFKEY('PART',IPAR,1,'INT ')
      CALL FFKEY('ETRA',ETRAN,1,'REAL')
      CALL FFKEY('FWHM',WIDTH,1,'REAL')
      CALL FFKEY('DIST',DIST,1,'REAL')
      CALL FFKEY('RILU',RILU,1,'REAL')
      CALL FFKEY('GERA',GERA,1,'REAL')
      CALL FFKEY('GELE',GELE,1,'REAL')
      CALL FFKEY('BMTI',BMTI,1,'REAL')
      CALL FFKEY('BMTO',BMTO,1,'REAL')
      CALL FFKEY('BMBI',BMBI,1,'REAL')
      CALL FFKEY('BMBO',BMBO,1,'REAL')
      CALL FFKEY('BMLE',BMLE,1,'REAL')
      CALL FFKEY('BBRA',BBRA,1,'REAL')
      CALL FFKEY('BBLE',BBLE,1,'REAL')
      CALL FFKEY('BNTI',BNTI,1,'REAL')
      CALL FFKEY('BNTO',BNTO,1,'REAL')
      CALL FFKEY('BNBI',BNBI,1,'REAL')
      CALL FFKEY('BNBO',BNBO,1,'REAL')
      CALL FFKEY('BNLE',BNLE,1,'REAL')
      CALL FFKEY('AIRA',AIRA,1,'REAL')
      CALL FFKEY('AILE',AILE,1,'REAL')
C
      RETURN
      END
C=======================================================================
C
      SUBROUTINE GUMATE
C.    7------------------------------------------------------------------
```

```
C.    I                                                    I
C.    I Define parameters of default  media (same as in GEXAM2 1.15)    I
C.    I Medium numbers are kept the same as material numbers            I
C.    I                                                    I
C.    ------------------------------------------------------------------
C
      IMPLICIT NONE
      REAL*4 AGER,ZGER,WGER,ABGO(3),ZBGO(3),WBGO(3)
      REAL*4 FIELDM,TMAXFD,DMAXMS,DEEMAX,EPSIL,STMIN,UBUFF
      REAL*4 ETRAN,WIDTH,DIST,RILU,GERA,GELE,BMTI,BMTO,
     *       BMBI,BMBO,BMLE,BBRA,BBLE,BNTI,BNTO,BNBI,BNBO,BNLE,
     *       AIRA,AILE
      INTEGER*4 ISENS1,ISENS0,IFIELD0,IFIELD1,NWBUFF
      INTEGER*4 IPAR,IAS,IMAG,IFIE,ITWI,MONO,IPLA,IHIT,ONLY,IRIN
      COMMON /USER/ ETRAN,WIDTH,DIST,RILU,GERA,GELE,BMTI,BMTO,
     *            BMBI,BMBO,BMLE,BBRA,BBLE,BNTI,BNTO,BNBI,BNBO,BNLE,
     *            AIRA,AILE
      COMMON /CONTROL/ IPAR,MONO,IPLA,IAS,IMAG,IFIE,ITWI,IHIT,ONLY,IRIN
C
C     BGO cristal- Bi4Ge3O12
C                  Bi     Ge      O
      DATA ABGO /208.982 ,72.59 ,15.999/
      DATA ZBGO / 83.    ,32.   , 8.  /
      DATA WBGO /  4.    , 3.   ,12.  /
C
C     Germanium cristal
C                  Ge
      DATA AGER / 72.59 /
      DATA ZGER / 32.   /
      DATA WGER /  1.   /
C
C     medium parameters same as in GEXAM2 1.15
      ISENS1 = 1                ! sensitivity flag
      ISENS0 = 0                ! sensitivity flag
      IFIELD0 = 0               ! no magnetic field
      IFIELD1 = 1               ! inhomogeneous magnetic field
      FIELDM = 0.               ! maximum field value
      TMAXFD = 0.               ! maximum angle due to field
      DMAXMS = 0.5              ! maximum step due to multipl. scatt.
      DEEMAX = 0.2              ! maximum fractional energy loss/step
      EPSIL  = 0.01             ! tracking precision
      STMIN  = 0.2              ! minimum step
      UBUFF  = 0.               ! additional user parameters
      NWBUFF = 0                ! number of UBUFF parameters
C
C     Definition of materials
      CALL GMATE                ! define standard materials
```

```
      CALL GSMIXT (17,'GE$',  AGER,ZGER,5.350,-1,WGER)
      CALL GSMIXT (18,'BGO$',  ABGO,ZBGO,7.13 ,-3,WBGO)
C
C     Definition of media
      CALL GSTMED (15,'AIR$'    ,    15,ISENS1
     + ,IFIELD0,FIELDM,TMAXFD,DMAXMS,DEEMAX,EPSIL,STMIN,UBUFF,NWBUFF)
      CALL GSTMED (16,'VACCUM$',    16,ISENS0
     + ,IFIELD0,FIELDM,TMAXFD,DMAXMS,DEEMAX,EPSIL,STMIN,UBUFF,NWBUFF)
      CALL GSTMED (17,'GE$'     ,    17,ISENS1
     + ,IFIELD0,FIELDM,TMAXFD,DMAXMS,DEEMAX,EPSIL,STMIN,UBUFF,NWBUFF)
      CALL GSTMED (18,'BGO$'    ,    18,ISENS1
     + ,IFIELD0,FIELDM,TMAXFD,DMAXMS,DEEMAX,EPSIL,STMIN,UBUFF,NWBUFF)
C
      RETURN
      END
C=======================================================================
C
      SUBROUTINE GUGEOM
C.    ------------------------------------------------------------------
C.    I                                                          I
C
      IMPLICIT NONE
      CHARACTER*4 KONLY
      REAL*4 ETRAN,WIDTH,DIST,RILU,GERA,GELE,BMTI,BMTO,
     *       BMBI,BMBO,BMLE,BBRA,BBLE,BNTI,BNTO,BNBI,BNBO,BNLE,
     *       AIRA,AILE
      REAL*4 PHALL(3),PGE(3),PBGOM(5),PBGOB(3),PBGON(5),PAIRCORE(3)
      REAL*4 RCEN,XCEN,YCEN,ZCEN,BASE
      INTEGER*4 IPAR,IAS,IMAG,IFIE,ITWI,MONO,IPLA,IHIT,ONLY,IRIN
      INTEGER*4 IBAF,IVOLM1,IVOLM2,IVOLM3,IVOLM4,IVOLM5,IVOLM6,IVOLM7,
     *          IVOLM8,IVOLM9,IVOLM10,IVOLM11,IVOLM12,IVOLM13,NEVE
      COMMON /USER/ ETRAN,WIDTH,DIST,RILU,GERA,GELE,BMTI,BMTO,
     *              BMBI,BMBO,BMLE,BBRA,BBLE,BNTI,BNTO,BNBI,
     *              BNBO,BNLE,AIRA,AILE
      COMMON /CONTROL/ IPAR,MONO,IPLA,IAS,IMAG,IFIE,ITWI,IHIT,ONLY,IRIN
      COMMON/NEVE/ NEVE
      COMMON /BASE/ BASE
      DATA PHALL /  7.5,  7.5,  40./     ! "ROOM"
C
C     Germanium
C
      PGE(1) = 0.0
      PGE(2) = GERA
      PGE(3) = GELE
C
C     BGO main
C
```

```
      PBGOM(1) = BMLE
      PBGOM(2) = BMTI
      PBGOM(3) = BMTO
      PBGOM(4) = BMBI
      PBGOM(5) = BMBO
C
C     BGO back
C
      PBGOB(1) = 0.0
      PBGOB(2) = BBRA
      PBGOB(3) = BBLE
C
C     BGO nose
C
      PBGON(1) = BNLE
      PBGON(2) = BNTI
      PBGON(3) = BNTO
      PBGON(4) = BNBI
      PBGON(5) = BNBO
C
C     AIR core
C
      PAIRCORE(1) = 0.0
      PAIRCORE(2) = AIRA
      PAIRCORE(3) = AILE
C
C
      CALL GSROTM (1,90.0,0.0,90.0,90.0,0.0,0.0) ! MaRS
      CALL GSVOLU ('ROOM','BOX ',15,PHALL, 3,IVOLM1)
      CALL GSVOLU ('GERM','TUBE',17,PGE  , 3,IVOLM2)
      CALL GSVOLU ('BGOM','CONE',18,PBGOM ,5,IVOLM3)
      CALL GSVOLU ('BGOB','TUBE',18,PBGOB ,3,IVOLM4)
      CALL GSVOLU ('BGON','CONE',18,PBGON ,5,IVOLM5)
      CALL GSVOLU ('AIRCORE','TUBE',16,PAIRCORE,3,IVOLM6)
C
C     Germanium
C
      XCEN = 0.0
      YCEN = 0.0
      ZCEN = DIST + GELE
      CALL GSPOS('GERM',1,'ROOM',XCEN,YCEN,ZCEN,1,'MANY')
C
      BASE = DIST + 2.*( GELE + BBLE)
C
C     BGO main
C
      ZCEN = BASE - BMLE
```

```
      CALL GSPOS('BGOM',1,'ROOM',XCEN,YCEN,ZCEN,1,'ONLY')
C
C     BGO back
C
      ZCEN = BASE -  BBLE
      CALL GSPOS('BGOB',2,'ROOM',XCEN,YCEN,ZCEN,1,'ONLY')
C
C     BGO nose
C
      ZCEN = BASE - (2*BMLE + BNLE)
      CALL GSPOS('BGON',3,'ROOM',XCEN,YCEN,ZCEN,1,'ONLY')
C
C     AIR core
C
      ZCEN = BASE - (2*BBLE + AILE)
      CALL GSPOS('AIRCORE',3,'ROOM',XCEN,YCEN,ZCEN,1,'ONLY')
C
C
      CALL GGCLOS    ! close geometry definition (obligatory system routine)
C
      RETURN
      END
C=======================================================================
C
      SUBROUTINE GUKINE
C.    ------------------------------------------------------------------
C.    I                                                                I
C.    I   Generates kinematics for primary particles.                  I
C.    I                                                                I
C.    ------------------------------------------------------------------
C
      IMPLICIT NONE
      INCLUDE 'CERN_GEANT:GEANT (GCBANK)'
      INCLUDE 'CERN_GEANT:GEANT (GCLIST)'
      INCLUDE 'CERN_GEANT:GEANT (GCFLAG)'
      REAL*4 PPLAB(3),PELAB(3),VERTZER(3),R(2),MTH$RANDOM,EDIS,THDIS,
     *       PHIRP,THERP,PHIRE,THERE,THEMAX,DCS,XM,PP,PE,THPAIR,PHPAIR,
     *       THPOS,PHPOS,THELE,PHELE,GAUSS,DUMMY
      REAL*4 ETRAN,WIDTH,DIST,RILU,GERA,GELE,BMTI,BMTO,
     *       BMBI,BMBO,BMLE,BBRA,BBLE,BNTI,BNTO,BNBI,BNBO,
     *       BNLE,AIRA,AILE
      REAL*4 EDEP,ZET,EKINP,EKINE,RAD,GERFIR,BGOFIR,ESC
      LOGICAL*1 THETOPEN
      INTEGER*4 JPA,NVERT,NTRACK,IDET,SEED,ITRTYP,IENE,ICH
      INTEGER*4 IPAR,NE,NTH,IAS,IMAG,IFIE,ITWI,MONO,IPLA,IHIT,ONLY,IRIN
      COMMON /USER/ ETRAN,WIDTH,DIST,RILU,GERA,GELE,BMTI,BMTO,
     *              BMBI,BMBO,BMLE,BBRA,BBLE,BNTI,BNTO,BNBI,BNBO,
```

```
     *              BNLE,AIRA,AILE
      COMMON /CONTROL/ IPAR,MONO,IPLA,IAS,IMAG,IFIE,ITWI,IHIT,ONLY,IRIN
      COMMON /UEVENT/ EDEP(4),GERFIR(3),BGOFIR(3),ESC(3)
      COMMON /SEED/ SEED
      DATA XM /0.511E-03/
      DATA VERTZER /3*0.0/
C
C     clear descriptors-variables for next event
      DO IDET=1,3
         EDEP(IDET) = 0.0
       GERFIR(IDET) = 0.0
       BGOFIR(IDET) = 0.0
          ESC(IDET) = 0.0
      ENDDO
      EDEP(4) = 0.0
C
      RAD = GERA
      IF(RILU.GT.0.0) RAD = RILU
C     calculate initial direction of PARTICLE
C     THETA----------
   10 R(1)=MTH$RANDOM(SEED)
      THEMAX= ATAND(RAD/DIST)
      DCS = 1. - COSD(THEMAX)
      THERP = ACOSD(1. - DCS * R(1))
C     PHI------------
      R(2)=MTH$RANDOM(SEED)
      PHIRP=360.0*R(2)
C
C     get PARTICLE mass from data structure
      JPA = LQ(JPART - IPAR)
      XM  = Q(JPA + 7)
      ITRTYP = Q(JPA + 6)
C
C     calculate momentum components of PARTICLE----------------------
      IF(WIDTH.NE.0.0) THEN
        EKINP = ETRAN*(1+WIDTH*GAUSS(DUMMY))
      ELSE
        EKINP = ETRAN
      ENDIF
      PP = SQRT(EKINP*(EKINP+2.*XM))
      PPLAB(1) = PP * SIND(THERP) * COSD(PHIRP)
      PPLAB(2) = PP * SIND(THERP) * SIND(PHIRP)
      PPLAB(3) = PP * COSD(THERP)
C
C     load vertex parameters-----------------------------
      CALL GSVERT (VERTZER,0,0,0.,0,NVERT)
C     load particles parameters--------------------------
```

```
      CALL GSKINE (PPLAB,IPAR,NVERT,0.,0,NTRACK)
C
C     print event initials for debugging
C      IF (LPRIN(2) .NE. 0) THEN
C        CALL GPVERT(NVERT)
C        CALL GPKINE(0)
C      ENDIF
C
      RETURN
      END
C=======================================================================
C
      SUBROUTINE GUTREV
C
      COMMON /STOP/ SKIP,ABORT,ESCAPE,FIRGER,FIRBGO
      LOGICAL*1 SKIP,ABORT,ESCAPE,FIRGER,FIRBGO
C
      ABORT=.FALSE.
      FIRGER=.TRUE.
      FIRBGO=.TRUE.
      ESCAPE=.TRUE.
C
      CALL GTREVE
      RETURN
      END
C
C
      SUBROUTINE GUTRAK
C
      COMMON /STOP/ SKIP,ABORT,ESCAPE,FIRGER,FIRBGO
      LOGICAL*1 SKIP,ABORT,ESCAPE,FIRGER,FIRBGO
C
      SKIP=.FALSE.
C
      CALL GTRACK
      RETURN
      END
C
C
      SUBROUTINE GUSTEP
C.    7------------------------------------------------------------------
C.    I                                                                  I
C.    I                                                                  I
C.    I                                                                  I
C.    ------------------------------------------------------------------
C
      IMPLICIT NONE
```

```
      INCLUDE 'CERN_GEANT:GEANT (GCFLAG)'
      INCLUDE 'CERN_GEANT:GEANT (GCKINE)'
      INCLUDE 'CERN_GEANT:GEANT (GCLIST)'
      INCLUDE 'CERN_GEANT:GEANT (GCTRAK)'
      INCLUDE 'CERN_GEANT:GEANT (GCTMED)'
      INCLUDE 'CERN_GEANT:GEANT (GCVOLU)'
      INTEGER*4 IPAR,IAS,IMAG,IFIE,ITWI,MONO,IPLA,IPOS,IHIT,ONLY,IRIN
      INTEGER*4 MAXLEV, IDET,NTH,MINY
      REAL*4 ETRAN,WIDTH,DIST,RILU,GERA,GELE,BMTI,BMTO,
     *       BMBI,BMBO,BMLE,BBRA,BBLE,BNTI,BNTO,BNBI,BNBO,BNLE,
     *       AIRA,AILE
      REAL*4 EDEP,ZET,GMX(3),GERFIR,BGOFIR,ESC
      LOGICAL*1 ABORT,SKIP,ESCAPE,FIRGER,FIRBGO
      COMMON /USER/ ETRAN,WIDTH,DIST,RILU,GERA,GELE,BMTI,BMTO,
     *              BMBI,BMBO,BMLE,BBRA,BBLE,BNTI,BNTO,BNBI,BNBO,
     *              BNLE,AIRA,AILE
      COMMON /CONTROL/ IPAR,MONO,IPLA,IAS,IMAG,IFIE,ITWI,IHIT,ONLY,IRIN
      COMMON /STOP/ SKIP,ABORT,ESCAPE,FIRGER,FIRBGO
      COMMON /UEVENT/ EDEP(4),GERFIR(3),BGOFIR(3),ESC(3)
C     locals
      DATA MAXLEV /3/
C
      IF(SKIP)  GOTO 10
      IF(ABORT) GOTO 20
C
      CALL GSKING(0)              ! store all secondaries
C     ----------WHAT IS HAPPENING INSIDE GERMANIUM ?----------
      IF(NUMED.EQ.17) THEN
        IF(DESTEP.GT.0.0) THEN
          IF(FIRGER) THEN
            GERFIR(1) = VECT(1)
            GERFIR(2) = VECT(2)
            GERFIR(3) = VECT(3)
            FIRGER =.FALSE.
          ENDIF
          EDEP(1)=EDEP(1)+DESTEP
        ENDIF
      ENDIF
C     ----------WHAT IS HAPPENING INSIDE BGO?----------
      IF(NUMED.EQ.18) THEN
        IDET=NUMBER(2)   ! number of BGO (1=MAIN,2=BACK,3=NOSE)
        IF(DESTEP.GT.0.0) THEN
          IF(FIRBGO) THEN
            BGOFIR(1) = VECT(1)
            BGOFIR(2) = VECT(2)
            BGOFIR(3) = VECT(3)
            FIRBGO =.FALSE.
```

```
        ENDIF
        EDEP(IDET+1)=EDEP(IDET+1)+DESTEP
       ENDIF
      ENDIF
C
      IF(.NOT.FIRGER.AND.NUMED.EQ.15) THEN
       IF(ESCAPE) THEN
        ESC(1) = VECT(1)
        ESC(2) = VECT(2)
        ESC(3) = VECT(3)
        ESCAPE =.FALSE.
       ENDIF
      ENDIF
C     stop tracking, if particle is out of set-up
      IF(INWVOL.EQ.3) GOTO 10
C
      GOTO 90
C     stop tracking of current particle
   10 SKIP=.TRUE.
C      NLEVEL=1
      ISTOP=2           ! particle is stopped
      RETURN
C     abort current event
   20 ABORT=.TRUE.
      IEOTRI=1          ! flag to abort current event if non zero
C
   90 RETURN
      END
C
C
C.    ----------------------------------------------------------------------
      SUBROUTINE GUDIGI
C.    ----------------------------------------------------------------------
C
      IMPLICIT NONE
      INCLUDE 'CERN_GEANT:GEANT (GCLIST)'
      CHARACTER*20 FILE
      REAL*4 ETRAN,WIDTH,DIST,RILU,GERA,GELE,BMTI,BMTO,
     *       BMBI,BMBO,BMLE,BBRA,BBLE,BNTI,BNTO,BNBI,BNBO,BNLE,
     *       AIRA,AILE
      REAL*4 EDEP,ZET(3),BASE
      REAL*4 FACT_E, FACT_Z,FACT_PHI,ETOT,GERFIR,BGOFIR,ESC,CIL(3)
      INTEGER*2 EVE(10)
      INTEGER M,CONTEXT
      INTEGER*4 IEE,ITT, LIMIT, I,ICH,ONLY,SEED,IRIN
      INTEGER*4 IPAR,NEVE,NE,NTH,IAS,IMAG,IFIE,ITWI,MONO,IPLA,IHIT
      LOGICAL*1 HIT(2),THETOPEN,SKIP,ABORT,ESCAPE,FIRGER,FIRBGO
```

```
      COMMON /USER/ ETRAN,WIDTH,DIST,RILU,GERA,GELE,BMTI,BMTO,
     *              BMBI,BMBO,BMLE,BBRA,BBLE,BNTI,BNTO,BNBI,BNBO,
     *              BNLE,AIRA,AILE
      COMMON /CONTROL/ IPAR,MONO,IPLA,IAS,IMAG,IFIE,ITWI,IHIT,ONLY,IRIN
      COMMON /NEVE/ NEVE
      COMMON /UEVENT/ EDEP(4),GERFIR(3),BGOFIR(3),ESC(3)
      COMMON /FILE/ FILE,CONTEXT
      COMMON /STOP/ SKIP,ABORT,ESCAPE,FIRGER,FIRBGO
      COMMON /BASE/ BASE
      DATA LIMIT /32767/
      DATA FACT_E   /0.5E+06/          ! conversion from GeV to  2  keV
      DATA FACT_Z   /1.0E+02/          ! conversion from cm  to  .1  mm
      DATA FACT_PHI /22.752777/         ! this makes 360 deg. = 8191 channel
C
      IF(EDEP(1).LE.0) RETURN
C
      CIL(1) = SQRT(GERFIR(1)**2 + GERFIR(2)**2)
      CIL(2) = SQRT(BGOFIR(1)**2 + BGOFIR(2)**2)
      CIL(3) = SQRT(ESC(1)**2 + ESC(2)**2)
      ZET(1) = BASE - GERFIR(3)
      ZET(2) = BASE - BGOFIR(3)
      ZET(3) = BASE - ESC(3)
C
      DO I=1,3
        EDEP(I)  = EDEP(I)*FACT_E      ! transformation to 1   keV units
        CIL(I)   = CIL(I)*FACT_Z
        ZET(I)   = ZET(I)*FACT_Z       ! transformation to 0.1 mm  units
      ENDDO
      EDEP(4)    = EDEP(4)*FACT_E
C
C     Overflows
C
      DO I=1,3
        IF(EDEP(I).GT.8191) EDEP(I)=8191
        IF(CIL(I).GT.8191)  ZET(I)=8191
        IF(ZET(I).GT.8191)  ZET(I)=8191
        IF(ZET(I).LT.0)     ZET(I)=0
      ENDDO
      IF(EDEP(4).GT.8191) EDEP(4)=8191
C
C     Filling an event buffer
      DO I=1,3
        EVE(I) = NINT(EDEP(I))
        EVE(2*I+3) = NINT(CIL(I))
        EVE(2*I+4) = NINT(ZET(I))
      ENDDO
        EVE(4) = NINT(EDEP(4))
```

```
      CALL PUTEVENT(%VAL(CONTEXT),EVE,10,0)
C
      RETURN
      END
C=============================================================
=====
C
     FUNCTION GAUSS(DUMMY)
C     Generates a gaussian distributed number with average 0
C     and standard deviation 1
      IMPLICIT NONE
      REAL*4 GAUSS,MTH$RANDOM,DUMMY
      INTEGER*4 INM,SEED
      COMMON /SEED/ SEED
C
      GAUSS=0.0
      DO INM=1,12
        GAUSS=GAUSS+MTH$RANDOM(SEED)-0.5
      ENDDO
      RETURN
      END
C
```

Appendix C Deduction of the transmission probability of the BGO-air-glass-grease-PMT read-out surface

Recall that the read-out surface is specular, so equation 3.2.2, 3.2.3, 3.2.4, 3.2.5. and 3.2.6 are valid. Then the transmission through one medium, without any reflections will be given by formula C1:

$$T_{i,i+2}(nr) = (1 - R_{i,i+1})\,(1 - R_{i+1,i+2})\,(1 - A_{i+1}) \qquad \text{(C1)}$$

with: $T_{i,i+2}(nr)$ = transmission through medium i+1 without any reflections.
A_{i+1} = absorbtion in medium i+1.
$R_{i,i+1}$ = reflection from medium i to medium i+1.
$R_{i+1,i+2}$ = reflection from medium i+1 to medium i+2.

The probability transmission after one reflection within medium i+1 is given by equation C2:

$$T_{i,i+2}(1r) = T_{i,i+2}(nr)\, R_{i+1,i+2}\, R_{i,i+1}\, (1 - A_{i+1})^2 \qquad \text{(C2)}$$

with: $T_{i,i+2}(1r)$ = transmission through one medium after one reflection inside this medium.

Summing all reflections possible inside medium i+1 then gives the total transmission possibility (formula C3):

$$T_{i,i+2} = (1 - R_{i,i+1})(1 - R_{i+1,i+2})(1 - A_{i+1}) \cdot \left[\frac{1}{1 - (1 - A_{i+1})^2\, R_{i,i+1} R_{i+1,i+2}}\right] \qquad \text{(C3)}$$

with: $T_{i,i+2}$ = transmission probability for a photon impinging interface i to reach medium i+2.

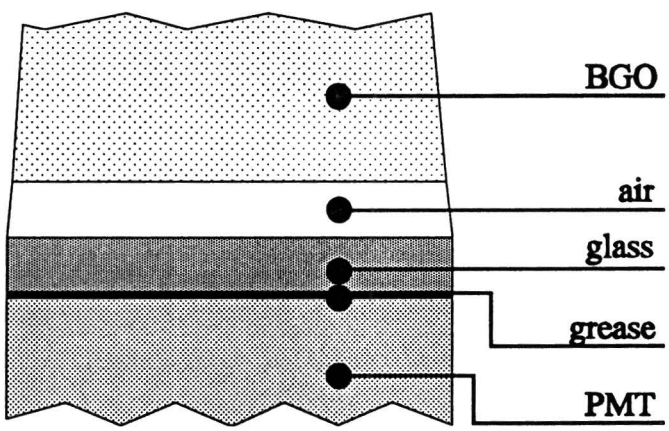

Figure 3.5.4. *Readout of scintillation photons.*

This equation can be generalized for the transmission through more than one medium. First let us change the notation. We now calculate the probability that a scintillation photon impinging on the readout surface of the BGO (1), is detected by the photomultiplier tube (5).

Between the photomultiplier and the BGO there are three different media, i.e. air (2), glass (3) and coupling grease (4) (See Figure 3.5.4).

The only difficulty is that light can be reflected within one medium, but also within more media (See Figure C1).

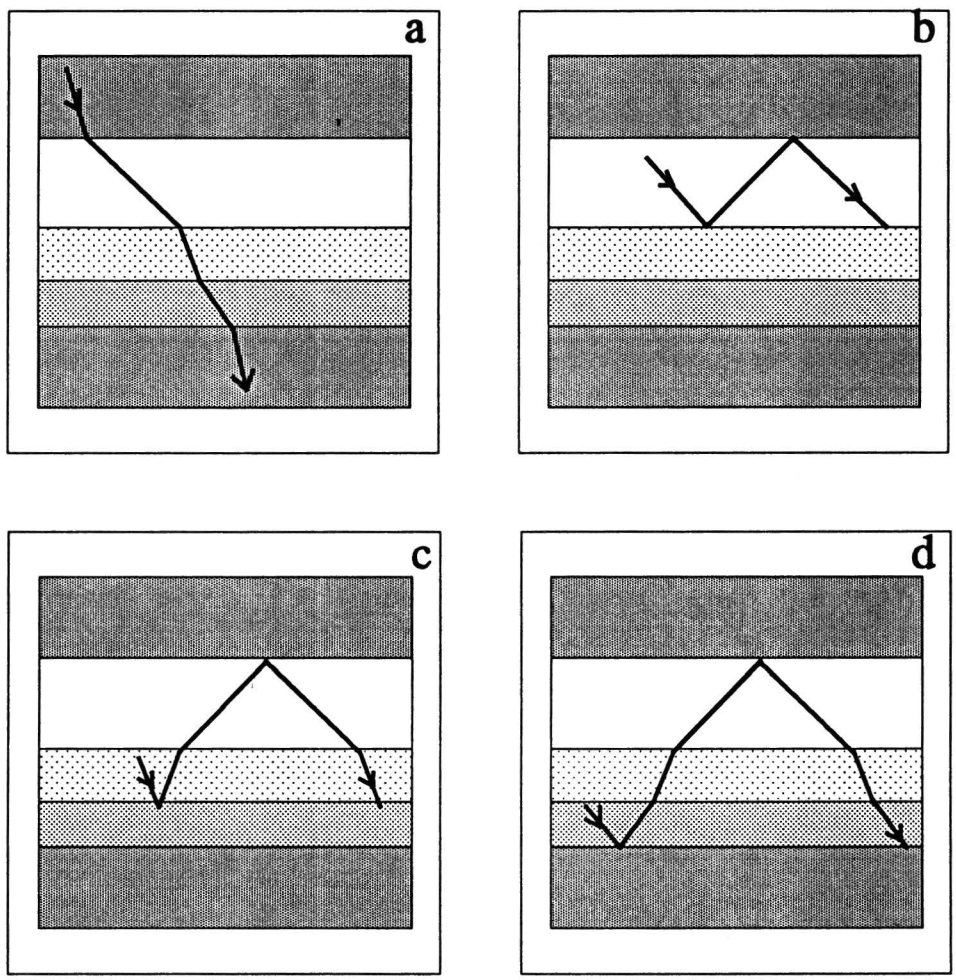

Figure C1. *Transmission and reflection of scintillation photons at a BGO-air-glass-grease-PMT readout surface; a: transmission through all interfaces, b: reflection within one medium, c: reflection within two media, d: reflection within three media.*

The transmission through three media is deducted in the same way we deducted the transmission through one medium and given by equation C4.

$$T_{1,5} = \left[\prod_{i=1}^{4} 1 - R_{i,i+1}\right] \cdot \left[\prod_{i=2}^{4} \frac{1 - A_i}{1 - R_{i-1,i}\, R_{i,i+1}(1 - A_i)^2}\right] \cdot$$

$$\left[\prod_{i=2}^{3} \frac{1}{1 - (1 - R_{i,i+1})^2 R_{i-1,i} R_{i,i+1} \left(\prod_{j=i}^{i+1} (1 - A_j)^2\right)}\right] \cdot \qquad \text{(C4)}$$

$$\left[\frac{1}{1 - \left(\prod_{i=2}^{3} (1 - R_{i,i+1})^2\right) \cdot \left(\prod_{i=3}^{3} R_{i-2,i-1} R_{i+1,i+2}\right) \cdot \left(\prod_{i=2}^{4} (1 - A_i)^2\right)}\right]$$

with: $T_{1,5}$ = Transmission of photons from BGO till detection in PMT.
$R_{i,i+1}$ = Reflectivity at surface i,i+1.
A_i = Absorbtion of photons in medium i.
i = medium index.

The first part decribes the transmission of the photons from BGO till PMT. The second terms accounts for reflections within one medium, the third reflections within two media (second line), and finally the fourth describes reflections within three media (third line).

Acknowledgement

I would like to thank all people who have been of any help during my graduate work.
Thanks to: my roommates;
A. Buda and J. Bacelar: KVI;
P. Schotanus: Q&S;
P. Vermeulen: Canberra.
Bedankt P. Magendans.
Dank aan de mannen van de werkplaats, met name J. van Asten. Bertha komt eraan.
Special thanks to M. de Voigt and S. Micek. It was a very educative and interesting year.